AD_____

Award Number: W81XWH-13-1-0130

TITLE: Understanding Selective Downregulation of c-Myc Expression through Inhibition of General Transcription Regulators in Multiple Myeloma

PRINCIPAL INVESTIGATOR: Dr. Charles Lin

CONTRACTING ORGANIZATION: Dana-Farber Cancer Institute, Inc.
Boston, MA 02115-6013

REPORT DATE: June 2015

TYPE OF REPORT: Annual

PREPARED FOR: U.S. Army Medical Research and Materiel Command
Fort Detrick, Maryland 21702-5012

REPORT DOCUMENTATION PAGE

Form Approved
OMB No. 0704-0188

1. REPORT DATE	2. REPORT TYPE	3. DATES COVERED
June 2015	Annual	06/15/2014-06/14/2015

4. TITLE AND SUBTITLE

Understanding Selective Downregulation of c-Myc Expression through Inhibition of General Transcription Regulators in Multiple Myeloma

5a. CONTRACT NUMBER
W81XWH-13-1-0130

5b. GRANT NUMBER

5c. PROGRAM ELEMENT NUMBER

6. AUTHOR(S)

Dr. Charles Lin

E-Mail: Charles_lin@dfci.harvard.edu

5d. PROJECT NUMBER

5e. TASK NUMBER

5f. WORK UNIT NUMBER

7. PERFORMING ORGANIZATION NAME(S) AND ADDRESS(ES)
Dana-Farber Cancer Institute
450 Brookline Ave.
Boston, MA 02115-5450

8. PERFORMING ORGANIZATION REPORT

9. SPONSORING / MONITORING AGENCY NAME(S) AND ADDRESS(ES)
U.S. Army Medical Research and Materiel Command
Fort Detrick, Maryland 21702-5012

10. SPONSOR/MONITOR'S ACRONYM(S)

11. SPONSOR/MONITOR'S REPORT NUMBER(S)

12. DISTRIBUTION / AVAILABILITY STATEMENT
Approved for Public Release; Distribution Unlimited

13. SUPPLEMENTARY NOTES

14. ABSTRACT

Through analysis of the chromatin and transcriptional landscape of Multiple Myeloma (MM) and other tumors, this project has endeavored to provide an explanatory mechanism for how treatment with inhibitors of chromatin regulators can selectively target oncogene transcription, and to understand how chromatin and transcription are altered to promote tumorigenesis. Here we report the discoveries that BET bromodomains are required to communicate enhancer mediated pro-inflammatory signal dependent transduction (Brown et al., 2014), that translocations of the *IgH* enhancer to the *MYC* locus in MM expose both enhancer driven and MYC/E2F driven regulatory programs to BET bromodomain inhibition (Fulciniti et al., submitted), and that master transcription factors co-operate with one another and BET bromodomains to establish oncogenic state in MM and other tumors (Lin et al., submitted). These efforts have yielded insights into the dynamic transcriptional control of oncogenic cell state, the development of novel and extendable experimental and computational approaches, and therapeutic insights into the consequences of systemic *in vivo* BET bromodomain inhibition.

15. SUBJECT TERMS
Multiple myeloma, chromatin, computational biology

16. SECURITY CLASSIFICATION OF:			17. LIMITATION OF ABSTRACT	18. NUMBER OF PAGES	19a. NAME OF RESPONSIBLE PERSON
a. REPORT	b. ABSTRACT	c. THIS PAGE			USAMRMC
U	U	U	UU	61	19b. TELEPHONE NUMBER *(include area code)*

Table of Contents

Introduction: Multiple Myeloma (MM) is an aggressive and incurable plasma cell malignancy often characterized by IgH Enhancer/*MYC* (IgH/*MYC*) translocations that drive excess levels of the c-Myc oncoprotein. Recently, the Bradner laboratory has shown that inhibition of the general transcriptional co-activator BRD4 with a selective chemical probe (JQ1) leads to dramatic down regulation of c-Myc expression and cell death in MM cell lines (Delmore et al., 2011). In other tumors, BRD4 inhibition does not lead to down regulation of the IgH/*MYC* translocation gene, but rather causes the selective down regulation of other key cancer genes (Dawson et al., 2011; Ott et al., 2012; Zuber et al., 2011). BRD4 is a BET (bromodomain and extra-terminal) family protein (Filippakopoulos et al., 2010) that binds to acetyl-lysine residues on histones and other chromatin associated factors. BRD4 is a key co-activator of the elongation factor P-TEFb and has been shown to co-activate transcription through co-operative interactions with master regulator transcription factors (Huang et al., 2009). P-TEFb is required for the transcription elongation of essentially all active genes (Rahl et al., 2010) suggesting a general role for BRD4 in broadly co-activating transcription. Thus, it is unexpected based on current paradigms of mammalian transcriptional regulation and chromatin structure, how inhibition of BRD4 can selectively inhibit the transcriptional activity of oncogenes in tumors. Currently, small molecule inhibitors of BRD4 (including derivatives of JQ1) are in FDA Phase I clinical trials, with recent reports of positive clinical response (AACR 2014). As such, it is imperative to understand how BRD4 regulates gene expression and the mechanisms by which inhibition of BRD4 leads to dramatic effects at a small subset of genes in a cell type specific manner. This study is focused on understanding mechanisms of JQ1 activity in MM and other tumors as it is critical for understanding both how chromatin regulators function in cancer and how general transcriptional regulator inhibitors can achieve selective effects against cancer.

Keywords: Chromatin, Transcription, Multiple Myeloma, MYC, Therapeutics, Gene Regulation

Key Research Accomplishments - *To explore the mechanisms by which inhibition of BRD4 leads to selective effects on oncogene transcription, we have undertaken the following aims:*

Major goals and accomplishments

Aim 1. To map Brd4 onto the transcriptional and epigenomic landscape of MM

Status: Completed

Reported in Loven et al., Cell 2013; Chapuy et al., Cancer Cell 2013, Fulciniti et al., submitted

Using genome wide ChIP-Seq (chromatin immunoprecipitation coupled to high throughput sequencing) approaches, we have mapped the comprehensive transcriptional and epigenomic landscape of MM in steady state and in response to treatment with increasing doses of JQ1. Given that BRD4 was present at all active promoters and enhancers, it was unclear how inhibition of such a broad co-factor could yield highly specific results. In several JQ1 sensitive cell lines, we integrated global BRD4 occupancy data with comprehensive chromatin landscapes and found that BRD4 was disproportionately found at only a handful of large enhancer domains that spanned tens of kilobases and were also highly occupied by all other chromatin and transcriptional co-activators. On the whole, these "super-enhancers" made up only 3% of the cell's enhancers, but encompassed 40% of all enhancer bound co-activators. In each tumor, super enhancers associated with key oncogenic genes, driving the not only continued cancer cell growth, but also genes specifying tumor cell identity itself.

The discovery and characterization of super-enhancers first published in this work (Loven et al., 2013) and its companion paper (Whyte et al., 2013) have now been extended and further studied in more than 40 publications. Data from this study has been curated and made publically available on the Epigenome gateway browser in the "Multiple Myeloma Epigenome Portal" (http://epigenomegateway.wustl.edu/browser/). Consequently, we have developed and made openly available analysis software that can quantify normalized factor occupancy genome wide to identify and rank super-enhancers, genomic regions of asymmetric chromatin co-activator loading (https://github.com/BradnerLab/pipeline). These methods have been used by more than 100 laboratories and have been incorporated into online databases including dbSuper (http://bioinfo.au.tsinghua.edu.cn/dbsuper/).

In subsequent work, we have employed this chromatin mapping framework in patient MM samples to investigate changes to the enhancer landscape of MM induced by the primary tumor microenvironment and have identified candidate primary tumor specific super-enhancers. We have also integrated a new chromatin mapping technique (ATAC-Seq) that identifies putative cis-regulatory elements from small cell samples (Buenrostro et al., 2013). These approaches have been extended to profile transcription factor occupancy in the MM.1S cell line (Figure 1), and also to profile chromatin landscapes in other MM cell lines (Fulciniti et al., in preparation). Here we have identified distinct regulatory axes governed by BRD4 and the cell cycle promoting transcription factor E2F and have incorporated this theme into our study of BRD4 cooperation with other transcriptional regulators (Aim 3). Finally, in collaboration with others, we have extended these approaches into other tumor model systems including Non Hodgkin's lymphoma (Chapuy et al., 2013), triple negative breast cancer (Shu et al., submitted), and medulloblastoma (Lin et al., submitted).

Aim 2. To examine the kinetic, transcriptional response to BET bromodomain inhibition

Status: Completed and extended with new objectives

Reported in Loven et al., Cell 2013; Chapuy et al., Cancer Cell 2013; Anand et al., Cell 2013; Brown et al., Molecular Cell 2014; Fulciniti et al., in preparation

From data generated in Aim 1, we hypothesized that asymmetric occupancy of chromatin regulators including BRD4 at oncogene driving super-enhancers might explain their sensitivity to chromatin co-activator inhibition. We have mapped JQ1 induced changes in gene expression and RNA Pol II genomic occupancy in both a time and concentration dependent manner in MM and other disease model systems (Anand et al., 2013; Brown et al., 2014; Chapuy et al., 2013; Loven et al., 2013). These data consistently show that BET bromodomain inhibition by JQ1 treatment leads to a global decrease in transcriptional activity, specifically a decrease in elongating RNA Pol II. This inhibition of transcription is most pronounced at super-enhancer proximal target genes and is supported at the chromatin level by evidence that both BRD4 and the active kinase subunit of the elongation P-TEFb are preferentially lost at super-enhancer loci upon JQ1 treatment. In MM, JQ1 treatment leads to rapid downregulation of *MYC* and other super-enhancer associated oncogenes. Interestingly in diffuse large B-cell lymphoma (DLBC), super-enhancers associate with different oncogenes and thus JQ1 treatment does not preferentially downregulate *MYC* transcription. Instead, in DLBCL, super-enhancers associate with other prominent B-cell factors including *BCL6* and *PAX5* that are strongly downregulated upon JQ1 treatment (Chapuy et al., 2013). In all profiled systems, inhibition of chromatin and transcriptional regulators including BET bromodomains (BRD4), the BAF complex (BRG1) and transcriptional kinases (CKD7) caused a selective inhibition of transcription at super-enhancer driven oncogenes as compared to other genes (Chapuy et al., 2013; Chipumuro et al., 2014; Kwiatkowski et al., 2014; Loven et al., 2013; Shi et al., 2013).

We next sought to explore the consequences BRD4 inhibition during dynamic cell state transitions. Previously, we had quantified BRD4 inhibition response in static, steadily growing tumor cell models. However, MM and other tumor cell states are often maintained through aberrant oncogenic signaling, necessitating an understanding of the role of BRD4 in stimulus coupled signal transduction response. *In vivo*, MM tumors exists in a pro-inflammatory environment in the bone marrow that is supported through increased NF-κB signaling and transcriptional activity (Demchenko and Kuehl, 2010). NF-κB transcription factors are known to directly interact with BRD4 (Huang et al., 2009) and we hypothesized that activation of NF-κB transcriptional response subsequent to pro-inflammatory stimulation requires BRD4 activity. Since *in vitro* immortalized MM cell line models fail to fully articulate *in vivo* inflammatory response, we utilized the well characterized NF-κB responsive primary human endothelial cell system to investigate basic mechanisms of signal dependent BRD4 function.

Treatment of endothelial cells with pro-inflammatory stimuli caused NF-κB to localize to the nucleus leading to transcriptional response and phenotypic cell state transition from resting to inflamed and activated endothelium. Surprisingly we found that NF-κB activation resulted in a rapid and comprehensive remodeling of the chromatin co-activator landscape, with more than 50% of all BRD4 bound super-enhancers redistributing to sites of newly acquired NF-κB binding. In inflammatory stimulated endothelial cells co-treated with JQ1, NF-κB still enters the nucleus and binds chromatin. However, BRD4 fails to redistribute to these sites of NF-κB binding, thus blocking super-enhancer formation and consequently abrogating NF-κB directed pro-inflammatory transcriptional response.

These data suggest a crucial role for BRD4 in dynamic cell state transitions where it communicates signals from signaling pathway terminal transcription factors to RNA Pol II. Further, JQ1 inhibited transcription of NF-κB directed *de novo* super-enhancer target genes an order of magnitude more than genes associated with resting endothelial super-enhancers at

baseline. This observation suggests that *in vivo* cell populations undergoing dynamic cell state transitions in response to cell signaling are most likely to be affected by JQ1. Results from this study of BRD4 and NF-κB dynamics were published in Molecular Cell (Brown et al., 2014) and is included in the appendices of this report.

Aim 3. To explore the contribution of cooperative binding and disproportionate load by BRD4 to transcriptional response

Status: 50% completed

Reported in Fulciniti et al., in preparation; Lin et al., submitted

The initial description of super-enhancers in MM revealed additional features of super-enhancers with potential utility in characterizing tumor epigenomes. Super-enhancers differ from typical enhancers in their underlying sequence composition, their response to perturbation, and their ability to drive high levels of transcription at target genes. Towards a mechanistic understanding of these features, we have now developed experimental and computational approaches to map transcription factor binding sites within super-enhancer loci using data derived from a combination of H3K27ac ChIP-Seq to map super-enhancers and ATAC-Seq to precisely identify high-resolution transcription factor binding sites. From this data we are able to computationally reconstruct enhancer gene regulatory networks and predict transcription factor regulated gene expression programs. Applying these methods to MM cells, we observed that many cell type specific transcription factors in MM were regulated by a super-enhancer and also bound to super-enhancers. These auto-regulatory patterns established a core regulatory circuitry in which a small number of transcription factors are super-enhancer associated, and in turn bind to and regulate super-enhancers (Figure 2). Analysis of core regulatory circuitry in MM and normal cd19+ plasma cells revealed many shared plasma cell transcription factors including XBP1 and IRF family factors. Differential analysis revealed the glucocorticoid receptor transcription factor as present only in the circuitry of MM cells. As MM are primarily treated with dexamethasone (a glucocorticoid receptor agonist), these data support a central role for glucocorticoid receptor signaling in driving MM oncogenesis and suggest that core circuitry network approaches accurately describe tumor cell identity.

We have also used methodology developed from this effort to elucidate core transcriptional regulatory circuitry in other poorly classified tumors. In collaboration with the German cancer research institute (DKFZ), we have deployed chromatin enhancer mapping and core regulatory circuitry inference methods to elucidate cellular origins of different medulloblastoma subgroups. Medulloblastoma is clinically classified into 4 different subgroups, each with different molecular pathologies. However, the cellular origins of individual subgroups are poorly understood. Here the use of core regulatory circuitry inference has elucidated the developmental and cellular origins of the previously uncharacterized Group 4 medulloblastoma. A manuscript describing these results has been submitted to Nature and is currently in revision (Lin et al., 2015 submitted).

Currently we are extending these chromatin profiling and computational approaches across a large number of hematopoietic lineage derived normal and tumor cell populations. To date H3K27ac ChIP-Seq in primary patient MM samples has proven technically challenging. Although ATAC-Seq is able to identify transcription factor binding sites in primary samples, it fails to adequately map super-enhancers, necessitating H3K27ac mapping approaches. To overcome technical challenges with ChIP-Seq, we are implementing the newly developed iChIP methodology that is able to produce ChIP-Seq equivalent data from small (< 1 million cell) patient samples (Lara-Astiaso et al., 2014).

Finally, analysis of the transcription factor occupancy in relation to BRD4 in MM has suggested new therapeutic strategies to target the disease. Previously we reported the concomitant inhibition of MYC and E2F activity in multiple myeloma (MM) upon treatment with the BET bromodomain inhibitor JQ1 (Delmore et al., 2011). BET bromodomains (BETs) are transcriptional co-activators that occupy active promoters and enhancers, but are asymmetrically localized to a small number of "super-enhancer" domains. JQ1 treatment results in disproportionate displacement of BETs from super-enhancers leading to potent and selective downregulation of super-enhancer target genes, including MYC which is > 90% depleted after 6 hours.

In contrast, E2F protein levels are relatively unperturbed by JQ1 treatment. Instead, JQ1 treatment inhibits the expression of super-enhancer driven upstream regulators of E2F including the MYC and CCND2. In tumors where MYC is not super-enhancer associated, JQ1 treatment fails to directly downregulate E2F activity. These observations suggest that the MYC translocation status of MM plays a key role in determining the sensitivity of E2F activity to BET inhibition. They also suggest an unexplored collaboration between MYC, E2F, and BETs in maintenance of MM.

In both MYC translocated and non MYC translocated MM, we mapped the global occupancy patterns of E2F1 and its dimerization partner DP1. We next utilized chemical and genetic perturbations to investigate the functional consequences of E2F depletion singly or in combination with JQ1 *in vitro* and *in vivo*. Across MM, we demonstrate that E2F activity is required for tumor growth both *in vitro* and *in vivo*, as depletion results in G1 arrest (Figure 3a,b). We find surprisingly that DP1, the dimerization partner of E2F1, is required for tumor growth, and that DP1 expression negatively correlates with patient outcome. Global chromatin analysis reveals distinct regulatory axes for E2F and BETs, with E2F predominantly localized to active gene promoters and BETs disproportionately found at super-enhancers (Figure 3 c-j). As MYC activates E2F, translocations of *MYC* to the *IgH* enhancer place both super-enhancer and E2F driven genes under BET control. Consequently BET inhibition is synergistic with E2F depletion only in non-*IgH/MYC* translocated MM (Figure 3k).

Our results implicate E2F as a dependency in MM and expose a vulnerability to BET inhibition imparted by *IgH/MYC* translocations. In non *IgH/MYC* translocated MM, E2F inhibition is synergistic with JQ1 treatment. These observations suggest targeting of E2F as promising therapeutic strategy in MM. A manuscript describing these results is currently under preparation for 2015 submission.

Summary of reported accomplishments: During this reporting period, data from these aims have been prepared in the following manuscripts.

1) Brown et al., Molecular Cell 2014
2) Lin et al., submitted 2015
3) Fulciniti et al., in preparation
4) Wolf et al., Trends in Cell Biology 2014

Opportunities for training and professional development: The work described in these aims was performed in collaboration with clinicians, molecular biologists, and computational biologists. Through collaborative interactions, I have gained knowledge and experience in the clinical management of cancer and translational research approaches. Conversely, I have been able to train several molecular biologists in computational bioinformatics.

Professional development during this reporting period include the presentation of invited seminars at the Dana-Farber Cancer Institute, Broad Institute, Memorial Sloan Kettering Cancer Institute, Baylor College of Medicine, and the National Institutes of Health.

Dissemination of results to communities of interest: In addition to the aforementioned public presentations, work from these aims was presented to disease advocacy groups and disease stakeholders at the Dana-Farber Cancer Institute, the Leukemia and Lymphoma Society, and the Multiple Myeloma Research Foundation. Emerging themes and concepts on oncogenic transcription regulation by the transcription factor MYC were also presented in a peer reviewed review article (Wolf et al., 2014).

Future plans: Research priorities for the next reporting period include submission and revision of results in Fulciniti et al., and the preparation of a manuscript on transcription factor networks in MM and other hematopoietic malignancies.

Impact:

The discovery and characterization of super-enhancers first published in this work (Loven et al., 2013) and its companion paper (Whyte et al., 2013) have now been extended and further studied in more than 40 publications. Data from this study has been curated and made publically available on the Epigenome gateway browser in the "Multiple Myeloma Epigenome Portal" (http://epigenomegateway.wustl.edu/browser/). Consequently, we have developed and made openly available analysis software that can quantify normalized factor occupancy genome wide to identify and rank super-enhancers, genomic regions of asymmetric chromatin co-activator loading (https://github.com/BradnerLab/pipeline). These methods have been used by more than 100 laboratories and have been incorporated into online databases including dbSuper (http://bioinfo.au.tsinghua.edu.cn/dbsuper/).

The discovery of BET bromodomain regulation of inflammatory signaling has prompted additional pre-clinical research on therapeutic strategies to target chromatin and transcription regulation in vascular disease by pharmaceutical companies developing BET bromodomain inhibitors for the clinic (Tensha Therapeutics & Glaxosmithkline).

The are no other significant impacts to report.

Changes and Problems:

We have experienced technical challenges in profiling chromatin in primary MM patient samples. This is largely due to the low cellularity of MM tumor samples, and sample preservation techniques that impede chromatin extraction. To overcome these problems, we have first orthogonally extended our approaches to other tumor systems as a way to prototype new analytical methods. We have also extended work in MM cell line models and *in vivo* xenograft models in collaboration with other MM researchers. Finally we are in the process of applying new low cell requirement chromatin profiling techniques including the newly developed iChIP methodology that is able to produce ChIP-Seq equivalent data from small (< 1 million cell) patient samples (Lara-Astiaso et al., 2014).

There are no other significant changes and problems to report.

Products:

Publications: During this reporting period, data from these aims have been prepared in the following manuscripts.

1) Brown et al., Molecular Cell 2014
2) Lin et al., submitted 2015
3) Fulciniti et al., in preparation
4) Wolf et al., Trends in Cell Biology 2014

Presentations: During this reporting period, this work was presented in invited seminars at the Dana-Farber Cancer Institute, Broad Institute, Memorial Sloan Kettering Cancer Institute, Baylor College of Medicine, and the National Institutes of Health.

Conferences: During this reporting period, this work was presented at conference poster proceedings at the Keystone Symposium on Epigenetics and Cancer and at the AACR meeting "MYC: From biology to therapy".

There are no other significant products to report.

Participants and Other Collaborating Organizations:

Name:	*Jonathan Brown, M.D.*
Project Role:	*Instructor*
Researcher Identifier	N/A
Nearest person month worked:	9
Contribution to Project:	*Dr. Brown contributed experimental analysis and direction as part of a collaboration reported in Brown et al., 2014.*
Funding Support:	*Dr. Brown is supported by the NIH-K08 HL105678, The Watkins Discovery Research Award and The Harris Family Award*

Name:	*Alexander Federation, Ph.D.*
Project Role:	*Graduate Student*
Researcher Identifier	N/A
Nearest person month worked:	4
Contribution to Project:	*Dr. Federation provided computational analysis as part of a collaboration reported in Aim 2 and in Lin et al., Submitted 2015*
Funding Support:	*Dr. Federation is supported by a Leukemia and Lymphoma Society SCOR, the National Science Foundation, and NIH grants 1R01 CA176745-01 and P01 CA109901*

Name:	*Mariateresa Fulciniti Ph.D.*
Project Role:	*Instructor*
Researcher Identifier	N/A
Nearest person month worked:	12
Contribution to Project:	*Dr. Fulciniti provided experimental analysis as part of a collaboration reported in Aims 1 and Aim 2.*
Funding Support:	*Dr. Fulciniti is supported by NIH PO1-CA078378, and RO1CA050947*

There are no other significant participants or collaborating organizations.

Special reporting requirements: There are no special reporting requirements to report

Appendices:

1. Figure Legends

Figure 1 Transcription factor and chromatin landscape of multiple myeloma:

a) A heatmap showing the pairwise similarities between spatial occupancy patterns of various transcription factors, chromatin regulators, and chromatin modifications in the MM1.S multiple myeloma cell line. Individual factors are hierarchically clustered to group spatially similar binding profiles.

Figure 2 Transcription regulatory circuitry of multiple myeloma:

a) Schematic showing methodology of constructing transcription factor networks. For each super-enhancer associated transcription factor a regulatory IN and OUT degree are calculated. For any transcription factor (TF_a) The IN degree represents the number of other super-enhancer associated transcription factors that binds to the super-enhancer of TF_a. The OUT degree represents the number of super-enhancers bound by the transcription factor TF_a.
b) Network of the most highly interconnected super-enhancer associated transcription factors in the multiple myeloma cell line MM1.S. Each node represents a super-enhancer associated transcription factor. Each edge represents binding of a transcription factor to the super-enhancer of another transcription factor.
c) Comparative network analysis of various hematopoietic lineage derived cells. Each comparison shows a rank ordered bar plot of the largest changes in total regulatory degree (IN + OUT) for each cell type comparison. At each transition, transcription factors with significant changes in total regulatory degree are highlighted.

Figure 3 E2F and BET bromodomains establish distinct oncogenic regulatory axes in multiple myeloma:

a) A panel of MM cell lines were infected with either scrambled (pLKO.1) or DP1-targeted shRNA and selected with puromycin for 72 hours. DP1 mRNA levels and cell growth were then evaluated by qPCR and Thymidine uptake respectively. The results are presented as mRNA (gray line) or cell growth (black bars) changes from cells infected with pLKO.1. Data are shown as the mean values ± s.d. of triplicates.
b) *In vivo* evaluation of the effects of DP1 knockdown on MM cells. Growth curve assess tumor size after injection of MM.1S cells transduced with DP1-specific shRNA or scrambled control vectors subcutaneously into the right posterior flank region of SCID mice. Data are shown as the mean values ± s.d.
c) Gene tracks showing RNA Pol II, H3K4me3, E2F1, and DP1 occupancy at the *E2F1* gene loci
d) Gene tracks showing BRD4, H3K27ac, E2F1, and DP1 occupancy at the *BCL-xL* gene loci. The *BCL-xL* intronic super-enhancer (SE) is annotated.
e,f) Pie charts showing the fraction of active promoters and enhancers bound by E2F1 and DP1
g) Scatter plot showing the contribution of BRD4 enhancer regulation and E2F promoter regulation for all active genes in MM1.S. The y-axis shows enhancer BRD4 signal and the x-axis shows promoter E2F signal. Units are in reads per million.
h) Venn diagram showing the overlap of high BRD4 SE regulated genes and high E2F promoter regulated genes.
i,j) Functional enrichment categories for high BRD4 SE regulated genes (i) and high E2F promoter regulated genes (j)
k) Isobologram of anti-E2F peptide and JQ1 treatment effects on cell proliferation.

2. References.

Anand, P., Brown, J.D., Lin, C.Y., Qi, J., Zhang, R., Artero, P.C., Alaiti, M.A., Bullard, J., Alazem, K., Margulies, K.B.*, et al.* (2013). BET bromodomains mediate transcriptional pause release in heart failure. Cell *154*, 569-582.

Brown, J.D., Lin, C.Y., Duan, Q., Griffin, G., Federation, A.J., Paranal, R.M., Bair, S., Newton, G., Lichtman, A.H., Kung, A.L.*, et al.* (2014). NF-kappaB Directs Dynamic Super Enhancer Formation in Inflammation and Atherogenesis. Molecular cell.

Buenrostro, J.D., Giresi, P.G., Zaba, L.C., Chang, H.Y., and Greenleaf, W.J. (2013). Transposition of native chromatin for fast and sensitive epigenomic profiling of open chromatin, DNA-binding proteins and nucleosome position. Nature methods *10*, 1213-1218.

Chapuy, B., McKeown, M.R., Lin, C.Y., Monti, S., Roemer, M.G., Qi, J., Rahl, P.B., Sun, H.H., Yeda, K.T., Doench, J.G.*, et al.* (2013). Discovery and characterization of super-enhancer-associated dependencies in diffuse large B cell lymphoma. Cancer cell *24*, 777-790.

Chipumuro, E., Marco, E., Christensen, C.L., Kwiatkowski, N., Zhang, T., Hatheway, C.M., Abraham, B.J., Sharma, B., Yeung, C., Altabef, A.*, et al.* (2014). CDK7 Inhibition Suppresses Super-Enhancer-Linked Oncogenic Transcription in MYCN-Driven Cancer. Cell *159*, 1126-1139.

Dawson, M.A., Prinjha, R.K., Dittmann, A., Giotopoulos, G., Bantscheff, M., Chan, W.I., Robson, S.C., Chung, C.W., Hopf, C., Savitski, M.M.*, et al.* (2011). Inhibition of BET recruitment to chromatin as an effective treatment for MLL-fusion leukaemia. Nature *478*, 529-533.

Delmore, J.E., Issa, G.C., Lemieux, M.E., Rahl, P.B., Shi, J., Jacobs, H.M., Kastritis, E., Gilpatrick, T., Paranal, R.M., Qi, J.*, et al.* (2011). BET bromodomain inhibition as a therapeutic strategy to target c-Myc. Cell *146*, 904-917.

Demchenko, Y.N., and Kuehl, W.M. (2010). A critical role for the NFkB pathway in multiple myeloma. Oncotarget *1*, 59-68.

Filippakopoulos, P., Qi, J., Picaud, S., Shen, Y., Smith, W.B., Fedorov, O., Morse, E.M., Keates, T., Hickman, T.T., Felletar, I.*, et al.* (2010). Selective inhibition of BET bromodomains. Nature *468*, 1067-1073.

Huang, B., Yang, X.D., Zhou, M.M., Ozato, K., and Chen, L.F. (2009). Brd4 coactivates transcriptional activation of NF-kappaB via specific binding to acetylated RelA. Molecular and cellular biology *29*, 1375-1387.

Kwiatkowski, N., Zhang, T., Rahl, P.B., Abraham, B.J., Reddy, J., Ficarro, S.B., Dastur, A., Amzallag, A., Ramaswamy, S., Tesar, B.*, et al.* (2014). Targeting transcription regulation in cancer with a covalent CDK7 inhibitor. Nature *511*, 616-620.

Lara-Astiaso, D., Weiner, A., Lorenzo-Vivas, E., Zaretsky, I., Jaitin, D.A., David, E., Keren-Shaul, H., Mildner, A., Winter, D., Jung, S.*, et al.* (2014). Immunogenetics. Chromatin state dynamics during blood formation. Science *345*, 943-949.

Loven, J., Hoke, H.A., Lin, C.Y., Lau, A., Orlando, D.A., Vakoc, C.R., Bradner, J.E., Lee, T.I., and Young, R.A. (2013). Selective inhibition of tumor oncogenes by disruption of super-enhancers. Cell *153*, 320-334.

Ott, C.J., Kopp, N., Bird, L., Paranal, R.M., Qi, J., Bowman, T., Rodig, S.J., Kung, A.L., Bradner, J.E., and Weinstock, D.M. (2012). BET bromodomain inhibition targets both c-MYC and IL7R in high-risk acute lymphoblastic leukemia. Blood.

Rahl, P.B., Lin, C.Y., Seila, A.C., Flynn, R.A., McCuine, S., Burge, C.B., Sharp, P.A., and Young, R.A. (2010). c-Myc regulates transcriptional pause release. Cell *141*, 432-445.

Shi, J., Whyte, W.A., Zepeda-Mendoza, C.J., Milazzo, J.P., Shen, C., Roe, J.S., Minder, J.L., Mercan, F., Wang, E., Eckersley-Maslin, M.A.*, et al.* (2013). Role of SWI/SNF in acute leukemia maintenance and enhancer-mediated Myc regulation. Genes & development *27*, 2648-2662.

Whyte, W.A., Orlando, D.A., Hnisz, D., Abraham, B.J., Lin, C.Y., Kagey, M.H., Rahl, P.B., Lee, T.I., and Young, R.A. (2013). Master transcription factors and mediator establish super-enhancers at key cell identity genes. Cell *153*, 307-319.

Wolf, E., Lin, C.Y., Eilers, M., and Levens, D.L. (2014). Taming of the beast: shaping Myc-dependent amplification. Trends in cell biology.

Zuber, J., Shi, J., Wang, E., Rappaport, A.R., Herrmann, H., Sison, E.A., Magoon, D., Qi, J., Blatt, K., Wunderlich, M.*, et al.* (2011). RNAi screen identifies Brd4 as a therapeutic target in acute myeloid leukaemia. Nature *478*, 524-528.

3. Attachments

a) Brown et al., Molecular Cell 2014
b) Lin et al., Submitted 2015
c) Wolf et al., Trends in Cell Biology 2014

Figure 1: Transcription factor and chromatin landscape of multiple myeloma

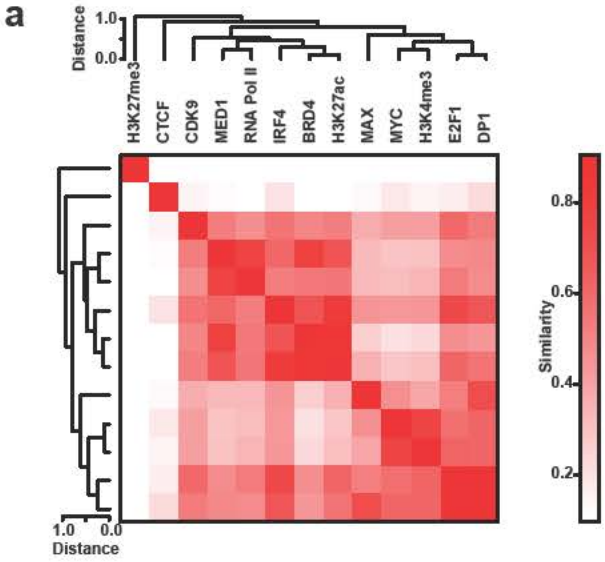

Figure 2: Transcriptional regulatory circuitry of multiple myeloma

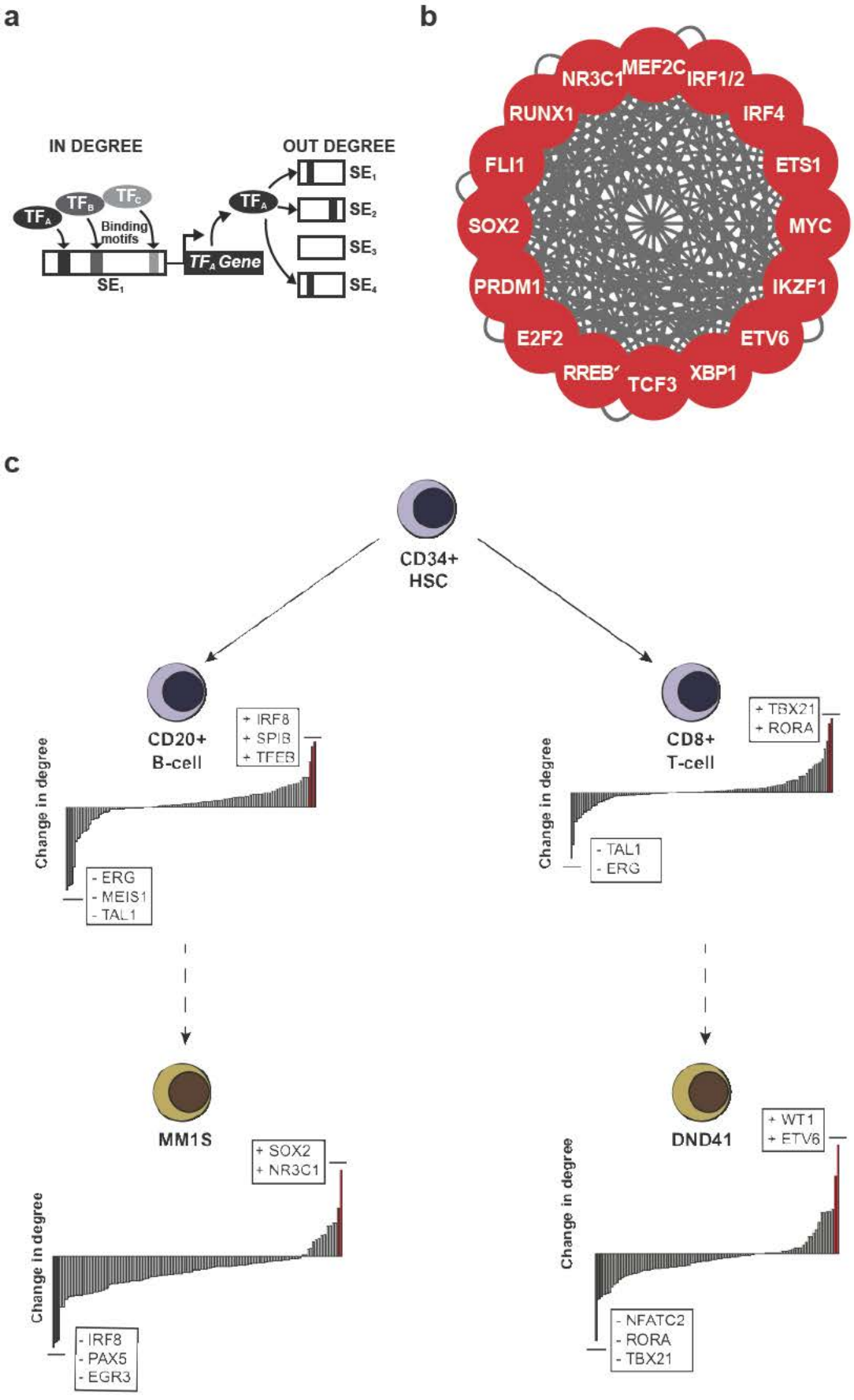

Figure 3: E2F and BET bromodomains establish distinct oncogenic regulatory axes in multiple myeloma

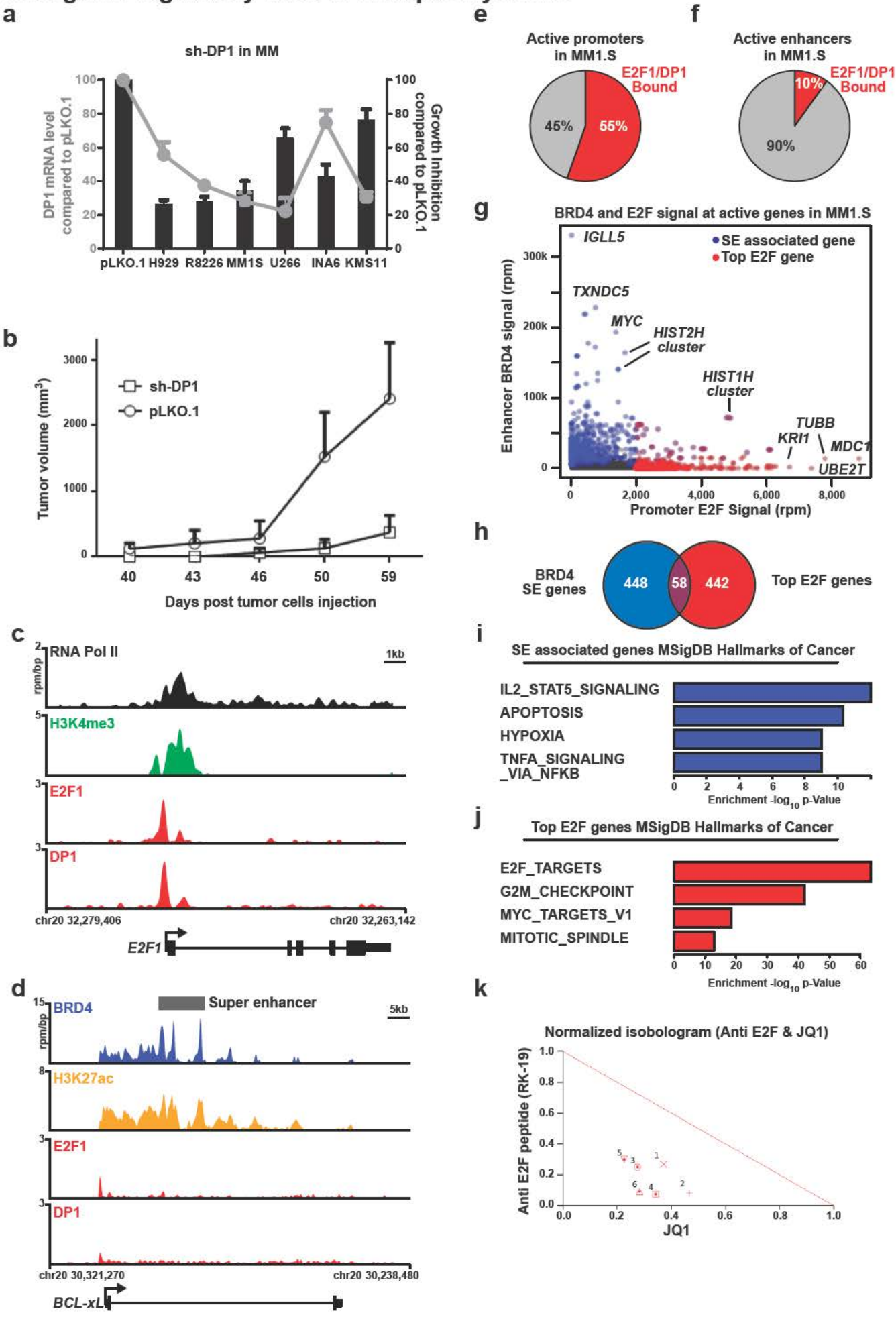

Please cite this article in press as: Brown et al., NF κB Directs Dynamic Super Enhancer Formation in Inflammation and Atherogenesis, Molecular Cell (2014), http://dx.doi.org/10.1016/j.molcel.2014.08.024

Molecular Cell
Article

NF-κB Directs Dynamic Super Enhancer Formation in Inflammation and Atherogenesis

Jonathan D. Brown,[1,6] Charles Y. Lin,[2,6] Qiong Duan,[1,3,6] Gabriel Griffin,[4] Alexander J. Federation,[2] Ronald M. Paranal,[2] Steven Bair,[2] Gail Newton,[4] Andrew H. Lichtman,[4] Andrew L. Kung,[2,5] Tianlun Yang,[3] Hong Wang,[1] Francis W. Luscinskas,[4] Kevin J. Croce,[1] James E. Bradner,[2,*] and Jorge Plutzky[1,*]
[1]Cardiovascular Division, Brigham and Women's Hospital, Harvard Medical School, Boston, MA 02115, USA
[2]Department of Medical Oncology, Dana Farber Cancer Institute, Harvard Medical School, Boston, MA 02115, USA
[3]Cardiovascular Division, Xiangya Hospital, Central South University, 410078 Changsha, Hunan, PR China
[4]Center for Excellence in Vascular Biology, Department of Pathology, Brigham and Women's Hospital, Harvard Medical School, Boston, MA 02115, USA
[5]Department of Pediatrics, Columbia University Medical Center, New York, NY 10032, USA
[6]Co-first author
*Correspondence: james_bradner@dfci.harvard.edu (J.E.B.), jplutzky@rics.bwh.harvard.edu (J.P.)
http://dx.doi.org/10.1016/j.molcel.2014.08.024

SUMMARY

Proinflammatory stimuli elicit rapid transcriptional responses via transduced signals to master regulatory transcription factors. To explore the role of chromatin-dependent signal transduction in the atherogenic inflammatory response, we characterized the dynamics, structure, and function of regulatory elements in the activated endothelial cell epigenome. Stimulation with tumor necrosis factor alpha prompted a dramatic and rapid global redistribution of chromatin activators to massive de novo clustered enhancer domains. Inflammatory super enhancers formed by nuclear factor-kappa B accumulate at the expense of immediately decommissioned, basal endothelial super enhancers, despite persistent histone hyperacetylation. Mass action of enhancer factor redistribution causes momentous swings in transcriptional initiation and elongation. A chemical genetic approach reveals a requirement for BET bromodomains in communicating enhancer remodeling to RNA Polymerase II and orchestrating the transition to the inflammatory cell state, demonstrated in activated endothelium and macrophages. BET bromodomain inhibition abrogates super enhancer-mediated inflammatory transcription, atherogenic endothelial responses, and atherosclerosis in vivo.

INTRODUCTION

Precise control of inflammation is essential for host defense. Defense against pyogenic infection requires rapid activation of tissue and circulating leukocytes and their recruitment by activated endothelium. However, inflammation is also integral to the pathophysiology of many common and life-threatening illnesses. Acute, high-grade inflammation accompanying sepsis features systemic inflammatory cell activation and contributes to multisystem organ failure and death (Medzhitov et al., 2012). Chronic, low-grade inflammation is a pathogenic feature of autoimmune disorders as well as highly prevalent and morbid conditions such as diabetes mellitus and atherosclerosis (Libby et al., 2011). As such, there is a pressing need to dissect inflammatory signaling for the elucidation of pathologic mechanisms of disease and the identification of targeted therapeutic interventions.

In inflammation, a primary mode of bidirectional cellular communication involves one set of cells releasing cytokines to activate surface receptors on effector cells. Transduced signals converge on activation and translocation of inflammatory transcription factors (Barnes and Karin, 1997). A central pathway common to the interaction between activated leukocytes and endothelium is tumor necrosis factor alpha (TNF-α)-mediated signal transduction to nuclear factor-kappa B (NF-κB)—a family of master regulatory, proinflammatory transcription factors canonically defined by the p50/p65 heterodimer (Baltimore, 2011). Following entry into the nucleus, NF-κB binds to DNA *cis*-regulatory elements at enhancers and promoters, prompting proinflammatory transcription (Pierce et al., 1988).

Genome-bound nuclear NF-κB interacts with transcriptional coactivators to stimulate transcription at multiple steps including the remodeling of chromatin as well as the initiation and elongation of RNA polymerase II (RNA Pol II; Barboric et al., 2001; Kaikkonen et al., 2013; Natoli, 2009). NF-κB recruits and interacts with defined chromatin regulators including histone acetyltransferases (P300), histone deacetylases, and epigenetic reader proteins, such as BRD4 (Ashburner et al., 2001; Huang et al., 2009; Zhong et al., 2002). Through these interactions, NF-κB engages in crosstalk with chromatin remodeling machinery.

BRD4 is a member of the bromodomain and extraterminal domain (BET) family of transcriptional coactivators and elongation factors (BRD2, BRD3, BRD4, and BRDT; Dey et al., 2000; LeRoy et al., 2008). At active genes, BET bromodomains recruit the positive transcription elongation factor complex (P-TEFb; Jang et al., 2005; Yang et al., 2005), and chromatin remodeling factors including the SWI/SNF complex (Shi et al., 2013) via molecular recognition of polyacetylated histone tails (Mujtaba et al.,

2007). Mechanistically, TNF-α or lipopolysaccharide (LPS) stimulation promotes direct acetylation of the p65 subunit (Lys310) of NF-κB by P300 (Chen et al., 2001), promoting a direct interaction with BRD4 through twin acetyl lysine-recognizing bromodomains (Huang et al., 2009). This interaction is needed for productive NF-κB transactivation (Huang et al., 2009), suggesting a central role for BRD4 in inflammatory transcriptional signaling.

Prior research from our group and others has identified that BET bromodomains localize genome-wide to promoter and enhancer regions (Anand et al., 2013; Chapuy et al., 2013; Lovén et al., 2013; Nicodeme et al., 2010). The majority of enhancer-bound BRD4 is found within a small number of massive enhancer regions termed super enhancers (SE). Like locus control regions or stretch enhancers, SEs concentrate chromatin-bound coactivators to genes essential for specialized cellular function (i.e., immunoglobulin production in plasma cells), and lineage specification (i.e., germinal center differentiation; Chapuy et al., 2013; Lovén et al., 2013; Parker et al., 2013; Whyte et al., 2013). Disruption of SE function by a first acetylated lysine-competitive small molecule BET bromodomain inhibitor from our group known as JQ1 (Filippakopoulos et al., 2010) suggests the mutability of these large chromatin structural elements (Chapuy et al., 2013). However, the role of SEs in the control of dynamic cell state transitions remains unknown. Recently, BET bromodomain inhibition has been shown to abrogate global, maladaptive transcriptional programs during sepsis and heart failure, implicating BRD4 in stress-induced cell state transitions (Anand et al., 2013; Nicodeme et al., 2010). These data provided a rationale for investigating the collaborative roles of NF-κB and BRD4 in regulating SEs during proinflammatory activation.

The endothelium is critical to the initiation and propagation of inflammation. Endothelial cells (ECs) prompt leukocyte recruitment, adhesion, and trafficking into tissues, thus mediating responses essential for many inflammatory disorders, including atherogenesis, in which activation of ECs is pathogenic (Gimbrone et al., 1990; Ley et al., 2007). Despite these important roles in disease, global studies of chromatin structure and function in vascular endothelium have to date not been undertaken. In this study, we investigate the role of BRD4 in determining the inflammatory activation of ECs through NF-κB and SE formation. Here, we provide evidence that EC activation by the archetypal proinflammatory stimulus TNF-α rapidly deploys NF-κB to enhancers and promoters genome-wide, where it recruits BRD4. Through the recruitment of BRD4, NF-κB establishes new SEs coincident with the surprising, rapid redistribution of BRD4 away from endothelial resting state SEs. Newly established NF-κB SEs are proximal to and drive canonical genes of the inflammatory response in ECs, including key effectors of chemotaxis, adhesion, migration, and thrombosis. BRD4 depletion from chromatin through small molecule BET bromodomain inhibition impedes NF-κB-directed SE reorganization. The failure to form proinflammatory SEs preferentially suppresses SE-dependent proinflammatory gene transcription, translating into functional suppression of key TNF-α-induced endothelial responses of leukocyte rolling, adhesion, and transmigration. In vivo, we find that BET bromodomain inhibition suppresses atherogenesis—a pathogenic process predicated on inflammatory endothelial activation. Together, these data establish BET bromodomain-containing proteins as key effectors of the integrated mammalian inflammatory response through their rapid, dynamic, global reorganization of SEs during NF-κB activation and suggest SE targeting during inflammatory cell state transitions as a therapeutic approach.

RESULTS

p65 and BRD4 Establish Super Enhancers during Proinflammatory Stimulation

To explore the role of NF-κB, BRD4, and SEs in the acute inflammatory activation of ECs, we activated NF-κB in primary human umbilical vein ECs with TNF-α, a canonical proinflammatory stimulus, for one hour. As expected, TNF-α resulted in NF-κB nuclear translocation (Figures 1A and 1B), a rapid change in EC state characterized by increased monocyte adhesion (Figure 1C), and induction of adhesion molecule gene expression including E-selectin (*SELE*) and vascular cell adhesion molecule (*VCAM1*; Figure 1D; Ley et al., 2007). The recognized capacity of BRD4 to bind acetylated NF-κB (Huang et al., 2009), suggests a coactivator role for the BET family in the robust p65-mediated EC inflammatory response observed. We therefore used chromatin immunoprecipitation coupled with high-throughput genome sequencing (ChIP-seq) to define p65 and BRD4 genomic occupancy in ECs before and following acute proinflammatory activation.

In TNF-α-stimulated ECs, p65 enrichment was evident at promoters (17.5%), intragenic (45.8%), and intergenic regulatory sequences (36.7%; Figures 1E and 1F). Striking colocalization of BRD4 and p65 was observed by global enrichment alignment and binding site motif analysis (Figure 1F; Figure S1A available online). TNF-α treatment prompts dynamic colocalization of p65 and BRD4 to enhancer and promoter regions marked by H3K27ac, which are significantly enriched for p65 consensus sequences (Figure S1A; Matys et al., 2006). At the exemplary *VCAM1* locus, TNF-α stimulation of resting ECs for one hour increased p65 occupancy at both promoters and upstream enhancer elements marked by acetylated chromatin (H3K27ac; Figure 1G). Coincident with these events, we identified recruitment of exceptionally high levels of BRD4 at discrete hyperacetylated enhancer elements (Figures 1F and 1G; Figure S1B), consistent with the formation of de novo SEs (SEs). Focal BRD4 colocalization with p65 was observed at each discrete peak, with complete concordance. Comparable evidence is provided at the *SELE* locus, where TNF-α stimulation recruits p65 and high levels of BRD4 to a gene regulatory region completely devoid of p65 and BRD4, augmenting regional hyperacetylation (Figure S1C). The dramatic remodeling of these loci in one hour in TNF-α stimulated ECs corroborates the robust transcriptional activation of these canonical EC inflammatory gene products (Figure 1D). Notably, typical enhancers are found at most other EC genes as exemplified by endothelial tyrosine kinase (*TEK*) and serpin peptidase inhibitor clade H1 (*SERPINH1*), where the levels of p65 and BRD4 are an order of magnitude lower compared to the *VCAM1* or *SELE* SE; and TNF-α does not induce mRNA expression (Figure 1H; Figures S1D and S1E).

To assess the genome-wide distribution of SEs during the EC inflammatory cell state transition, we characterized and compared the enhancer landscape in resting and TNF-α-activated

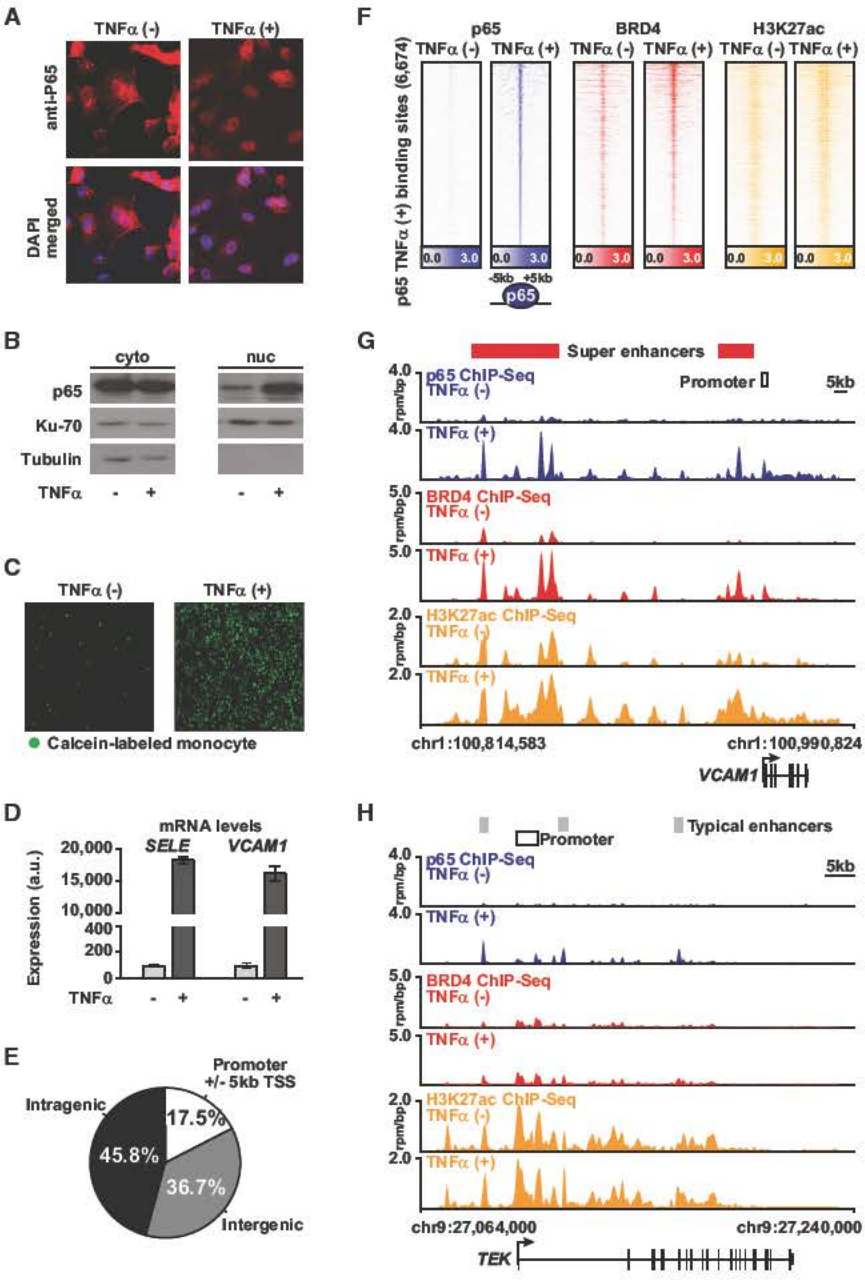

Figure 1. p65 and BRD4 Genome Binding during Proinflammatory Activation in ECs

(A) Images of ECs ± TNF α stained for p65 (red) or DAPI (blue) (25 ng/ml, 1 hr).

(B) Western blot for p65, Ku 70, and tubulin in cytosolic (left) and nuclear (right) protein fraction lysates in ECs ± TNF α.

(C) Images showing adhesion of calcein labeled THP 1 monocytes to ECs ± TNF α (25 ng/ml, 3 hr).

(D) Bar plots showing cell count normalized expression levels of *SELE* and *VCAM1* in ECs ± TNF α (25 ng/ml, 3 hr). Error bars represent SEM.

(E) Pie chart of p65 binding site distribution in EC genome in TNF α(+).

(F) Heatmap of p65 (blue), BRD4 (red), and H3K27ac (yellow) levels in resting ECs and after TNF α (25 ng/ml, 1 hr). Each row shows ± 5kb centered on p65 peak. Rows are ordered by max p65 in each region. ChIP seq signal (rpm/bp) is depicted by color scaled intensities.

(G and H) Gene tracks of ChIP seq signal for p65, BRD4, and H3K27ac at the *VCAM1* and *TEK* gene loci in untreated (top) or TNF α(+) (bottom) ECs. The y axis shows ChIP seq signal (rpm/bp). The x axis depicts genomic position with TNF α gained typical enhancers (TE, gray) and SEs (SE, red) and promoter regions (white) marked.

See also Figure S1.

ECs using BRD4 ChIP-seq data sets. When ranked by increasing BRD4 enrichment, 347 and 271 SEs were identified in resting and TNF-α-activated ECs, respectively. These SEs comprised ~7% of the total number of discrete EC enhancer loci (Figure 2A; Figure S2A), but represented more than one-fourth of the total amount of enhancer size and more than one-third of enhancer-bound BRD4 (Figures 2A and 2B). Compared to typical enhancers, SE loci are significantly larger in DNA length, total BRD4 signal, and signal density and share less overlap between resting and TNF-α-activated ECs (Figure 2C; Figures S2A and S2B). Following TNF-α stimulation, the absolute change in BRD4 total signal and density at SEs was greater compared to typical enhancers (Figure 2D; Figure S2C). We observed higher p65 total binding signal and density at SE loci when compared to either typical enhancer regions or active gene transcriptional start sites (Figure 2E; Figure S2D). As exemplified by the *VCAM1* SE locus and also observed globally, ECs feature dense clustering of multiple regulatory transcription factor binding sites known to be involved in EC proinflammatory responses including p65, p50, ETS1/2, and transcription factor 3/4 (TCF3/4; Figure 2F; Figure S2E; De Val et al., 2008; Masckauchán et al., 2005). In contrast, typical enhancer sites typified by the TEK locus possess a much lower density of these motifs (Figure 2G; Figure S2E).

To dissect the temporal relationship between p65 and BRD4 localization to enhancers, we next performed time-ranging chromatin binding studies. ChIP for p65 and BRD4 followed by real-time PCR centered on the most prominent NF-κB binding site in the 5′ *VCAM1* and *CCL2* SEs revealed enrichment of p65 five minutes after TNF-α stimulation, with peak occupancy detected by 30 min (Figure 2H; Figure S2F). BRD4 recruitment followed the identical temporal pattern of recruitment at these sites. Inhibition of NF-κB phosphorylation and function by IκB kinase inhibition (BAY 11-7082, "BAY") (Pierce et al., 1997) completely abrogated TNFα-induced p65 and BRD4 accumulation at both NF-κB sites at all time points, while also suppressing *VCAM1* gene induction (Figure S2G). As expected,

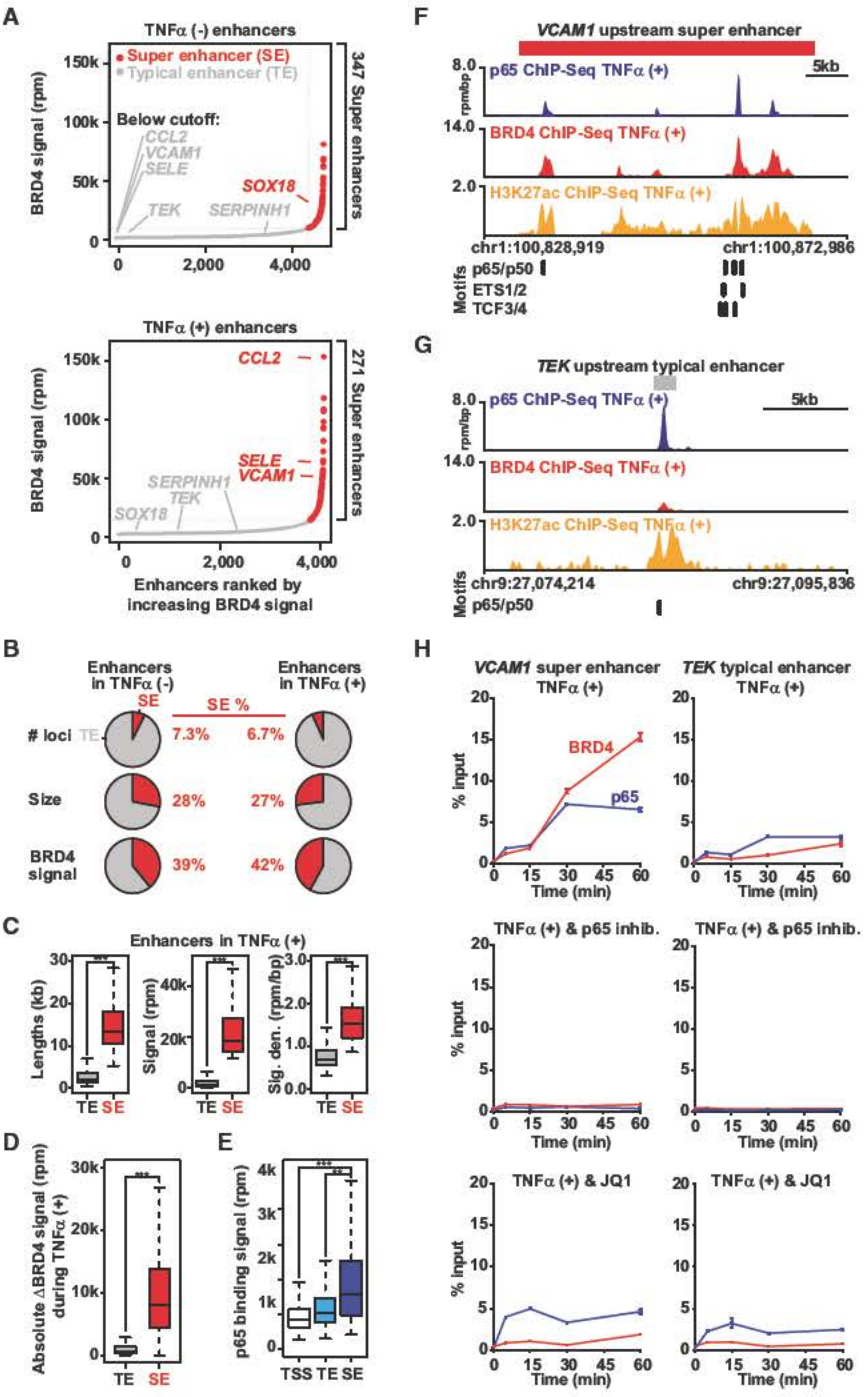

Figure 2. p65 and BRD4 Establish Super Enhancers during Proinflammatory Stimulation

(A) Ranked plots of enhancers defined in resting (top) or TNF α(+) (bottom) ECs ranked by increasing BRD4 signal (units: rpm). Enhancers are defined as regions of BRD4 ChIP seq binding not contained in promoters. The cutoff discriminating TEs from SEs is shown as a dashed line. Genes associated with enhancers that are considered typical or super are colored gray and red, respectively.

(B) Pie charts displaying characteristics of TE and SE regions including number of loci, size, and BRD4 signal.

(C) Boxplots of median enhancer length (kb), signal (rpm), and density (rpm/bp) in TNF α gained en hancers. Significance of the difference between distributions determined using a two tailed t test. $^{***}p < 1 \times 10^{-10}$.

(D) Boxplot of absolute change in BRD4 signal in response to TNF α measured at all enhancers in TNF α( ) and TNF α(+). Significance of the differ ence between distributions determined using a two tailed t test. $^{***}p < 1 \times 10^{-10}$.

(E) Boxplot of p65 binding signal (rpm) at all active gene promoters (TSS), TEs, and SEs in TNF α treated ECs. Significance of the difference be tween distributions determined using a two tailed t test. $^{**}p < 1 \times 10^{-5}$, $^{***}p < 1 \times 10^{-10}$.

(F and G) Schematic of transcription factor motif binding sites at the *VCAM1* SE (red box; F) or *TEK* TE (gray box; G) loci in ECs treated with TNFα.

(H) Line plots of kinetic ChIP PCR showing enrichment (percent input normalized to time 0) of p65 and BRD4 at an NF κB binding site in the *VCAM1* (left) SE and *TEK* TE (right) in ECs treated with TNF α (25 ng/ml; 0, 5, 15, 30, 60 min). The effect of cotreatment with vehicle (top), BAY (NF κB inhibitor, middle), and JQ1 (bottom) is shown. See also Figure S2.

NF-κB Provokes Rapid Global Redistribution of BRD4 at Super Enhancers

We next explored the dynamics and function of SEs in inflammation in both ECs and macrophages. One hour following TNF-α stimulation, we observed the formation of pronounced, prototypical SEs at canonical inflammatory genes, such as the *CCL2* chemokine (Figure 3A). There, a density of upstream and intragenic enhancer elements was identified, characterized by regional hyperacetylation (H3K27ac) and peaks of BRD4 enrichment coinciding with focal p65 binding sites (Figure 3A). Functionally, rapid SE formation was associated with recruitment of RNA Pol II (Figure 3A) and marked transcriptional activation (Figure S3A). These data provide a demonstration that the canonical proinflammatory stimulus TNF-α rapidly induces de novo formation of SEs established by p65 at proinflammatory

cotreatment of ECs with JQ1 reduced TNF-α-induced enrichment of BRD4 at these NF-κB binding sites. However, in contrast to BAY, JQ1 had no effect on immediate early p65 recruitment (Figure 2H; Figure S2F). Compared to SEs, typical enhancers featured less TNF-α-induced recruitment of both NF-κB and BRD4 (Figure 2H; Figure S2F). Collectively, these results establish that p65 is required for TNF-α-induced recruitment of BRD4 to SE regions in ECs.

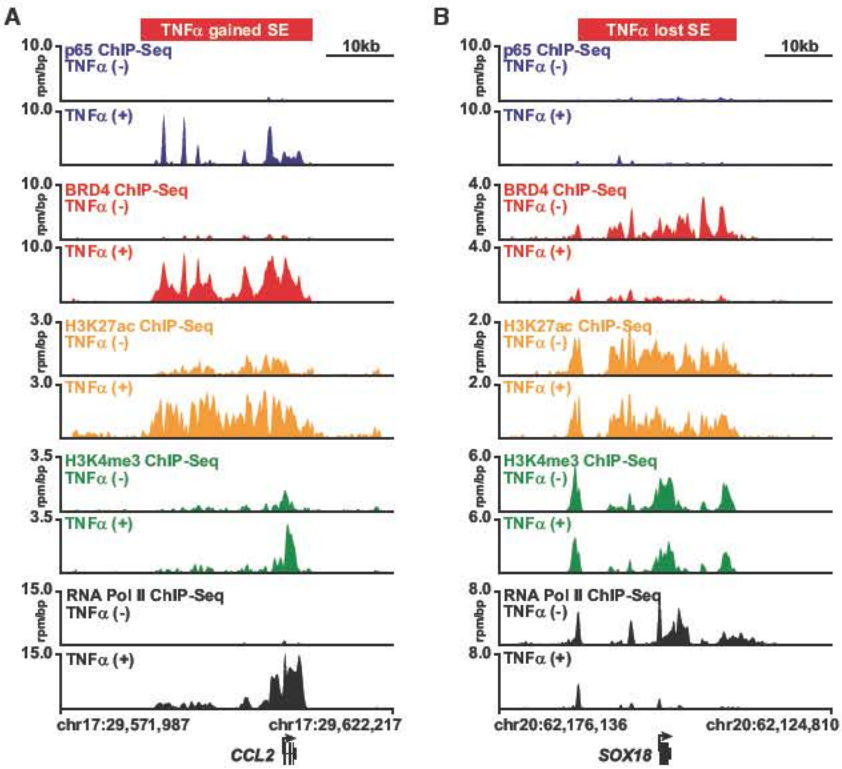

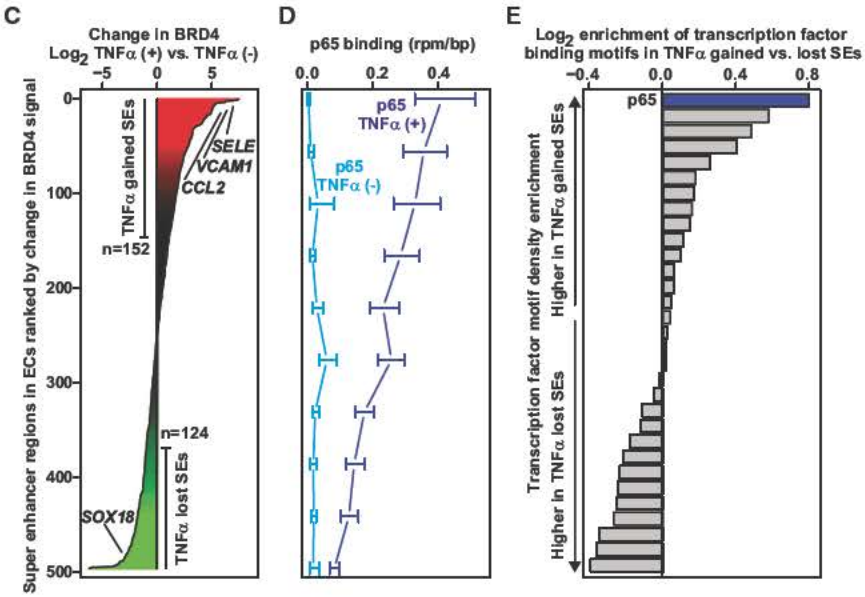

Figure 3. NF κB Provokes Rapid, Global Redistribution of BRD4

(A and B) Gene tracks of ChIP seq signal (rpm/bp) for p65, BRD4, H3K27ac, H3K4me3, and RNA Pol II at the *CCL2* gene (A) or *SOX18* (B) locus in TNFα( ) (top) and TNFα(+) (bottom) ECs.

(C) All genomic regions containing a SE in TNFα( ) and TNF α(+) ECs are shown ranked by $\log_2$ change in BRD4 signal (treated versus untreated). The x axis shows the $\log_2$ fold change in BRD4 signal. Change in BRD4 levels at SEs is colored by intensity of change (green to red).

(D) Line plot showing the median levels of p65 binding (rpm/bp) at SEs in either TNF α( ) light blue or TNF α(+) dark blue conditions. SEs were ranked by change in BRD4 and binned (50/bin). The median p65 level was calculated in each bin. Error bars represent 95% confidence intervals (CI) of the median determined by empirical resampling.

(E) Horizontal bar plot showing the ratio of transcription factor motif density between TNFα gained and TNF α lost SEs. Twenty one transcription factors are displayed whose motifs occur more frequently than expected based on dinucleotide background model. The transcription factor motifs are ranked by $\log_2$ fold change in density between TNF α gained versus TNF α lost SEs. See also Figure S3.

target genes, also including *VCAM1* and *SELE* (Figures 1G and S1C).

Unexpectedly, the enrichment of BRD4 at inflammatory EC SEs was associated with the rapid, reciprocal depletion of BRD4 at resting EC SEs. ECs grown in culture feature 347 canonical SEs, including SEs associated with genes critical for noninflammatory EC function, such as the *SOX18* transcription factor implicated in vasculogenesis (Matsui et al., 2006). In such resting ECs, regional enrichment for H3K27ac is observed at the *SOX18* locus, accompanied by characteristic BRD4 occupancy and evident enrichment for RNA Pol II throughout the gene body. In the inflammatory EC state, TNF-α fails to drive NF-κB to the *SOX18* locus, RNA Pol II enrichment is markedly diminished and transcription is muted (Figure 3B; Figure S3A). Only 1 hour following TNF-α stimulation, BRD4 is effectively depleted, despite persistent hyperacetylation (H3K27ac) of the *SOX18* SE (Figure 3B).

To explore the relevance of changes in SEs provoked by proinflammatory activation across the genome, a systematic analysis of dynamic alterations in SE formation was undertaken. BRD4 enrichment was selected here as a preferred marker for SE identity owing to a concern that H3K27ac, or other more biochemically stable enhancer modifications (such as H3K4me1/2), may lag behind BRD4 redistribution globally in a dynamic cell state change, as above at the *SOX18* locus. We identified a dramatic redistribution of genomic BRD4 occupancy following TNF-α stimulation (Figure 3C). Differential enhancer analysis revealed an evident global balance in chromatin-associated BRD4, but importantly TNF-α stimulation resulted in the reclassification of multiple enhancers from typical enhancer to SE (N = 152) and from SE to typical enhancer (N = 124; Figure 3C). Gains in BRD4 occupancy were strongly and directly associated with site-specific

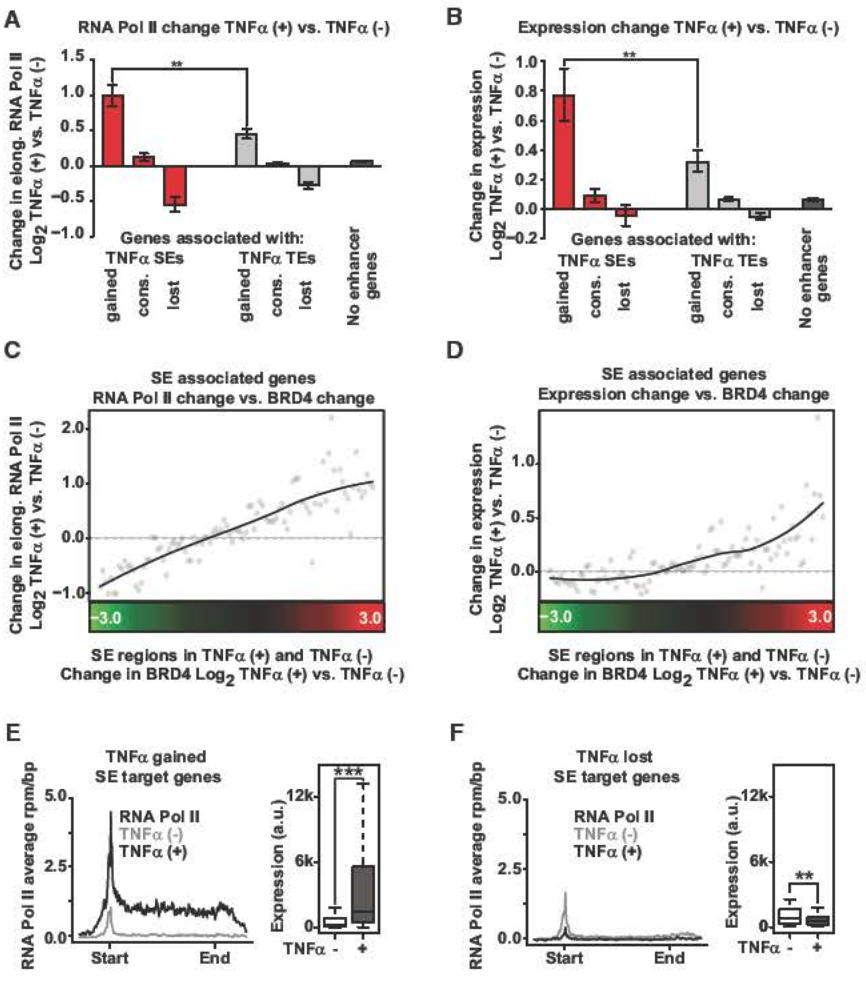

Figure 4. NF κB Formed Super Enhancers Drive Proinflammatory Transcription

(A and B) Bar plot of average change in elongating RNA Pol II (A) or mRNA expression (B) at genes associated with TNF α gained, TNF α lost, or TNF α conserved SEs (red), TEs (gray), and no enhancers (black). Error bars represent 95% CI of the mean determined by empirical resampling. Significance of the difference between distributions determined using a two tailed t test. $^{**}p < 1 \times 10^{-5}$, $^{***}p < 1 \times 10^{-10}$.

(C and D) Change in elongating RNA Pol II in the gene body region of genes (C, y axis) or change in mRNA levels (D, y axis) are plotted ranked by change in BRD4 at proximal SEs (x axis). Dots represent median change sampled across 50 evenly distributed bins with a loess fitted line overlaid. Change in BRD4 levels at proximal SEs are colored by intensity of change (green to red).

(E and F) Metagene representations of average RNA Pol II ChIP seq signal (gray, untreated; black, TNF α treated) in units of rpm/bp at a meta composite of target genes of SEs that are gained (E) or lost (F) in response to TNF α treatment. Boxplots of cell count normalized expression levels are shown to the right of each metagene in arbitrary units for genes with associated SEs (gray, untreated; black, TNF α treated) that are gained (E) or lost (F) in response to TNF α treatment. Significance of the difference between distributions determined using a two tailed t test. $^{**}p < 1 \times 10^{-5}$, $^{***}p < 1 \times 10^{-10}$.

(G and H) Table showing the functional categories of selected genes that are targets of SEs gained (G) or lost (H) in response to TNF α treatment.

See also Figure S4.

G

TNFα gained SE target genes (62 total)	
Cytokine signalling	*LTB; TNFAIP3; TNFRSF11B; IRAK2; CSF2RB*
Chemotaxis	*CCL2; CSF2; CXCL1,2,3,8; CXCR7; ICOSLG*
Adhesion and migration	*EFNA1; ICAM1,4,5; ITGAV; NUAK2; SELE; TRIO; VCAM1*
Thrombosis	*COX-2, SERPINE1 FS3*

H

TNFα lost SE target genes (55 total)	
Angiogenesis	*SOX18; EGFL7*
Anti-thrombotic	*THBD*
Barrier function	*PALMD; LYVE1 ESAM*

increases in p65 binding occupancy genome-wide (Figure 3D). As expected, TNF-α-gained SEs are characterized by coordinate increases in BRD4 and H3K27ac enrichment at regions of increased p65 occupancy, which correlates directly with SE formation (Figures 3C and S3B). Consistent with the *SOX18* regulatory region, lost SEs are defined by a significant reduction of BRD4 occupancy following TNF-α stimulation that is disproportionate to minimal changes in p65 and modest reductions in H3K27ac (Figures 3D and S3C). Finally, the p65 motif was found at much higher density in TNF-α-gained versus TNF-α-lost SEs regions in ECs, further suggesting p65 direct binding to clustered sites in TNF-α-gained SEs as a causal event in BRD4 SE redistribution during inflammatory activation (Figure 3E), akin to comparable "stretch enhancers" as described by Francis Collins and colleagues (Parker et al., 2013).

NF-κB-Formed Super Enhancers Drive Proinflammatory Transcription

To assess the consequences of SE redistribution on transcriptional output, we integrated genome-wide ChIP-seq data with cell count-normalized, array-based absolute gene expression profiling measurements obtained before and 1 hour after TNF-α stimulation. Compared to typical and conserved enhancer regions, the gain or loss of SEs provoked by TNF-α resulted in the largest changes to RNA Pol II occupancy and expression of adjacent genes (Figures 4A and 4B). This global relationship was also evident when specifically comparing the change in the levels of SE constituent BRD4 versus change in nearby gene elongating RNA Pol II levels and expression (Figures 4C and 4D). Those genes positioned near TNF-α gained SEs, which also feature BRD4 enrichment at their promoters

suggestive of promoter-enhancer communication, demonstrated marked induction of transcriptional initiation, elongation, and gene expression (Figure 4E; Figure S4A). Functional classification of TNF-α-gained SE marked genes reveals known drivers of key functional facets of EC inflammatory responses: cytokine signaling, chemotaxis, adhesion and migration, and thrombosis (Figure 4G; Figure S4F). In contrast, the reciprocal loss of BRD4 at resting EC SEs resulted in a proportionate decrease in transcription and expression of nearby genes (Figures 4A, 4B, and 4F), such as *THBD* and genes involved in angiogenesis and endothelial barrier function (Figure 4H; Figure S4G). Notably, the cohort of lost SE genes featured marked decreases in transcriptional initiation and elongation by RNA Pol II enrichment metagene analysis in advance of changes in promoter modification (H3K4me3 enrichment; Figure S4B). Genes with conserved enhancers show minimal change in expression and serve pathways that govern homeostatic function in ECs (Figures 4A and 4B; Figure S4H). Globally, this chromatin restructuring results in a strong induction of proinflammatory SE driven transcription compared to typical enhancer associated genes. The 62 TNF-α-gained, SE-associated genes comprise only ~8% of all genes with >2-fold increase in mRNA expression, but account for ~60% of the total increase in upregulated gene expression and ~20% of the increase in cellular mRNA within 3 hr of TNF-α stimulation (Figures S4C–S4E). These data provide discrete examples and global evidence of dynamic, functional remodeling of enhancer factors even preceding the structural decommissioning of abandoned enhancers.

NF-κB-Formed Super Enhancers Drive Proinflammatory Gene Expression in a BET Bromodomain-Dependent Manner

Disruption of SEs by disrupting enhancer factors, such as BRD4, has been observed to selectively influence the expression of genes associated with SEs (Lovén et al., 2013). In cancer, we have observed that competitive displacement of BET bromodomains from nuclear chromatin provokes coordinated inhibition of the MYC transcriptional program, often associated with downregulation of *MYC* itself (Chapuy et al., 2013; Delmore et al., 2011; Zuber et al., 2011). Using a chemical genetic approach, we assessed the role of BET bromodomains in the rapid transcriptional response of SE-associated, proinflammatory genes in TNF-α-stimulated ECs. Small molecule probes, such as the BET bromodomain inhibitor JQ1, are particularly appealing in the study of dynamic processes, because they offer precise temporal perturbation of the biological system (Frye, 2010; Strausberg and Schreiber, 2003). We therefore performed a dynamic, genome-wide analysis of BET bromodomain inhibition on inflammatory SE integrity, global chromatin structure, gene expression, and EC postinflammatory function.

First, we characterized the effect of JQ1 on EC chromatin structure and function immediately following TNF-α exposure. ECs were treated with JQ1 (500 nM) to displace BET bromodomains, then stimulated with TNFα for 1 hour. Chromatin from treated and untreated ECs was subjected to ChIP-seq for promoters (H3K4me3), enhancers (H3K27ac), RNA Pol II, the p65 transcription factor, and the BRD4 coactivator. At the *SELE* locus, BET inhibition had no effect on TNF-α-mediated recruitment of p65 (Figures 5A and 5B). However, JQ1 depleted BRD4 resulting in abrogated *SELE* expression assessed by decreased RNA Pol II enrichment (Figure 5A and cell surface protein levels assessed by flow cytometry (Figure S5E). Comparable observations are evident at the *CCL2* and *IRAK2* loci, where BET inhibition selectively displaces BRD4 leading to impaired transcription induction and elongation by RNA Pol II (Figures S5A and S5B).

Global analysis of TNF-α-stimulated ECs revealed preferential loss of BRD4 at TNF-α-gained SEs compared to typical enhancers, with minimal effect on TNFα-induced p65 binding or H3K27ac levels (Figure 5B). TNF-α-gained SEs possessed a diminished capacity to drive proinflammatory transcription initiation and elongation in the presence of the BRD4 inhibitor, JQ1 (Figure 5C), and these dynamic effects on RNA Pol II enrichment were independent of alterations in promoter modification by differential metagene analysis of H3K4me3 enrichment at the transcriptional start sites (Figure S5C). Functionally, preferential JQ1-induced loss of transcription at TNF-α-gained SE-associated genes culminated in more potent suppression of their proinflammatory gene expression program relative to genes driven by typical enhancers (Figure 5C; Figure S5D). Treatment of ECs with TNF-α and JQ1 suppressed the maximal mRNA induction of SE-associated genes (*FS3*, *CCL2*, *VCAM1*) at a lower concentration of JQ1 and to a greater degree compared to TE-associated genes (*LOX*, *TEK*, *NLRP1*; Figure 5D). Together, these data support a model in which BET bromodomains mediate dynamic and immediate inflammatory EC response gene transcription, by facilitating chromatin-dependent signal transduction from NF-κB to RNA Pol II.

To determine whether JQ1 transcriptional effects resulted from specific engagement of BETs at nuclear chromatin, we spatially localized the JQ1 molecule genome-wide using a new biotechnology called Chem-seq (Anders et al., 2014). This technique maps the interactions of small molecules with chromatin in the human genome, in this instance by using a retrievable synthetic derivative of JQ1 (biotin-JQ1). Notably, despite high levels of acetylated HK27ac at enhancers, we detected no biotin-JQ1 occupancy with Chem-seq at *SELE* and other SEs (Figure 5E; Figures S5F and S5G) in resting ECs. Rather, at these loci, biotin-JQ1 binding to chromatin perfectly colocalized with BRD4 spatially and temporally following TNF-α–stimulation. Genome-wide analysis demonstrated a dose-dependent relationship between biotin-JQ1 localization and the decrease in genomic BRD4 occupancy, not H3K27ac, in ECs treated with TNF-α + JQ1 compared to TNF-α alone (Figures 5F and 5G). Taken together, these data reveal that JQ1 directly targets BRD4 during proinflammatory activation in ECs. Preferential loss of BRD4 at inflammatory SEs by BET bromodomain inhibition serves mechanistically to underscore the observed selective effects on transcription.

To assess the generalizability of these observations, we tested whether the BRD4-dependent formation of proinflammatory SEs is relevant for other immune effector cells. We integrated robust, publically available acetyl-histone data (H4K12ac) with RNA Pol II ChIP-seq data in LPS-stimulated macrophages (Nicodeme et al., 2010), to map SEs and explore the effect of BET inhibition on enhancer-mediated transcriptional signaling. H4K12ac is a

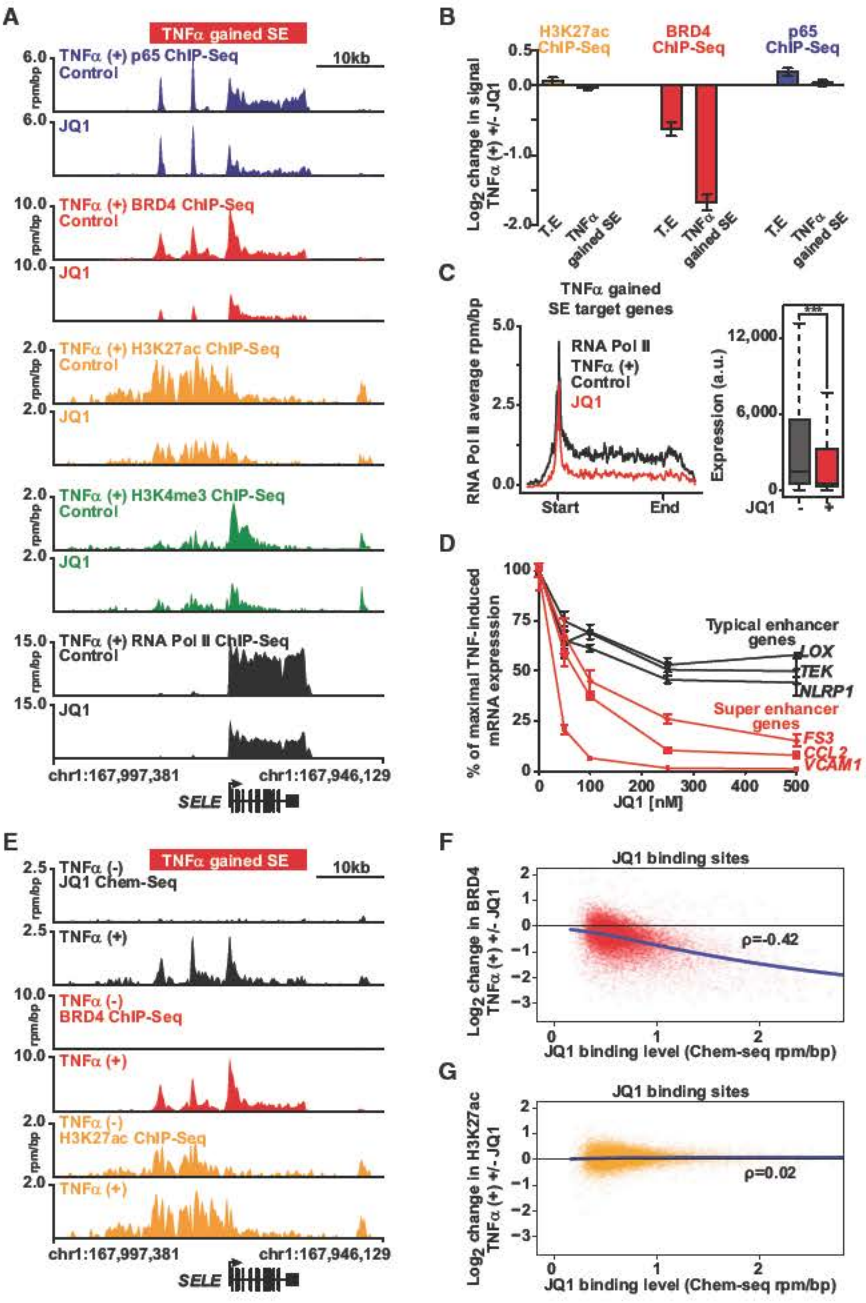

Figure 5. NF κB Formed Super Enhancers Drive Proinflammatory Gene Expression in a BET Bromodomain Dependent Manner

(A) Gene tracks of ChIP seq signal (rpm/bp) for p65, BRD4, H3K27ac, H3K4me3, and RNA Pol II at the *SELE* locus in TNF α treated ECs cotreated with vehicle (top) or JQ1 (bottom).

(B) The mean $\log_2$ fold change in H3K27ac (yellow), BRD4 (red), and p65 (blue) ChIP seq signal in TNF α treated cells ± JQ1 at either TEs or SEs gained in response to TNF α treatment. Error bars represent 95% CI of the mean determined by empirical re sampling.

(C) Metagene representations of average RNA Pol II ChIP seq signal (black, TNF α treated; red, JQ1 treated) in units of rpm/bp at a meta composite of target genes of SEs gained in response to TNFα treatment. Boxplots (right) show cell count normalized expression levels in TNF α (25 ng/ml, 3 hr) treated ECs ± JQ1. Significance of the dif ference between distributions determined using a two tailed t test. ***$p < 1 \times 10^{-10}$.

(D) Line plots of mRNA levels (qRT PCR) of three representative genes associated with TEs (*LOX*, *TEK*, *NLRP1* in black) and SEs (*FS3*, *CCL2*, *VCAM1* in red) in response to TNF α and JQ1 (50, 100, 250, 500 nM). The mRNA levels from TNF α + VEH (10 ng/ml, 3 hr) treated ECs were set to 100%. Results displayed as the percent reduction from maximum. Error bars represent SEM. Representative results from two independent ex periments are shown.

(E) Gene tracks from Chem seq (JQ1) and ChIP seq (BRD4, H3K27ac) data sets of the *SELE* SE locus (rpm/bp) for JQ1, BRD4, and H3K27ac from TNF α( ) or TNF α(+) stimulated ECs.

(F and G) Scatter plot of JQ1 genome wide binding levels on the x axis compared to the $\log_2$ change in BRD4 (F) or H3K27ac (G) ChIP seq signal on the y axis. The change in BRD4 and H3K27ac signal was determined comparing TNF α + JQ1 versus TNF α.

See also Figures S5 and S6.

histone mark defining active enhancers that can be used to identify SEs in the absence of specific enhancer coactivator data (Hnisz et al., 2013; Whyte et al., 2013).

Large gains of histone acetylation were identified in macrophages following LPS stimulation at the *Irak2* proinflammatory gene locus (Figure S6A). LPS treatment provoked an immediate increase in promoter and intergenic acetylation, accompanied by an increase in RNA Pol II enrichment throughout the gene body. Globally, SE analysis identified 122 gained SEs following LPS treatment near proinflammatory genes involved in cytokine signaling, cell adhesion, and chemotaxis (Figures S6B and S6C). Unlike inflammatory ECs, the target genes induced and associated with proinflammatory SEs in macrophages are largely distinct from those found in ECs (Figure S6D). Transcription at SE-associated genes was more strongly induced by LPS compared to genes controlled by typical enhancers, as revealed by composite analysis of RNA Pol II enrichment and elongation (Figures S6E and S6F). As in activated ECs, BET bromodomain inhibition in macrophages preferentially suppressed transcription of genes driven by proinflammatory SEs as compared to genes controlled by typical enhancers (Figures S6G and S6H). The *Irak2* locus provides an exemplary illustration of the effect of BET bromodomain inhibition using the structurally analogous I-BET inhibitor (Nicodeme et al., 2010), on depletion of RNA Pol II enrichment (Figure S6A). Collectively, these data from ECs and macrophages demonstrate that proinflammatory SEs drive proinflammatory gene activation in a cell context specific manner.

BET Bromodomain Inhibition Suppresses Leukocyte Rolling, Adhesion, and Transmigration in Endothelium

In response to proinflammatory stimuli, endothelial-leukocyte interactions follow a sequential cascade involving leukocyte chemoattraction, their slow rolling, and subsequent firm adhesion to ECs, culminating in leukocyte endothelial transmigration into tissue (Ley et al., 2007). To explore a phenotypic effect of SE disruption by BET bromodomain inhibition, we tested the functional effects of JQ1 on leukocyte rolling across TNF-α-activated endothelium in vivo. C57Bl/6 mice were pretreated with JQ1 (50 mg/kg) 12 hours before TNF-α injection. As depicted with intravital microscopy of leukocyte rolling in the cremaster postcapillary venule, BET bromodomain inhibition significantly reduced the leukocyte rolling flux (15.8 versus 7.5, $p < 0.01$; Figure 6A) and the number of leukocyte rollers/minute (42.8 versus 25.14, $p < 0.05$; data not shown), without changing systemic white blood cell count or shear stress (Figure S7A). BET bromodomain inhibition also shifted the distribution of leukocyte velocity and increased mean velocity (2.89 μm/s versus 3.91 μm/s, $p < 0.01$), consistent with an effect on E-selectin-mediated slow rolling (Figures 6B and 6C).

Next, we examined firm adhesion of the human monocytic cell line (THP1) to activated ECs in vitro. TNF-α-stimulated ECs had significantly increased numbers of attached THP1 cells (Figure 6D). JQ1 pretreatment of ECs suppressed THP1 adhesion to TNF-α-activated ECs by 70% (Figures 6D and 6E). Similarly, siRNA inhibition of BRD4 expression in ECs recapitulated JQ1's effects on THP1 adhesion to ECs (Figures 6F and 6G). Lastly, we tested BET bromodomain inhibitor effects on leukocyte transmigration in a parallel-plate flow chamber. TNF-α stimulation of ECs resulted in transmigration of 67% of human neutrophils (Figure 6H). Pretreatment of ECs with JQ1 prior to TNF-α stimulation reduced neutrophil transmigration in a concentration-dependent manner (Figure 6H). In kinetic studies of transcription response of TNF-α-stimulated ECs, JQ1 demonstrated prolonged inhibitory effects on expression of SE-associated genes (*SELE*, *VCAM1*, *CXCL8*, *CCL2*) over 48 hr (Figures 6I–6L). These data establish BET bromodomain inhibition as a functional suppressor of the phenotypic features of EC proinflammatory activation.

BET Bromodomain Inhibition Suppresses Atherogenesis in Hypercholesterolemic Mice

Proinflammatory activation of ECs is a seminal, early event in atherogenesis, a process driven by vascular inflammation that also involves monocytes/macrophages and precedes atherosclerosis (Cybulsky et al., 2001). The transcriptional and functional effects of BET bromodomain inhibition in ECs prompted us to examine their role in atherogenesis using the well-established low-density lipoprotein (LDL) receptor-deficient ($Ldlr^{-/-}$) mouse model. Vehicle-treated mice fed a cholesterol-enriched diet (10 weeks) developed atherosclerosis, as measured by oil red O staining (Figure 7A). Once-daily JQ1 treatment (50 mg/kg) reduced aortic plaque area by 40% (Figure 7A). Notably, there was no difference in LDL and high-density lipoprotein cholesterol between the vehicle and JQ1 treatment groups (168 versus 164 mg/dL and 56 versus 59 mg/dL, respectively; total cholesterol 911 versus 1,349 mg/dl; see also Table S6.). Early atherosclerotic lesions are comprised of macrophages (98%–99%) with lesser amounts of T lymphocytes (1%–2%). Mac-3 staining demonstrated that JQ1 treatment significantly lowered total macrophage staining area, CD4-positive T lymphocytes, and levels of VCAM1 protein (Figures 7B–7D). Oil red O staining of en face thoracoabdominal aortas revealed decreased atherosclerotic plaque beyond the aortic root (Figures 7E and 7F). Soluble VCAM1 and ICAM1 levels were also significantly reduced in JQ1-treated animals compared to vehicle (Figures S7B and S7C), suggesting an effect of BET bromodomain inhibition on systemic proinflammatory activation in vivo. We next tested whether BET bromodomain inhibition mitigated the activation of proadhesion pathways in aortic endothelium, which occurs during the first 10 weeks of exposure to an atherogenic diet. In ex vivo aortic adhesion assays, the aortas harvested from animals (6 weeks on diet) treated with JQ1 supported less adhesion of fluorescently labeled monocytes (Figures S7D and S7E). These data demonstrate BET inhibition significantly decreased atherogenesis and accumulation of inflammatory cells in a well-characterized murine model of atherosclerosis.

DISCUSSION

The inflammatory response underlies numerous chronic diseases. NF-κB is a master regulatory transcription factor in several dominant inflammatory signaling cascades, which cooperate with chromatin-associated regulatory complexes to direct inflammatory transcription (Natoli, 2009). Enhancer-bound NF-κB arises following nuclear translocation in a manner influenced by pioneer transcription factors (Kaikkonen et al., 2013; Natoli, 2009; Ostuni et al., 2013) and a preestablished topology that places distal enhancer regions and target genes in spatial proximity (Jin et al., 2013). Here, we explore the role of chromatin in terminal signal transduction from NF-κB to RNA polymerase, specifically at massive regulatory regions.

Super or stretch enhancers represent less than 5% of the enhancers in a cell, yet they use almost half of all enhancer coactivator proteins (Lovén et al., 2013; Parker et al., 2013; Whyte et al., 2013) and are highly transcribed, producing large amounts of enhancer RNA that may itself facilitate target gene activation (Hnisz et al., 2013; Kaikkonen et al., 2013). The SE landscape is remarkably cell-type specific, driving expression of the genes that define and maintain cell identity in different tissues and cell lineages. The present study demonstrates that NF-κB engages most endothelial enhancers following proinflammatory activation, yet significant BRD4 recruitment to form de novo SEs is restricted to a subset of these enhancer regions. NF-κB-directed SE formation causes global reorganization of the BRD4 SE landscape and induces the transcription of many canonical proinflammatory endothelial genes. Whereas previous studies have studied the importance of SEs in the maintenance of cell identity (Whyte et al., 2013), here we describe de novo SE formation as a mechanism by which stimulus-coupled master regulatory transcription factors such as NF-κB can coordinate a rapid transcriptional response that drives a dynamic change in cell state.

This study of kinetic transcriptional response during the inflammatory cell state transition in ECs unexpectedly identified a rapid loss of SEs upon cytokine stimulation. As orchestrated

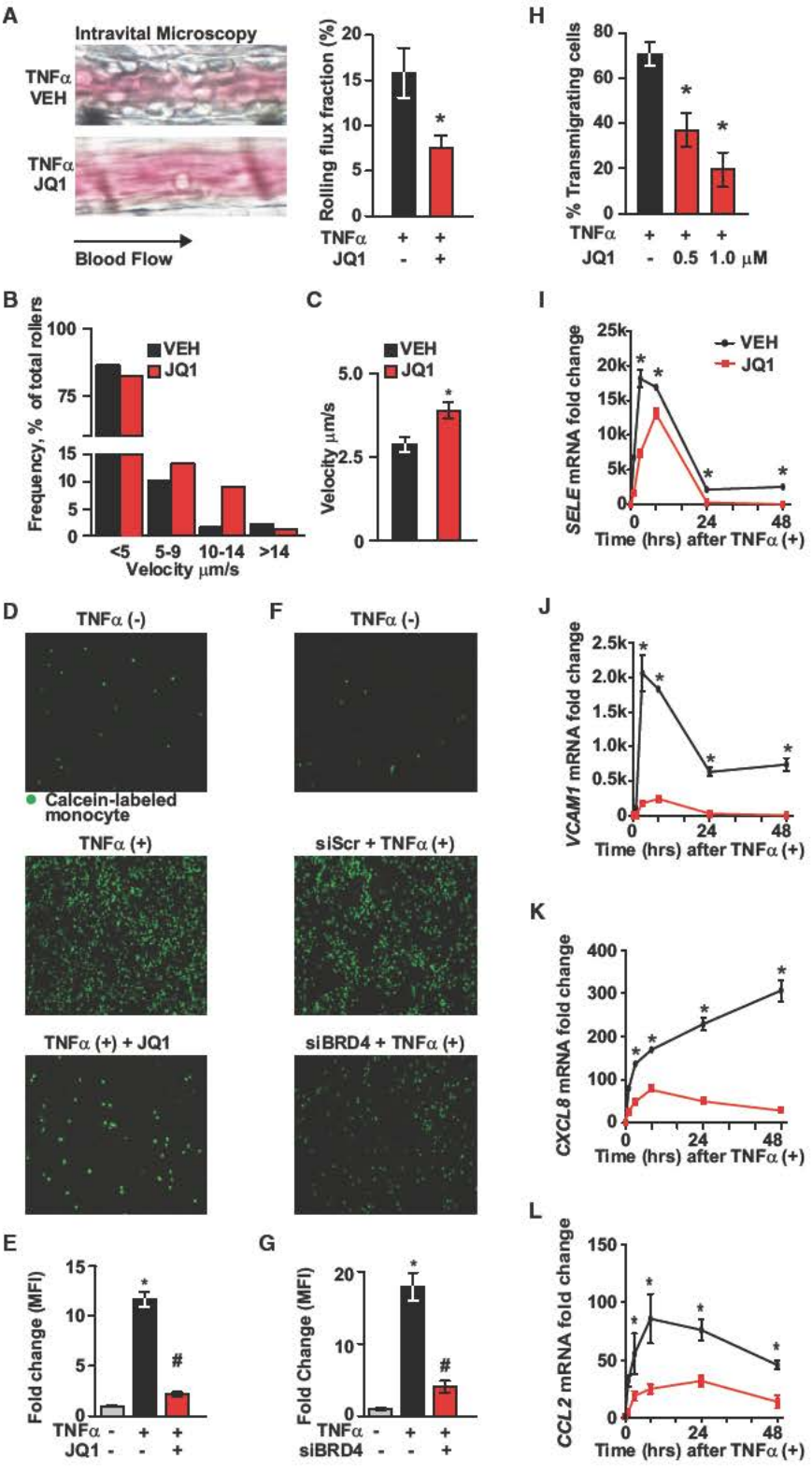

Figure 6. Phenotypic Consequences of BET Bromodomain Inhibition in Endothelium

(A) Intravital microscopy image (left) and bar plot quantification (right) of leukocyte flux fraction in the cremaster postcapillary venule after TNF α (2 hr, n = 7/group) in VEH or JQ1 treated samples. Error bars represent SEM. The statistical significance of the difference between JQ1 and VEH treated samples was determined using a two tailed t test. *p < 0.05.

(B) Velocity distribution of leukocytes measured in (A).

(C) Bar plot showing mean leukocyte velocity in cremaster postcapillary venule in TNF α(+) animals ± BET bromodomain inhibition. Error bars represent SEM.

(D and F) Representative fluorescence microscopy images showing adhesion of calcein labeled THP1 cells to (D) ECs pretreated with JQ1 then activated with TNFα (4 hr) as well as (F) TNF α treated ECs after siRNA knockdown of BRD4.

(E and G) Bar plots showing quantification of fluorescence from (D) and (F).

(H) Bar plots showing quantification of trans migrating neutrophils on TNF α activated EC monolayers. Results pooled from three indepen dent experiments. Data represent mean ± SEM. The statistical significance of the difference be tween JQ1 and VEH treated samples was deter mined using a two tailed t test. *p < 0.05.

(I L) Line plots of mRNA levels (qRT PCR) for (I) *SELE*, (J) *VCAM1*, (K) *CXCL8*, and (L) *CCL2* measured after stimulation of ECs with TNF α (12.5 ng/ml; 1, 3, 8, 24, 48 hr) ± JQ1 (500 nM). The statistical significance of the difference be tween samples was determined using a two tailed t test. *p < 0.05 in TNF α(+) versus TNF α( ); #p < 0.05 in JQ1 versus VEH. Data represent mean ± SEM of fold change versus 0 hr. See also Figure S7.

by the master regulatory inflammatory transcription factor NF-κB, SE formation comes at the immediate expense of SEs associated with active transcription of genes in unstimulated ECs, including targets involved in cell specification and noninflammatory cell states. Many of these lost SE associated genes, such as *SOX18*, will be down-regulated. Curiously, we find persistent marks of open, active euchromatin at the *SOX18* locus (H3K27ac), yet BRD4 depletion is associated with loss of RNA pol II transcription. In studies of dynamic cell state transitions, as here, we find that experimental measurements of canonical enhancer marks (i.e., H3K27ac, H3K4me1/2) are inferior to assessments of enhancer coactivators (i.e., BRD4) for characterizing rapid changes in enhancer structure and function. As such, BRD4 may be viewed and used as a rheostat for enhancer output, converting typical enhancers into SEs, thereby driving rapid and robust induction of inflammatory transcription.

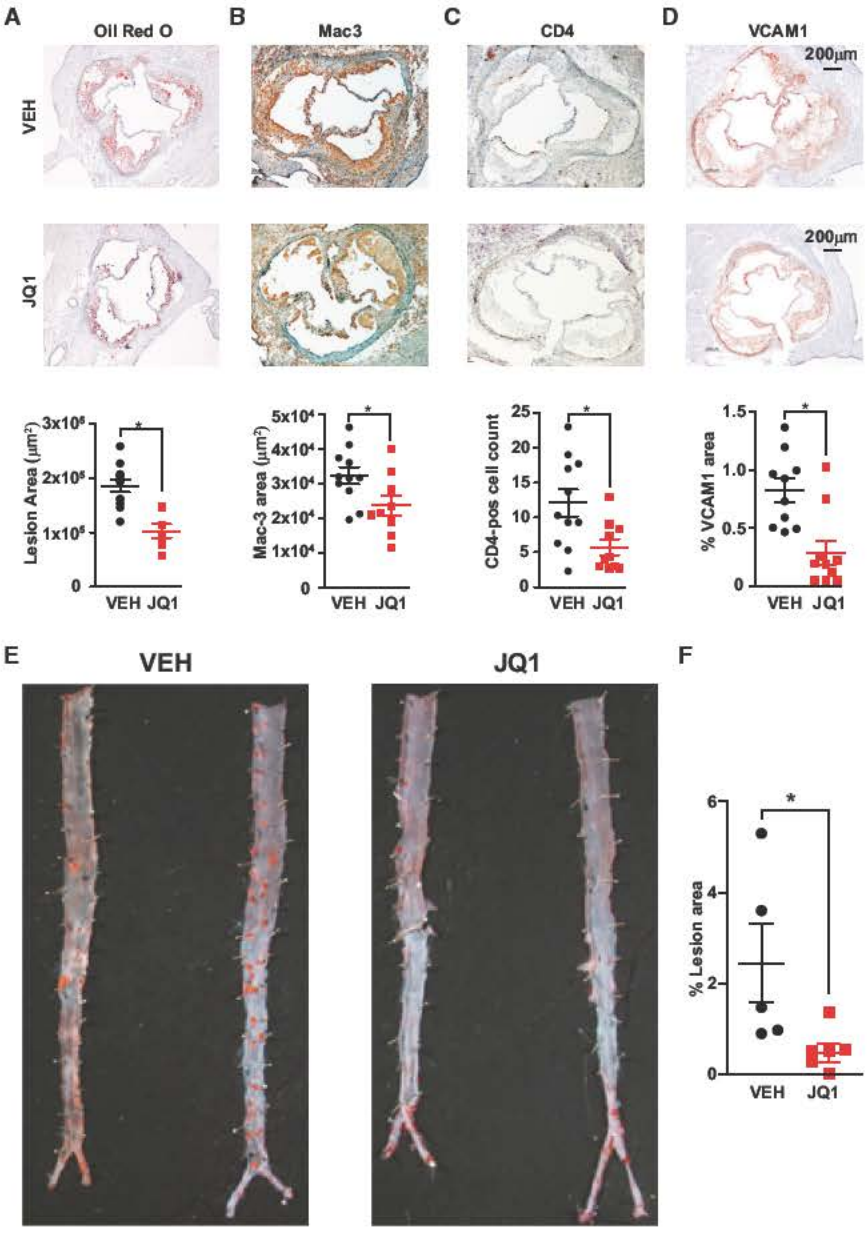

Figure 7. BET Bromodomain Inhibition Suppresses Atherogenesis in Ldlr$^{-/-}$ Mice

(A D) Photomicrographs of aortic root sections from Ldlr $^{-/-}$ animals treated with VEH or JQ1 stained for (A) oil red O, (B) Mac 3, (C) CD 4, or (D) VCAM1. Quantification of staining is shown below. Results represent mean ± SEM. The statistical significance of the difference between JQ1 and VEH treated samples was determined using a two tailed t test. *p = 0.002 for (A); and *p < 0.05 for (B) (D).

(E) Oil red O staining of en face aortas prepared from cohort in (A) (D).

(F) Quantification of lesion area (%) between VEH and JQ1 treated en face aortas. The statistical significance of the difference between JQ1 and VEH treated samples was determined using a two tailed t test. *p < 0.05.

See also Figure S7.

In our previous studies, genes with the highest occupancy of BRD4 at their proximal SEs were the most selectively downregulated by BET bromodomain inhibition (Chapuy et al., 2013; Lovén et al., 2013). However, these studies characterized effects on cells at ground state, where stable, preestablished SEs predominate. During cell state transitions, such as the present study of EC and macrophage activation, we observe potent and selective effects on upregulated genes associated with de novo SEs. Preferential disruption of dynamic SEs by BET bromodomain inhibition abrogates the induction of inflammatory transcription. The direct relationship between BRD4 enrichment and transcription suggests that modulating BRD4 levels at enhancers may influence the pathogenesis of inflammatory diseases. Changes in eRNA levels by NF-κB-directed BRD4 SE formation may also be an important factor in proinflammatory transcription in ECs, but await future study. Further granularity on dynamic enhancer remodeling will accompany progress in genome-wide enhancer detection and assignment.

In many disease settings, the degree of the host inflammatory response is a key determinant of severity (Medzhitov et al., 2012). Here we show small molecule BET bromodomain inhibition (JQ1) significantly attenuated endothelial activation during acute inflammation in vitro and ex vivo, as revealed by suppression of TNF-α induced leukocyte rolling, adhesion and transmigration. Finally, in a hypercholesterolemic murine model of atherosclerosis, in which EC proinflammatory activation is a seminal early event, 10-week treatment with JQ1 suppressed cardinal histopathologic features of atherogenesis. These data in vascular endothelial activation establish a critical and early role for BET bromodomains in dynamic enhancer remodeling. They describe a mechanism for rapid inflammatory gene activation by NF-κB-mediated formation of SEs. Taken in the context of prior research in macrophage activation, spermatogenesis, and myocyte hypertrophy (Anand et al., 2013; Delmore et al., 2011; Matzuk et al., 2012; Nicodeme et al., 2010), these data support a model where localization of BET bromodomains to chromatin facilitates cell state transitions. The existence of BET bromodomain inhibitors provides, then, a broad opportunity for inflammatory gene control through modulation of chromatin structure and function.

EXPERIMENTAL PROCEDURES

Animal Models

LDL receptor knockout mice (4 weeks old) on a C57Bl/6 background were purchased from Jackson Laboratories. Mice were fed an atherogenic diet (Clinton/Cybulsky Rodent Diet, D12108 with 1.25% cholesterol, Research Diets) for 10 weeks. While on the diet, the animals were treated with vehicle (DMSO) or JQ1 (50 mg/kg) by intraperitoneal injection, once daily (N = 10/group). Oil red O staining was used to quantify atherosclerotic plaque lesion area in the aortic root. Macrophage (Mac 3) and T lymphocyte (CD 4) accumulation was assessed in the aortic root, and the total staining area was analyzed using computer assisted imaging analysis. For CD 4 cells, total cell numbers were counted. Whole aorta from the left subclavian artery to the iliac bifurcation, was used for en face preparation and stained with oil red O. All protocols concerning animal use were approved by the Harvard Medical School Institutional Animal Care and Use Committee and conducted in accordance with the NIH Guide for the Care and Use of Laboratory Animals. All studies were performed in C57Bl/6J mice (Jackson Laboratories), maintained in a pathogen free facility with standard light/dark cycling and ad libitum access to food and water.

Reagents and Cell Culture

ECs from pooled human umbilical cords were cultured in M199 medium supplemented with 20% fetal bovine serum (FBS), 0.1% heparin, 50 μg/ml endothelial cell growth factor (Biomedical Technologies), penicillin/streptomycin on gelatin coated tissue culture plates. U937 cells (ATCC) were maintained in RPMI with 10% FBS and antibiotics. For transendothelial migration (see below), human umbilical vein ECs (subculture 2) were grown on fibronectin coated glass coverslips (5 mg/ml; BD Biosciences) and treated with JQ1 (500 nM) or vehicle (DMSO) for 1 hr before TNF α stimulation (10 ng/ml, 4 hr). Recombinant human TNF α was obtained from PeproTech. JQ1 was dissolved in DMSO at a concentration of 50 mg/ml. Working stocks of JQ1 were prepared by diluting 1:10 in 10% beta cyclodextrin solution (Filippakopoulos et al., 2010). Animals were treated at 50 mg/kg once daily by intraperitoneal injection.

ChIP-Seq and Data Analysis

ChIP was performed in ECs in the presence or absence of TNF α (1 hr, 25 ng/ml) and JQ1 (3 hr pretreatment, 500 nM). Specific antibodies and detailed methods are described in the Supplemental Experimental Procedures. ChIP was carried out as described elsewhere (Lovén et al., 2013). All ChIP seq data sets were aligned using Bowtie (version 1.0.0; Langmead et al., 2009) to build version NCBI36/HG18 of the human genome or build version NCBI37/MM9 of the mouse genome. Enhancers and super enhancers were mapped as described elsewhere (Lovén et al., 2013). Additional details are provided in the Supplemental Experimental Procedures.

ACCESSION NUMBERS

The GEO (http://www.ncbi.nlm.nih.gov/geo) accession numbers for all ChIP seq and Chem seq data (including microarray data) and aligned and raw data reported in this work are GSE53998 and GSE54000, respectively.

SUPPLEMENTAL INFORMATION

Supplemental Information includes Supplemental Experimental Procedures, seven figures, and six tables and can be found with this article online at http://dx.doi.org/10.1016/j.molcel.2014.08.024.

AUTHOR CONTRIBUTIONS

J.D.B., C.Y.L., Q.D., J.E.B., and J.P. designed research. J.D.B. and Q.D. performed in vitro and in vivo endothelial function studies with assistance from G.G., G.N., A.H.L., F.W.L., K.C. J.D.B. and C.Y.L. performed ChIP studies and analyzed ChIP data. A.J.F. developed motif analysis code. A.L.K. treated mice with JQ1 for atherogenesis studies. J.D.B., C.Y.L., J.E.B., and J.P. wrote manuscript.

ACKNOWLEDGMENTS

We are grateful to R. Young, P. Rahl, T. Graf, and C. Van Oevelen for stimulating discussions; M. Berkeley, Z. Herbert, and the late E. Fox (DFCI Microarray Core) for assistance with microarray experiments; and T. Volkert, J. Love, and S. Gupta at the Whitehead Genome Core for assistance with genome sequencing. This research was supported by NIH K08 HL105678, The Watkins Discovery Research Award and The Harris Family Award (to J.D.B.); US Department of Defense CDMRP CA120184 (to C.Y.L.); Sarnoff Cardiovascular Research Foundation (to G.G. and S.B.); NIH PO1 HL36028 (to F.W.L. and A.H.L.); NIH K08 HL086672 3 and Watkins Family Foundation (to K.C.); NIH K08 CA128972, the Burroughs Wellcome Fund, the Damon Runyon Cancer Research Foundation, the Richard and Susan Smith Family Foundation, and the Next Generation Award (to J.E.B.); and the Neissa Foundation and NHLBI P01 HL048743 (to J.P.). J.E.B. is the scientific founder of Tensha Therapeutics, which is clinically translating drug like derivatives of the JQ1 chemical probe of BET bromodomains used in this study as cancer therapeutics. As such, the Dana Farber Cancer Institute and J.E.B. have been granted minority equity in Tensha.

Received: March 19, 2014
Revised: July 7, 2014
Accepted: August 20, 2014
Published: September 25, 2014

REFERENCES

Anand, P., Brown, J.D., Lin, C.Y., Qi, J., Zhang, R., Artero, P.C., Alaiti, M.A., Bullard, J., Alazem, K., Margulies, K.B., et al. (2013). BET bromodomains mediate transcriptional pause release in heart failure. Cell *154*, 569–582.

Anders, L., Guenther, M.G., Qi, J., Fan, Z.P., Marineau, J.J., Rahl, P.B., Lovén, J., Sigova, A.A., Smith, W.B., Lee, T.I., et al. (2014). Genome-wide localization of small molecules. Nat. Biotechnol. *32*, 92–96.

Ashburner, B.P., Westerheide, S.D., and Baldwin, A.S., Jr. (2001). The p65 (RelA) subunit of NF-kappaB interacts with the histone deacetylase (HDAC) corepressors HDAC1 and HDAC2 to negatively regulate gene expression. Mol. Cell. Biol. *21*, 7065–7077.

Baltimore, D. (2011). NF-κB is 25. Nat. Immunol. *12*, 683–685.

Barboric, M., Nissen, R.M., Kanazawa, S., Jabrane-Ferrat, N., and Peterlin, B.M. (2001). NF-kappaB binds P-TEFb to stimulate transcriptional elongation by RNA polymerase II. Mol. Cell *8*, 327–337.

Barnes, P.J., and Karin, M. (1997). Nuclear factor kappaB: a pivotal transcription factor in chronic inflammatory diseases. N. Engl. J. Med. *336*, 1066–1071.

Chapuy, B., McKeown, M.R., Lin, C.Y., Monti, S., Roemer, M.G., Qi, J., Rahl, P.B., Sun, H.H., Yeda, K.T., Doench, J.G., et al. (2013). Discovery and characterization of super-enhancer-associated dependencies in diffuse large B cell lymphoma. Cancer Cell *24*, 777–790.

Chen, L.f., Fischle, W., Verdin, E., and Greene, W.C. (2001). Duration of nuclear NF-kappaB action regulated by reversible acetylation. Science *293*, 1653–1657.

Cybulsky, M.I., Iiyama, K., Li, H., Zhu, S., Chen, M., Iiyama, M., Davis, V., Gutierrez-Ramos, J.C., Connelly, P.W., and Milstone, D.S. (2001). A major role for VCAM-1, but not ICAM-1, in early atherosclerosis. J. Clin. Invest. *107*, 1255–1262.

De Val, S., Chi, N.C., Meadows, S.M., Minovitsky, S., Anderson, J.P., Harris, I.S., Ehlers, M.L., Agarwal, P., Visel, A., Xu, S.M., et al. (2008). Combinatorial regulation of endothelial gene expression by ets and forkhead transcription factors. Cell *135*, 1053–1064.

Delmore, J.E., Issa, G.C., Lemieux, M.E., Rahl, P.B., Shi, J., Jacobs, H.M., Kastritis, E., Gilpatrick, T., Paranal, R.M., Qi, J., et al. (2011). BET bromodomain inhibition as a therapeutic strategy to target c-Myc. Cell *146*, 904–917.

Dey, A., Ellenberg, J., Farina, A., Coleman, A.E., Maruyama, T., Sciortino, S., Lippincott-Schwartz, J., and Ozato, K. (2000). A bromodomain protein,

MCAP, associates with mitotic chromosomes and affects G(2) to M transition. Mol. Cell. Biol. *20*, 6537 6549.

Filippakopoulos, P., Qi, J., Picaud, S., Shen, Y., Smith, W.B., Fedorov, O., Morse, E.M., Keates, T., Hickman, T.T., Felletar, I., et al. (2010). Selective inhi bition of BET bromodomains. Nature *468*, 1067 1073.

Frye, S.V. (2010). The art of the chemical probe. Nat. Chem. Biol. *6*, 159 161.

Gimbrone, M.A., Jr., Bevilacqua, M.P., and Cybulsky, M.I. (1990). Endothelial dependent mechanisms of leukocyte adhesion in inflammation and athero sclerosis. Ann. N Y Acad. Sci. *598*, 77 85.

Hnisz, D., Abraham, B.J., Lee, T.I., Lau, A., Saint André, V., Sigova, A.A., Hoke, H.A., and Young, R.A. (2013). Super enhancers in the control of cell identity and disease. Cell *155*, 934 947.

Huang, B., Yang, X.D., Zhou, M.M., Ozato, K., and Chen, L.F. (2009). Brd4 coactivates transcriptional activation of NF kappaB via specific binding to acetylated RelA. Mol. Cell. Biol. *29*, 1375 1387.

Jang, M.K., Mochizuki, K., Zhou, M., Jeong, H.S., Brady, J.N., and Ozato, K. (2005). The bromodomain protein Brd4 is a positive regulatory component of P TEFb and stimulates RNA polymerase II dependent transcription. Mol. Cell *19*, 523 534.

Jin, F., Li, Y., Dixon, J.R., Selvaraj, S., Ye, Z., Lee, A.Y., Yen, C.A., Schmitt, A.D., Espinoza, C.A., and Ren, B. (2013). A high resolution map of the three dimensional chromatin interactome in human cells. Nature *503*, 290 294.

Kaikkonen, M.U., Spann, N.J., Heinz, S., Romanoski, C.E., Allison, K.A., Stender, J.D., Chun, H.B., Tough, D.F., Prinjha, R.K., Benner, C., and Glass, C.K. (2013). Remodeling of the enhancer landscape during macrophage acti vation is coupled to enhancer transcription. Mol. Cell *51*, 310 325.

Langmead, B., Trapnell, C., Pop, M., and Salzberg, S.L. (2009). Ultrafast and memory efficient alignment of short DNA sequences to the human genome. Genome Biol. *10*, R25.

LeRoy, G., Rickards, B., and Flint, S.J. (2008). The double bromodomain pro teins Brd2 and Brd3 couple histone acetylation to transcription. Mol. Cell *30*, 51 60.

Ley, K., Laudanna, C., Cybulsky, M.I., and Nourshargh, S. (2007). Getting to the site of inflammation: the leukocyte adhesion cascade updated. Nat. Rev. Immunol. *7*, 678 689.

Libby, P., Ridker, P.M., and Hansson, G.K. (2011). Progress and challenges in translating the biology of atherosclerosis. Nature *473*, 317 325.

Lovén, J., Hoke, H.A., Lin, C.Y., Lau, A., Orlando, D.A., Vakoc, C.R., Bradner, J.E., Lee, T.I., and Young, R.A. (2013). Selective inhibition of tumor oncogenes by disruption of super enhancers. Cell *153*, 320 334.

Masckauchán, T.N., Shawber, C.J., Funahashi, Y., Li, C.M., and Kitajewski, J. (2005). Wnt/beta catenin signaling induces proliferation, survival and inter leukin 8 in human endothelial cells. Angiogenesis *8*, 43 51.

Matsui, T., Kanai Azuma, M., Hara, K., Matoba, S., Hiramatsu, R., Kawakami, H., Kurohmaru, M., Koopman, P., and Kanai, Y. (2006). Redundant roles of Sox17 and Sox18 in postnatal angiogenesis in mice. J. Cell Sci. *119*, 3513 3526.

Matys, V., Kel Margoulis, O.V., Fricke, E., Liebich, I., Land, S., Barre Dirrie, A., Reuter, I., Chekmenev, D., Krull, M., Hornischer, K., et al. (2006). TRANSFAC and its module TRANSCompel: transcriptional gene regulation in eukaryotes. Nucleic Acids Res. *34*, D108 D110.

Matzuk, M.M., McKeown, M.R., Filippakopoulos, P., Li, Q., Ma, L., Agno, J.E., Lemieux, M.E., Picaud, S., Yu, R.N., Qi, J., et al. (2012). Small molecule inhibi tion of BRDT for male contraception. Cell *150*, 673 684.

Medzhitov, R., Schneider, D.S., and Soares, M.P. (2012). Disease tolerance as a defense strategy. Science *335*, 936 941.

Mujtaba, S., Zeng, L., and Zhou, M.M. (2007). Structure and acetyl lysine recognition of the bromodomain. Oncogene *26*, 5521 5527.

Natoli, G. (2009). Control of NF kappaB dependent transcriptional responses by chromatin organization. Cold Spring Harb. Perspect. Biol. *1*, a000224.

Nicodeme, E., Jeffrey, K.L., Schaefer, U., Beinke, S., Dewell, S., Chung, C.W., Chandwani, R., Marazzi, I., Wilson, P., Coste, H., et al. (2010). Suppression of inflammation by a synthetic histone mimic. Nature *468*, 1119 1123.

Ostuni, R., Piccolo, V., Barozzi, I., Polletti, S., Termanini, A., Bonifacio, S., Curina, A., Prosperini, E., Ghisletti, S., and Natoli, G. (2013). Latent enhancers activated by stimulation in differentiated cells. Cell *152*, 157 171.

Parker, S.C., Stitzel, M.L., Taylor, D.L., Orozco, J.M., Erdos, M.R., Akiyama, J.A., van Bueren, K.L., Chines, P.S., Narisu, N., Black, B.L., et al.; NISC Comparative Sequencing Program; National Institutes of Health Intramural Sequencing Center Comparative Sequencing Program Authors; NISC Comparative Sequencing Program Authors (2013). Chromatin stretch enhancer states drive cell specific gene regulation and harbor human disease risk variants. Proc. Natl. Acad. Sci. USA *110*, 17921 17926.

Pierce, J.W., Lenardo, M., and Baltimore, D. (1988). Oligonucleotide that binds nuclear factor NF kappa B acts as a lymphoid specific and inducible enhancer element. Proc. Natl. Acad. Sci. USA *85*, 1482 1486.

Pierce, J.W., Schoenleber, R., Jesmok, G., Best, J., Moore, S.A., Collins, T., and Gerritsen, M.E. (1997). Novel inhibitors of cytokine induced IkappaBalpha phosphorylation and endothelial cell adhesion molecule expression show anti inflammatory effects in vivo. J. Biol. Chem. *272*, 21096 21103.

Shi, J., Whyte, W.A., Zepeda Mendoza, C.J., Milazzo, J.P., Shen, C., Roe, J.S., Minder, J.L., Mercan, F., Wang, E., Eckersley Maslin, M.A., et al. (2013). Role of SWI/SNF in acute leukemia maintenance and enhancer medi ated Myc regulation. Genes Dev. *27*, 2648 2662.

Strausberg, R.L., and Schreiber, S.L. (2003). From knowing to controlling: a path from genomics to drugs using small molecule probes. Science *300*, 294 295.

Whyte, W.A., Orlando, D.A., Hnisz, D., Abraham, B.J., Lin, C.Y., Kagey, M.H., Rahl, P.B., Lee, T.I., and Young, R.A. (2013). Master transcription factors and mediator establish super enhancers at key cell identity genes. Cell *153*, 307 319.

Yang, Z., Yik, J.H., Chen, R., He, N., Jang, M.K., Ozato, K., and Zhou, Q. (2005). Recruitment of P TEFb for stimulation of transcriptional elongation by the bromodomain protein Brd4. Mol. Cell *19*, 535 545.

Zhong, H., May, M.J., Jimi, E., and Ghosh, S. (2002). The phosphorylation sta tus of nuclear NF kappa B determines its association with CBP/p300 or HDAC 1. Mol. Cell *9*, 625 636.

Zuber, J., Shi, J., Wang, E., Rappaport, A.R., Herrmann, H., Sison, E.A., Magoon, D., Qi, J., Blatt, K., Wunderlich, M., et al. (2011). RNAi screen iden tifies Brd4 as a therapeutic target in acute myeloid leukaemia. Nature *478*, 524 528.

Medulloblastoma regulatory circuitries reveal subgroup-specific cellular origins

Charles Y. Lin[1]*, Serap Erkek[2,3]*, Daisuke Kawauchi[3], Alexander J. Federation[1], Rhamy Zeid[1], Marc Zapatka[4], Thomas Risch[5], Hans-Jörg Warnatz[5], Barbara Worst[3], Sebastian M. Waszak[2], David T.W. Jones[3], Marcel Kool[3], Volker Hovestadt[4], Ivo Buchhalter[6], Laura Sieber[3], Pascal Johann[3], Stefan Gröschel[7], Marina Ryzhova[8], Andrey Korshunov[9], Vyacheslav Amstislavskiy[5], Hans Lehrach[5], Marie-Laure Yaspo[5], Roland Eils[6,10], Peter Lichter[4], Jan O. Korbel[2], Stefan M. Pfister[3,11#], James E. Bradner[1#] and Paul A. Northcott[3,12#]

[1]Dana Farber Cancer Institute (DFCI), Medical Oncology, Boston, MA, USA
[2]European Molecular Biology Laboratory (EMBL), Genome Biology Unit, Heidelberg, Germany
[3]German Cancer Research Center (DKFZ), Division of Pediatric Neurooncology, Heidelberg, Germany
[4]German Cancer Research Center (DKFZ), Division of Molecular Genetics, Heidelberg, Germany
[5]Max Planck Institute for Molecular Genetics, Department of Vertebrate Genomics, Berlin, Germany
[6]German Cancer Research Center (DKFZ), Division of Theoretical Bioinformatics, Heidelberg, Germany
[7]NCT Heidelberg, Department of Translational Oncology, Heidelberg, Germany
[8]NN Burdenko Neurosurgical Institute, Department of Neuropathology, Moscow, Russia
[9]Clinical Cooperation Unit Neuropathology, German Cancer Research Center (DKFZ), and Department of Neuropathology University Hospital, Heidelberg, Germany
[10]Institute of Pharmacy and Molecular Biotechnology and BioQuant, University of Heidelberg
[11]University of Heidelberg, Department of Pediatrics, Heidelberg, Germany
[12]St. Jude Children's Research Hospital, Developmental Neurobiology, Memphis, TN, USA

*These authors contributed equally to this study
[#]Co-senior authorship

Manuscript correspondence:

Stefan M. Pfister, M.D.
Group Leader & Division Head, Division of Pediatric Neurooncology
German Cancer Research Center (DKFZ)
Im Neuenheimer Feld 280
D-69120 Heidelberg, Germany
S.Pfister@dkfz-heidelberg.de
+49.62 21.42-4618 (P)
+49.62 21.42-4639 (F)

James E. Bradner, M.D.
Associate Professor
Dana-Farber Cancer Institute
Harvard Medical School
Boston, MA
james_bradner@dfci.harvard.edu

http://bradner.dfci.harvard.edu
617-632-3352 (P)

Paul A. Northcott, Ph.D.
Assistant Member, Department of Developmental Neurobiology
St. Jude Children's Research Hospital
262 Danny Thomas Place
Mailstop 325
Memphis, TN 38105
paul.northcott@stjude.org
www.stjude.org/northcott
901-595-2816 (P)
901-595-7478 (F)

Summary (148 words):

Medulloblastoma is a highly malignant paediatric brain tumour, often inflicting devastating consequences on the developing child. Genomic studies have revealed four transcriptionally distinct molecular subgroups with divergent biology and clinical behaviour. An understanding of the regulatory circuitry governing the transcriptional landscapes of medulloblastoma subgroups, and how this relates to their respective developmental origins, is currently lacking. Using H3K27ac and BRD4 ChIP-Seq, coupled with tissue-matched DNA methylation and transcriptome data, we describe the active *cis*-regulatory landscape across 28 primary medulloblastoma specimens. Analysis of differentially regulated enhancers and super-enhancers reinforced inter-subgroup heterogeneity and revealed clinically relevant insights into oncogenic TGFβ signaling in Group 3. Computational reconstruction of core regulatory circuitry identified a master set of transcription factors responsible for subgroup divergence and revealed candidate cellular origins for Group 4. The integrated analysis of *cis*-regulatory elements in primary human tumour samples reveals insights into *cis*-regulatory architecture, unrecognized dependencies, and cellular origins.

Introduction (465 words):

Medulloblastoma is a highly malignant paediatric brain tumour classified into four biologically and clinically distinct molecular subgroups[1-3]. Transcriptional diversity underlying WNT, SHH, Group 3, and Group 4 subgroup medulloblastoma is partially explained by active and discriminatory signaling pathways, such as the Wingless/WNT and Sonic hedgehog/SHH developmental cascades inherent to WNT and SHH medulloblastomas, respectively. Recurrent, somatically altered driver genes such as *MYC* (Group 3), *KDM6A* (Group 4), the recently implicated *GFI1/GFI1B* (Group 3 and Group 4), and others contribute to further diversity between medulloblastoma subgroups[4-6]. Whereas distinct cellular origins have been experimentally substantiated for WNT[7] and SHH[8-10] tumours, the origins of Group 3 and Group 4 medulloblastoma remain unknown. Underscoring the need for new subgroup-specific therapeutic insights, the present clinical approach to medulloblastoma involves invasive surgery, cranio-spinal radiation and cytotoxicity, together associated with profound morbidity in the developing child.

Recent next-generation sequencing studies of medulloblastoma have defined recurrently mutated genes and pathways, the proportion of cases affected by such alterations, and their respective subgroup distribution[4,11-14]. The bulk of these efforts have thus far been focused on somatic, DNA-level genomic alterations, especially non-synonymous single nucleotide variants, indels, and focal copy-number aberrations[5]. Recurrent targeting of genes involved in chromatin modification has been the most consistent theme to emerge from these studies[11,15,16], strongly suggesting deregulation of the epigenome as a critical step during medulloblastoma pathogenesis. However, this hypothesis has yet to be substantiated and knowledge pertaining to how the medulloblastoma epigenome influences subgroup-specific transcriptional programs remains in its infancy. Recent analysis of DNA cytidine methylation in medulloblastoma corroborated transcriptional differences in subgroups and enumerated putative master regulatory factors[17]. Still, a detailed analysis of the *cis*-regulatory epigenome of this disease has not been undertaken.

Enhancers are *cis*-acting regulatory elements that serve as sites of recruitment for transcription factors and chromatin-associated regulatory complexes, which together signal to RNA polymerase in control of target gene expression[18]. Massive catalogues of genome-wide enhancers have been inferred and published by large consortia such as ENCODE[19,20] and Roadmap[21], dramatically advancing our understanding of enhancer-gene regulation across a comprehensive spectrum of cell lines and tissues from different species. These resources empower our understanding of the complex cartography of the human regulatory landscape, provide testable hypotheses regarding disease-risk association, contribute evolutionary inferences, and establish facile analytical techniques. To deeply characterize the active *cis*-regulatory circuitry of a single disease entity, here medulloblastoma, we performed high-resolution chromatin immunoprecipitation with sequencing (ChIP-Seq) for active enhancers (H3K27ac) in 28 primary tumour specimens and three established cell lines, collectively accounting for known molecular subgroups. Our approach to studying enhancers genome-wide in a large set of primary tissue samples led to a regulatory explanation for subgroup transcriptional diversity, previously unrecognized subgroup-specific dependencies and firm insights into medulloblastoma cellular origins, in particular for the poorly characterized and aggressive Group 3 and Group 4 subgroups.

Results: (2,491 words):

The enhancer landscape of primary medulloblastoma

Recent publications of large-scale efforts to annotate active regulatory elements genome-wide in human tissues (*e.g.* through DNase I hypersensitivity, H3K27ac and BRD4 ChIP-seq)[19,21], have focused on immortalized or malignant cell lines and normal human tissues for cataloguing active enhancers. Discrete disease entities have been under-represented in these comprehensive surveys, such as medulloblastoma, which has been the subject of only a single long-term culture cell line (D721; first reported in 1997) included amongst 125 cell types initially studied by ENCODE[20]. Further, cancer cell lines often exhibit drastic genomic and transcriptional divergence from their corresponding primary tumour tissues. This is exemplified in Non-Hodgkin's lymphoma where our prior epigenomic analyses identified greater likeness between primary tumour samples and normal lymphoid tissues than between tumours and cell lines[22]. Given the apparent limitations of using cell lines to faithfully study the tumour epigenome, and the recognized subgroup-dependent heterogeneity of medulloblastoma, we collected a series of 28 treatment-naïve, fresh-frozen medulloblastoma specimens for studying the active enhancer landscape by H3K27ac ChIP-Seq (Figure 1a,b, Extended Data Figure 1a,b).

The cohort was selected to be inclusive of all four medulloblastoma subgroups (Supplemental Table S1; WNT, n=3, SHH, n=5, Group 3, n=9, Group 4, n=11). Three additional Group 3 cell lines (MED8A, D425, and HD-MB03) were also included in our experimental workflow. Using MACS[23] to identify significantly enriched H3K27ac peaks, we inferred 78,516 medulloblastoma enhancers, which mainly (~80%) covered introns and intergenic regions (Extended Data Figure 1b). Parallel ChIP-Seq was performed for *Bromodomain Containing 4* (BRD4), an enhancer-associated transcriptional coactivator[22,24], in 27/31 cases (Figure 1c). Enrichment of H3K27ac and BRD4 ChIP-Seq signals was highly correlated at putative enhancer loci (Pearson correlation, r=0.949), confirming that the selected regions are indeed active enhancers (Figure 1c)[22,24]. In contrast, regions enriched for H3K27ac were strongly anti-correlated with DNA methylation (Pearson correlation, r=-0.577; Figure 1d). Finally, analyzing strand-specific RNA-Seq data generated from the same medulloblastomas subjected to ChIP-Seq, we observed short, unspliced, bidirectional RNA transcripts overlapping active enhancers (Figure 1e), in accordance with recently described enhancer RNAs (eRNAs), known also to arise from active enhancers[25]. Comparison of predicted medulloblastoma enhancers with those reported using analogous methods employed by the ENCODE and Roadmap Epigenomics Projects revealed 19,850 novel regulatory regions, indicative of potentially cerebellar cell type- or medulloblastoma-specific enhancers in our dataset (Figure 1f, g). Importantly, primary medulloblastoma enhancer landscapes exhibited poor overlap and correlation with those generated from medulloblastoma cell lines (Extended Data Figure 1c, d), further emphasizing the importance of studying the epigenome in primary tumours.

Since medulloblastoma subgroups were first described based on their transcriptional diversity[26], we sought to explore subgroup-specific enhancers to gain insight into the *cis*-regulatory landscape defining subgroup identity. ANOVA was used to identify sets of enhancers differing according to known molecular subgroup, revealing 20,406 differentially regulated enhancers (26% of all inferred medulloblastoma enhancers; Figure 2a, b). The remaining 74% (n=58,110) displayed activity across all groups

suggesting a general role in medulloblastoma or cerebellar identity (Figure 2a; Supplemental Table S2). K-means clustering of differentially regulated enhancers delineated six distinct medulloblastoma enhancer classes, including one for each subgroup (i.e. WNT, SHH, Group 3 and Group 4) as well as WNT-SHH and Group 3-Group 4 shared classes (Figure 2b, c). Group 3 and Group 4 subgroups are known to exhibit some degree of transcriptional similarity[27-29], consistent with the enhancer clustering results. In contrast, WNT and SHH subgroups tend to be mostly dissimilar from a transcriptional perspective, and thus a common subset of shared enhancers between these groups was unexpected and intriguing.

We next sought to assign enhancer elements to target genes, a process typically hindered by the fact that the majority of enhancer/promoter interactions occur over extensive genomic distances[30]. To overcome challenges in enhancer/gene assignment, we leveraged sample-matched RNA-Seq gene expression data to identify putative enhancer/gene interactions that are (i) contained in the same topologically associated domain (TAD[31]) and (ii) exhibit strong positive correlations between enhancer H3K27ac levels and gene expression ($\rho > 0.6$ and FDR <0.05, Extended Data Figures 2 & 3). TADs are megabase scale genomic regions of interacting chromatin that form a fundamental unit of genome structure. This approach assigned 8,775 enhancers (including 43% of all differential enhancers) to at least one protein-coding target gene (Supplemental Table S3). The majority (44%) of inferred target genes were assigned to a single enhancer, but in many cases, several enhancers were predicted to converge on the regulation of a single gene (Figure 2d). Likewise, 73% of enhancers were assigned to only a single gene target and rarely was a given enhancer assigned to more than two candidate genes (Figure 2e). Compelling subgroup-related diversity with respect to inferred enhancer-target gene regulation was prevalent in our dataset (Figure 2f-i), with numerous genes exhibiting convergent regulation by distinct subgroup-specific differential enhancer loci. For example, we identified alternative subgroup-specific enhancers predicted to regulate known oncogenes, including WNT-specific and SHH-specific enhancers inferred to target *ALK*, and WNT-specific and Group 3-specific enhancers inferred to target *MYC* (Figure 2g-i; Extended Data Figure 2j). These data provide a rational, computationally robust approach for assigning medulloblastoma enhancers to their potential targets and underscore the apparent complexity inherent to enhancer-gene regulation across medulloblastoma subgroups.

Subgroup-specific enhancers reveal aberrant TGFβ signaling in Group 3

Group 3 and Group 4 medulloblastoma remain the least well understood subgroups of the disease, despite collectively accounting for ~60% of all diagnoses[2,11]. Group 3 patients have a particularly grave prognosis, suffer commonly from metastatic disease, and fall ill in infancy or early childhood. Group 4 disease affects children of all ages and prognoses have been demonstrated to vary according to metastatic status and the presence of certain cytogenetic anomalies[32]. In contrast to WNT patients (who almost universally survive current treatment regimens), and SHH patients (who represent rational candidates for SHH pathway inhibitors such as SMO inhibitors), mechanism-based treatment options remain scarce for Group 3 and Group 4 patients. As such, additional insights are needed to direct future mechanistic and translational research.

We therefore applied differential enhancer analysis to identify divergent regulatory programs between Group 3 and Group 4 tumours. First, we validated that Group 3 or Group 4 differential enhancer target genes showed reciprocal patterns of H3K27ac

enrichment. We ranked the top 1,000 enhancers (by H3K27ac signal) in either Group 3 or Group 4 by fold-change in acetylation and found a strong leading edge enrichment of Group 3- and Group 4-specific target genes (Figure 3a). Functional pathway analysis (see Supplementary Methods) performed on Group 3 and Group 4 enhancer-gene target assignments identified prominent neuronal gene sets enriched in both subgroups (Figure 3b, c), consistent with published transcriptional studies[27-29] and validating the computational approach implemented to assign enhancers to target genes. Neuronal development driven by transcriptional regulators dominated the Group 4 functional annotation, whereas Group 3 enhancer target genes prominently included thematic pathways associated with TGFβ signaling (Figure 3b,c; Extended Data Figure 4a). Group 3-specific enhancers included the TGFβ family type I and II membrane receptors (*ACVR2A* and *TGFBR1*) as target genes (Figure 3c), whereas enhancers regulating *SMAD5*, *TGFB1*, and *TGFB3* showed equivalent acetylation between Group 3 and Group 4. Overall, components of the TGFβ signaling pathway showed a strong enrichment for enhancer regulation in Group 3 (Figure 3d). Notably, we uncovered a ~450kb focal amplification at the *ACVR2A* locus in one Group 3 sample that encompassed both the gene and the upstream enhancer regions (Extended Data Figure 4b). These data, combined with our prior observations that TGFβ receptor genes are recurrently amplified at low frequency in Group 3[5], further implicate TGFβ signaling as a putative oncogenic driver in Group 3 medulloblastoma.

Medulloblastoma super-enhancers define subgroup identity

The large, Group 3-specific enhancer clusters adjacent to genes defining the TGFβ signaling pathway prompted a consideration that super-enhancers (SEs), broad spatially co-localized enhancer domains[33-36], might play an essential role in establishing subgroup-specific identity. SEs are established by cell state-defining transcription factors (TFs) and TFs at the termini of signaling pathways[34,36]. In multiple tumour types, SEs have been shown to drive oncogenes, genes required for maintenance of tumour cell identity, and genes associated with cell type-specific functions. We therefore next undertook a systematic mapping of SEs across all 28 medulloblastoma samples (Figure 4a). Massive (>50kb) SE domains were identified at the cerebellar-specific TFs, *ZIC1* and *ZIC4*[37 38] (Figure 4b, c), and at 70% of a queried set of established medulloblastoma driver/signature genes, including *GLI2*, *MYC*, *OTX2* and others[5] (Extended Data Figure 5a).

To identify subgroup-specific SEs, we ranked average H3K27ac enrichment across all samples from a given subgroup at the union of all enhancer regions identified in that subgroup. Subgroup SEs were identified from this meta H3K27ac signal using previously established methods[36], resulting in ~3,000 distinct SE containing loci with ~600-1,100 SEs identified per subgroup (Figure 4a, Supplemental Table S4). Compared to typical enhancers, subgroup SEs showed higher occupancy of BRD4 and greater enhancer signal dynamic range between subgroups (Extended Data Figure 5b-d). Targets of differential enhancers contained within SEs (i.e. SE target genes) included a large fraction of established medulloblastoma signature genes (32%; Supplemental Table S3), as well as novel candidates, including *NKD1/NKD2* (WNT subgroup), *PCNT* (SHH subgroup), *HLX* (Group 3), and *SNCAIP* (Group 4) (Figure 4d-f). Medulloblastoma SEs were inferred to regulate known Cancer Gene Census genes, including *ALK* in WNT, *SMO* and *NTRK3* in SHH, *LMO1*, *LMO2*, and *MYC* in Group 3, and *ETV4* and *PAX5* in Group 4, among others (Supplemental Table S3). Furthermore, several actionable, SE-

regulated genes were revealed in our analysis including kinases (NTRK1, SGK1) and chromatin modifying enzymes (PNMT, HDAC4) (Supplemental Table S5).

Rank transformation of subgroup SE loci across all samples enabled a systematic identification of SEs displaying either conserved SE activity across samples, or highly subgroup-specific patterns of activity (Figure 4b-f, Supplemental Table S6). Unbiased hierarchical clustering of SEs across all primary medulloblastoma samples was sufficient to recapitulate transcriptional subgroupings using no prior knowledge of subgroup status, suggesting that SEs might play a role in driving subgroup-specific identity (Figure 4a). As shown with all enhancer elements (Extended Data Figure 1c,d), SEs from established Group 3 medulloblastoma cell lines clustered with one another, but failed to show similarity to primary Group 3 samples or samples from any other subgroup.

Super-enhancer regulated transcription factors implicate Group 4 cellular origins

Among subgroup-specific SE target genes, we observed an enrichment of TFs involved in neuronal development (*P*~0.0001, Fisher's exact test; Extended Data Figure 6a). ~30% of these SEs are previously unreported suggesting a lineage-specific regulatory role. Overall, subgroup-specific TFs displayed similar patterns of expression, enhancer motif enrichment, and overlap of target genes (Extended Data Figures 6 & 7). TFs were also enriched in subgroup-specific SE targets as compared to subgroup-specific non-SE targets (*P*~0.002, Fisher's exact test), consistent with prior observations in other cancers that SEs regulate key TFs required for tumour identity and maintenance[22,24,34]. Given evidence in embryonic stem cells that pluripotency master regulator TFs (OCT4, SOX2, NANOG) are driven by SEs and themselves bind to and establish SEs[36], we hypothesized that a *reverse* analysis of SEs in medulloblastoma might enable a *de novo* reconstruction of tumour identity-defining TFs and their associated regulatory circuitry, thereby providing novel insights into medulloblastoma origins.

Pursuant to this idea, we proposed a set of criteria for TF inclusion into the core regulatory circuitry of medulloblastoma. Specifically, (i) core regulatory circuitry TFs are SE-regulated and (ii) the TFs themselves bind to SEs of one another (Figure 5a). For each SE-regulated TF, these criteria can be quantified through a measurement of the *in* and *out* degree of regulation, whereby the *in degree* represents the total number of SE-regulated TFs that bind to a TF's SE, and the *out degree* represents the total number of other TF SEs bound by a given TF (Figure 5a). Using these criteria in the poorly characterized Group 4 medulloblastoma, we observe interconnected binding at the SEs of three neuronal TFs: *LMX1A*, *LHX2*, and *EOMES* (Figure 5b). Inspection of their respective gene loci revealed large SEs containing clustered binding sites for these factors present only in Group 3 and Group 4 (Figure 5b,c). Additionally, Group 4-specific enhancers for *LMX1A, LHX2,* and *EOMES* binding sites linked those TFs with Group 4-specific target genes (Extended Data Figure 8). Extending regulatory circuitry reconstruction across all SE-associated TFs in medulloblastoma, we identified regulatory cliques of TFs with similar patterns of *in/out* degree, strong interconnectivity via motif binding, and higher likelihoods of pairwise protein/protein interaction and motif co-occurrence at enhancers (Figure 5d, Extended Data Figure 9). This reconstruction creates for the first time a candidate core regulatory circuitry in each subgroup, and implicates specific sets of TFs in establishing medulloblastoma subgroup identity (Figure 5d).

Cellular origins for WNT and SHH medulloblastomas have been experimentally established using mouse models genetically engineered to aberrantly activate the WNT and SHH signaling pathways, respectively, in distinct hindbrain stem/progenitor cells during development[7-10]. The origins of Group 3 and Group 4 medulloblastoma, however, are unknown and yet essential to define as these tumours account for ~60% of all diagnoses, lack targeted therapies, and are frequently associated with a poor clinical outcome secondary to current standard of care[2].

Cell identity is most essentially defined by the activity of master regulator TFs. In reprograming and trans-differentiation studies, the activity of these TFs (e.g. OCT4, SOX2, and NANOG in embryonic stem cells, Pu.1 in B cells, ATOH1 in sensory hair cells, and BARHL1/BARHL2 in spinal commissural neurons) is sufficient to induce transitions between cell states[39-42]. As such, we hypothesized that the regulatory SE regions governing endogenous expression of candidate master TFs and embedded in the core regulatory circuitry of medulloblastoma subgroups might inform the cellular origins of the disease via their cell type-specific activity. Examination of the expression of Lmx1a, Eomes, and Lhx2 in the developing mouse hindbrain (e13.5) using the Mouse Allen Brain Atlas Database showed spatiotemporal patterns of restricted expression in the nuclear transitory zone (NTZ), an assembly point for immature deep cerebellar nuclei (DCN) (Figure 5e). DCN residing in the NTZ at this time point are predominantly glutamatergic projection neurons that originate from earlier progenitors of the rhombic lip, a transient structure producing progenitors with distinct cellular fates, including DCN and cerebellar granule neurons[43] (Figure 5g). Immunohistochemical staining for Lmx1a and Eomes at the same developmental stage (e13.5) recapitulated these findings (Figure 5f). To investigate the spatiotemporal distribution of cells in which Group 4-specific TFs are regulated by their SEs, we cloned constituent regions of the Lmx1a SE into a *LacZ* reporter construct, introduced the reporter into the e11.5 developing mouse hindbrain by *exo utero* electroporation, and assayed enhancer activity via x-gal staining at 48 hours post-transfection (Figure 5g). X-gal staining revealed spatially restricted activity of the Lmx1a SE reporter in the developing cerebellum (Figure 5h). These findings validate the specific activity of the Lmx1a SE observed in Group 4 medulloblastoma and implicate precursors of glutamatergic DCN as potential cells-of-origin for this subgroup. Finally, these findings establish SE core regulatory circuitry as a novel method to infer cell of origin for poorly classified primary tumours.

Discussion (450 words):

We describe the active medulloblastoma enhancer landscape across a series of 28 fresh-frozen, treatment-naïve tissue samples and three cultured cell lines, to our knowledge representing the largest such dataset for any single cancer entity. Our data reveal dramatic divergence between primary tumour and tumour cell line material and uncover considerable *cis*-regulatory element heterogeneity between subgroups of the disease that would be overlooked and unsubstantiated in series limited to just a few cases.

Clinically relevant medulloblastoma subgroups are principally defined based on their underlying transcriptional profiles. Differentially regulated medulloblastoma enhancers and SEs are here shown to recapitulate these subgroups, and importantly extend our understanding of this disease to inferences regarding cell specification and actionable tumour dependencies. Biological themes and signaling networks extracted from transcriptional data have served as the primary source of annotation for

medulloblastoma subgroups, with WNT and SHH subgroups characterized by activation of their respective signaling pathways, and Group 3 and Group 4 recognized for their GABAergic and glutamatergic expression phenotypes, respectively. Although these data provide a functional and phenotypic annotation of medulloblastoma, they fail to articulate the cell of origin and developmental identity of individual subgroups. Using a reverse analysis of the medulloblastoma chromatin landscape starting at the level of differentially-regulated enhancers and SEs, we have reconstructed a model of the core regulatory circuitry inherent to medulloblastoma subgroups, and inferred master transcriptional regulators responsible for subgroup-specific divergence. The majority of these master regulator TFs were not previously implicated in medulloblastoma developmental biology, nor were they visible amongst transcriptionally-derived gene sets dominated by aberrant signaling and overwhelming phenotypic signatures. Through tracing the spatiotemporal activity of a subset of Group 4 master TFs, these studies identified DCN of the cerebellar NTZ, or plausibly their earlier precursors originating from the rhombic lip, as putative cells-of-origin for this large subgroup of patients. Together these approaches establish a framework for the inference of tumour cell of origin through enhancer core regulatory circuitry mapping.

Understanding the cellular origins of cancer has broad implications for the understanding and treatment of the disease[44]. Numerous cancers, especially those of the immune compartment are treated through targeting of the lineage (*e.g.* anti-B cell therapies)[45,46]. As medulloblastoma is believed to originate from cell populations that normally exist ephemerally during development, targeting the aberrant persistence of tumour cells from these lineages may represent a novel therapeutic strategy. Moreover, elucidation of core regulatory circuitry implicates upstream signaling dependent regulators of master TFs, their co-activators, and their downstream effectors as potential, rational subgroup-specific therapeutic targets. These insights demonstrate the critical importance of epigenetic analyses of primary tumours as opposed to cell line model systems and highlight the broad utility of core regulatory circuitry inference especially in poorly characterized and clinically diverse malignancies.

Methods Summary

All patient material included in this study was collected after receiving informed consent from the patients and their families. Medulloblastoma samples were collected at first resection, before adjuvant chemotherapy or radiotherapy. Subgroup assignments were made using the Illumina 450K DNA methylation array as described[47]. Chromatin extraction and library preparation for ChIP-seq of H3K27ac and BRD4 were performed at ActiveMotif (Carlsbad, CA) using proprietary protocols. Alignment and filtering of ChIP-seq data was performed as described[6]. H3K27ac enhancer peaks were called using MACS[23]. H3K27ac peaks were classified as being subgroup-specific or as common enhancers by first calculating H3K27ac enrichment on the merged peaks followed by ANOVA and k-means clustering. Target gene identification of enhancers was performed by correlating H3K27ac enrichment at the enhancers with expression levels of genes located in the same TAD[31] as the enhancers. Candidate gene(s) showing the highest correlation were selected as the putative target(s) of the enhancer. Gene Ontology/Pathway analysis of enhancer-gene targets was performed using the ClueGO plugin for cytoscape[48]. SEs were called using ROSE2 (https://github.com/BradnerLab/pipeline)[49] and subgroup specificity of super-enhancers were assigned via ranking average H3K27ac signal across the subgroups. Medulloblastoma core regulatory circuitry analysis was performed by calculating inward

and outward degree regulation of SE-regulated TFs. Reporter assays for validating enhancers *in vivo* were performed by *exo utero* electroporation of reporter constructs into the hindbrain of murine CD1 embryos (e11.5). Enhancer activity was measured by x-gal staining of transfected cerebella. Endogenous expression of candidate TFs was determined by querying the Allen Brain Atlas Data Portal (http://developingmouse.brain-map.org) or by immunohistochemistry performed on the murine embryonic hindbrain (e13.5).

Acknowledgements

CYL was supported by funding from the U.S. Department of Defense CDMRP (CA120184). SE was supported by a Long-Term Fellowship from the Human Frontier Science Program (LT000432/2014). SMW was supported by a European Molecular Biology Organization Long-Term Fellowship (ALTF 755-2014) and a Swiss National Science Foundation Early Postdoctoral Mobility Fellowship (P2ELP3_155365). JEB was supported by the Grand Challenge Award for Cure Search. We thank Creative Science Studios (http://www.creativesciencestudios.com) for assistance with artwork.

Figure Legends:

Figure 1. The enhancer landscape of primary medulloblastoma.

- **(a)** Experimental workflow for studying enhancers and super-enhancers in primary medulloblastomas.
- **(b)** H3K27ac ChIP-seq data across all 28 primary medulloblastoma samples from our series showing a highly active enhancer at the *OTX2* locus, especially in Group 3 and Group 4.
- **(c)** Scatter plot comparing the enrichment (log_2) of H3K27ac signal versus BRD4 signal at medulloblastoma enhancers (n=78,516) as determined by ChIP-seq.
- **(d)** Scatter plot comparing the enrichment (log_2) of H3K27ac signal versus DNA methylation at medulloblastoma enhancers (n=78,516) as determined by ChIP-seq and WGBS, respectively.
- **(e)** RNA-seq data showing Group 3-specific enhancer RNA (eRNA) expression (lower left) overlapping a Group 3-specific *MYC* enhancer (upper left) in a subset of Group 3 and Group 4 medulloblastomas. MYC gene expression (RPKM) is also shown for the same subset of cases (lower right).
- **(f)** Venn diagram showing the overlap of medulloblastoma enhancers with those reported by ENCODE and Roadmap.
- **(g)** Pie chart summarizing the results presented in **(f)**.

Figure 2. Differentially regulated enhancers and enhancer-gene assignments in medulloblastoma subgroups.

- **(a)** ANOVA classification of medulloblastoma enhancers displayed as a pie chart.
- **(b)** Pie chart showing the distribution of differentially-regulated enhancers among medulloblastoma enhancer classes.
- **(c)** K-means clustering of differentially-regulated medulloblastoma enhancers (n=20,406).
- **(d)** Bar plot showing the proportion of enhancer/gene assignments to N enhancers.
- **(e)** Bar plot displaying the proportion of enhancer/gene assignments to N genes.

(f) Bar plot summarizing the proportion of enhancer-gene assignments to N subgroups.
(g) WNT (E2) and SHH (E3) subgroup-specific enhancers inferred to regulate *ALK*.
(h, i) Scatter plots correlating sample-matched gene expression (RPKM, x-axis) of *ALK* with H3K27ac enrichment (log_2; y-axis) for the WNT-specific (E2) and SHH-specific (E3) enhancers shown in **(g)**.

Figure 3. Functional characterization of enhancer/gene targets in medulloblastoma subgroups.

(a) Waterfall plot discriminating the top 1,000 Group 3 and Group 4 subgroup-specific enhancers as defined by total H3K27ac signal. The distribution of assigned targets in Group 3, Group 4, and shared Group 3-4 targets are shown below the waterfall.
(b, c) Functional annotation of target genes assigned to Group 3 and Group 4 subgroup-specific enhancers based on their significant overlap with gene sets annotated in Gene Ontology (GO Biological Process) and pathway databases (KEGG, Reactome).
(d) Convergence of Group 3-specific enhancers on TGFβ pathway genes. Subgroup-specific enhancers are summarized as nodes according to their respective medulloblastoma enhancer class – Group 3, Group 4, and shared Group 3-4 – with edges representing individual enhancer/TGFβ pathway gene assignments.

Figure 4. Medulloblastoma super-enhancers define subgroup-specific identity.

(a) Unsupervised hierarchical clustering of primary medulloblastomas and cell lines using H3K27ac signal calculated at all SEs identified in each individual sample.
(b) Meta tracks of H3K27ac ChIP-seq signal for the conserved *ZIC1/ZIC4* SE locus. Expression (mean RPKM) for both *ZIC4* (left) and *ZIC1* (right) is displayed as bar graphs to the right of each H3K27ac track.
(c) Line plot showing the enhancer rank for the conserved *ZIC1/ZIC4* SE locus across all samples according to subgroup.
(d) Ranked plots of enhancers defined across composite H3K27ac landscapes of WNT, SHH, Group 3, and Group 4 medulloblastomas. Enhancers are ranked by increasing group average H3K27ac signal (rpm). The cut-off discriminating typical enhancers (TEs) from super-enhancers (SEs) is shown as a dashed line. Select genes associated with SEs in each subgroup are highlighted and shaded according to enhancer class specificity.
(e) Line plots showing the enhancer rank for candidate SE loci across all samples according to subgroup. Examples of subgroup-specific (WNT=*NKD2*, SHH=*PCNT*, Group 3=*HLX*, Group 4=*SNCAIP*) SEs are shown.
(f) Meta tracks of H3K27ac ChIP-Seq signal across medulloblastoma subgroups for the loci described in **(e)**. The y-axis shows ChIP-Seq signal (rpm/bp) for each individual sample (shaded regions) with the average signal across the group shown in a line. The x-axis depicts genomic position with SE boundaries demarcated as rectangles. Bar graphs shown to the right of each H3K27ac track summarize the expression (mean RPKM) of the relevant candidate genes as determined by RNA-seq.

Figure 5. Super-enhancers define medulloblastoma regulatory circuitry and identify putative cellular origins.

- **(a)** Methodology for inferring transcriptional regulatory circuitry driven by medulloblastoma SEs.
- **(b)** Subset of the Group 4-specific transcriptional network predicted to be driven by *LMX1A*, *LHX2*, and *EOMES*.
- **(c)** H3K27ac ChIP-seq meta tracks for the SE-regulated TFs *LMX1A*, *LHX2*, and *EOMES*. Locations of enriched motifs for each of the respective TFs are highlighted at the top of the panel.
- **(d)** Subgroup-specific TF circuitry. Nodes are TFs associated with a SE in a subgroup-specific context. Edges indicate co-regulating TFs as defined by enrichment of TF binding motifs in respective regulatory regions.
- **(e)** In situ hybridization data showing highly localized expression of Lmx1a (upper panel) and Eomes (middle panel) in the embryonic cerebellum at e13.5. Red arrows indicate highly specific focal expression of both TFs in deep cerebellar nuclei (DCN) of the nuclear transitory zone (NTZ). Atoh1 expression (lower panel) is shown at the same developmental time-point to serve as a marker of the external granule layer (EGL).
- **(f)** Immunofluorescence microscopy for Lmx1a (upper panel) and Eomes (middle panel) performed on sagittal sections of the e13.5 murine cerebellum. Red arrows indicate highly localized expression of both TFs in DCN of the NTZ. Atoh1 staining (lower panel) is shown at the same developmental time-point to serve as a marker of the EGL. Neighbouring sections.
- **(g)** Strategy for validating medulloblastoma subgroup-specific enhancers *in vivo*. An Atlas (sagittal) of the e13.5 murine cerebellum, highlighting the main cell types and compartments contributing to the cerebellar anlage at this developmental stage is included as a reference.
- **(h)** X-gal staining of an embryonic hindbrain (e13.5) transfected with the reporter construct shown in **(g)** containing constituents of the Group 4-specific *Lmx1a* SE. Red arrow indicates cells positive for *in vivo* enhancer activity driving LacZ expression. Dorsal view.

References:

1 Northcott, P. A., Dubuc, A. M., Pfister, S. & Taylor, M. D. Molecular subgroups of medulloblastoma. *Expert review of neurotherapeutics* **12**, 871-884, doi:10.1586/ern.12.66 (2012).

2 Northcott, P. A., Korshunov, A., Pfister, S. M. & Taylor, M. D. The clinical implications of medulloblastoma subgroups. *Nature reviews. Neurology* **8**, 340-351, doi:10.1038/nrneurol.2012.78 (2012).

3 Taylor, M. D. *et al.* Molecular subgroups of medulloblastoma: the current consensus. *Acta neuropathologica* **123**, 465-472, doi:10.1007/s00401-011-0922-z (2012).

4 Jones, D. T. *et al.* Dissecting the genomic complexity underlying medulloblastoma. *Nature* **488**, 100-105, doi:10.1038/nature11284 (2012).

5 Northcott, P. A. *et al.* Subgroup-specific structural variation across 1,000 medulloblastoma genomes. *Nature* **488**, 49-56, doi:10.1038/nature11327 (2012).

6 Northcott, P. A. *et al.* Enhancer hijacking activates GFI1 family oncogenes in medulloblastoma. *Nature* **511**, 428-434, doi:10.1038/nature13379 (2014).

7 Gibson, P. *et al.* Subtypes of medulloblastoma have distinct developmental origins. *Nature* **468**, 1095-1099, doi:10.1038/nature09587 (2010).

8 Grammel, D. *et al.* Sonic hedgehog-associated medulloblastoma arising from the cochlear nuclei of the brainstem. *Acta neuropathologica* **123**, 601-614, doi:10.1007/s00401-012-0961-0 (2012).

9 Yang, Z. J. *et al.* Medulloblastoma can be initiated by deletion of Patched in lineage-restricted progenitors or stem cells. *Cancer cell* **14**, 135-145, doi:10.1016/j.ccr.2008.07.003 (2008).

10 Schuller, U. *et al.* Acquisition of granule neuron precursor identity is a critical determinant of progenitor cell competence to form Shh-induced medulloblastoma. *Cancer cell* **14**, 123-134, doi:10.1016/j.ccr.2008.07.005 (2008).

11 Northcott, P. A. *et al.* Medulloblastomics: the end of the beginning. *Nature reviews. Cancer* **12**, 818-834, doi:10.1038/nrc3410 (2012).

12 Kool, M. *et al.* Genome sequencing of SHH medulloblastoma predicts genotype-related response to smoothened inhibition. *Cancer cell* **25**, 393-405, doi:10.1016/j.ccr.2014.02.004 (2014).

13 Robinson, G. *et al.* Novel mutations target distinct subgroups of medulloblastoma. *Nature* **488**, 43-48, doi:10.1038/nature11213 (2012).

14 Pugh, T. J. *et al.* Medulloblastoma exome sequencing uncovers subtype-specific somatic mutations. *Nature* **488**, 106-110, doi:10.1038/nature11329 (2012).

15 Batora, N. V. *et al.* Transitioning from genotypes to epigenotypes: why the time has come for medulloblastoma epigenomics. *Neuroscience* **264**, 171-185, doi:10.1016/j.neuroscience.2013.07.030 (2014).

16 Jones, D. T., Northcott, P. A., Kool, M. & Pfister, S. M. The role of chromatin remodeling in medulloblastoma. *Brain pathology* **23**, 193-199, doi:10.1111/bpa.12019 (2013).

17 Hovestadt, V. *et al.* Decoding the regulatory landscape of medulloblastoma using DNA methylation sequencing. *Nature* **510**, 537-541, doi:10.1038/nature13268 (2014).

18 Shlyueva, D., Stampfel, G. & Stark, A. Transcriptional enhancers: from properties to genome-wide predictions. *Nature reviews. Genetics* **15**, 272-286, doi:10.1038/nrg3682 (2014).

19 Consortium, E. P. An integrated encyclopedia of DNA elements in the human genome. *Nature* **489**, 57-74, doi:10.1038/nature11247 (2012).

20 Thurman, R. E. *et al.* The accessible chromatin landscape of the human genome. *Nature* **489**, 75-82, doi:10.1038/nature11232 (2012).
21 Roadmap Epigenomics, C. *et al.* Integrative analysis of 111 reference human epigenomes. *Nature* **518**, 317-330, doi:10.1038/nature14248 (2015).
22 Chapuy, B. *et al.* Discovery and characterization of super-enhancer-associated dependencies in diffuse large B cell lymphoma. *Cancer cell* **24**, 777-790, doi:10.1016/j.ccr.2013.11.003 (2013).
23 Zhang, Y. *et al.* Model-based analysis of ChIP-Seq (MACS). *Genome biology* **9**, R137, doi:10.1186/gb-2008-9-9-r137 (2008).
24 Loven, J. *et al.* Selective inhibition of tumor oncogenes by disruption of super-enhancers. *Cell* **153**, 320-334, doi:10.1016/j.cell.2013.03.036 (2013).
25 Kim, T. K. *et al.* Widespread transcription at neuronal activity-regulated enhancers. *Nature* **465**, 182-187, doi:10.1038/nature09033 (2010).
26 Thompson, M. C. *et al.* Genomics identifies medulloblastoma subgroups that are enriched for specific genetic alterations. *Journal of clinical oncology : official journal of the American Society of Clinical Oncology* **24**, 1924-1931, doi:10.1200/JCO.2005.04.4974 (2006).
27 Cho, Y. J. *et al.* Integrative genomic analysis of medulloblastoma identifies a molecular subgroup that drives poor clinical outcome. *Journal of clinical oncology : official journal of the American Society of Clinical Oncology* **29**, 1424-1430, doi:10.1200/JCO.2010.28.5148 (2011).
28 Northcott, P. A. *et al.* Medulloblastoma comprises four distinct molecular variants. *Journal of clinical oncology : official journal of the American Society of Clinical Oncology* **29**, 1408-1414, doi:10.1200/JCO.2009.27.4324 (2011).
29 Kool, M. *et al.* Integrated genomics identifies five medulloblastoma subtypes with distinct genetic profiles, pathway signatures and clinicopathological features. *PloS one* **3**, e3088, doi:10.1371/journal.pone.0003088 (2008).
30 Jin, F. *et al.* A high-resolution map of the three-dimensional chromatin interactome in human cells. *Nature* **503**, 290-294, doi:10.1038/nature12644 (2013).
31 Pope, B. D. *et al.* Topologically associating domains are stable units of replication-timing regulation. *Nature* **515**, 402-405, doi:10.1038/nature13986 (2014).
32 Shih, D. J. *et al.* Cytogenetic prognostication within medulloblastoma subgroups. *Journal of clinical oncology : official journal of the American Society of Clinical Oncology* **32**, 886-896, doi:10.1200/JCO.2013.50.9539 (2014).
33 Dowen, J. M. *et al.* Control of cell identity genes occurs in insulated neighborhoods in mammalian chromosomes. *Cell* **159**, 374-387, doi:10.1016/j.cell.2014.09.030 (2014).
34 Hnisz, D. *et al.* Super-enhancers in the control of cell identity and disease. *Cell* **155**, 934-947, doi:10.1016/j.cell.2013.09.053 (2013).
35 Parker, S. C. *et al.* Chromatin stretch enhancer states drive cell-specific gene regulation and harbor human disease risk variants. *Proceedings of the National Academy of Sciences of the United States of America* **110**, 17921-17926, doi:10.1073/pnas.1317023110 (2013).
36 Whyte, W. A. *et al.* Master transcription factors and mediator establish super-enhancers at key cell identity genes. *Cell* **153**, 307-319, doi:10.1016/j.cell.2013.03.035 (2013).
37 Aruga, J. *et al.* Mouse Zic1 is involved in cerebellar development. *The Journal of neuroscience : the official journal of the Society for Neuroscience* **18**, 284-293 (1998).

38 Grinberg, I. *et al.* Heterozygous deletion of the linked genes ZIC1 and ZIC4 is involved in Dandy-Walker malformation. *Nature genetics* **36**, 1053-1055, doi:10.1038/ng1420 (2004).
39 Graf, T. & Enver, T. Forcing cells to change lineages. *Nature* **462**, 587-594, doi:10.1038/nature08533 (2009).
40 Lee, T. I. & Young, R. A. Transcriptional regulation and its misregulation in disease. *Cell* **152**, 1237-1251, doi:10.1016/j.cell.2013.02.014 (2013).
41 Liu, Z. *et al.* Age-dependent in vivo conversion of mouse cochlear pillar and Deiters' cells to immature hair cells by Atoh1 ectopic expression. *The Journal of neuroscience : the official journal of the Society for Neuroscience* **32**, 6600-6610, doi:10.1523/JNEUROSCI.0818-12.2012 (2012).
42 Saba, R., Nakatsuji, N. & Saito, T. Mammalian BarH1 confers commissural neuron identity on dorsal cells in the spinal cord. *The Journal of neuroscience : the official journal of the Society for Neuroscience* **23**, 1987-1991 (2003).
43 Fink, A. J. *et al.* Development of the deep cerebellar nuclei: transcription factors and cell migration from the rhombic lip. *The Journal of neuroscience : the official journal of the Society for Neuroscience* **26**, 3066-3076, doi:10.1523/JNEUROSCI.5203-05.2006 (2006).
44 Gilbertson, R. J. Mapping cancer origins. *Cell* **145**, 25-29, doi:10.1016/j.cell.2011.03.019 (2011).
45 Byrd, J. C. *et al.* Targeting BTK with ibrutinib in relapsed chronic lymphocytic leukemia. *The New England journal of medicine* **369**, 32-42, doi:10.1056/NEJMoa1215637 (2013).
46 Hale, G. *et al.* Remission induction in non-Hodgkin lymphoma with reshaped human monoclonal antibody CAMPATH-1H. *Lancet* **2**, 1394-1399 (1988).
47 Hovestadt, V. *et al.* Robust molecular subgrouping and copy-number profiling of medulloblastoma from small amounts of archival tumour material using high-density DNA methylation arrays. *Acta neuropathologica* **125**, 913-916, doi:10.1007/s00401-013-1126-5 (2013).
48 Bindea, G. *et al.* ClueGO: a Cytoscape plug-in to decipher functionally grouped gene ontology and pathway annotation networks. *Bioinformatics* **25**, 1091-1093, doi:10.1093/bioinformatics/btp101 (2009).
49 Brown, J. D. *et al.* NF-kappaB directs dynamic super enhancer formation in inflammation and atherogenesis. *Molecular cell* **56**, 219-231, doi:10.1016/j.molcel.2014.08.024 (2014).

Figure 1. The enhancer landscape of primary medulloblastoma.

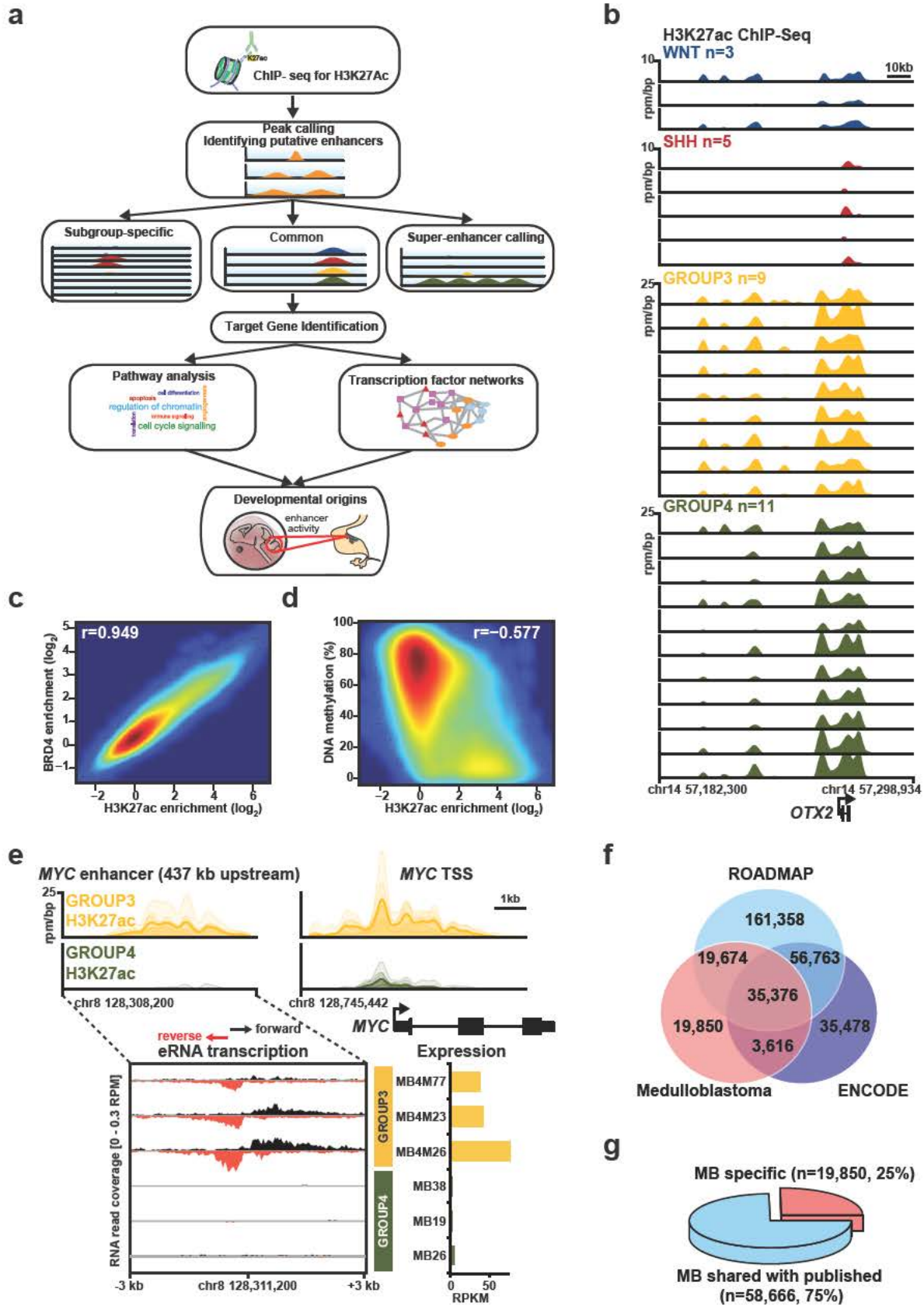

Figure 2. Differentially regulated enhancers and enhancer-gene assignments in medulloblastoma subgroups.

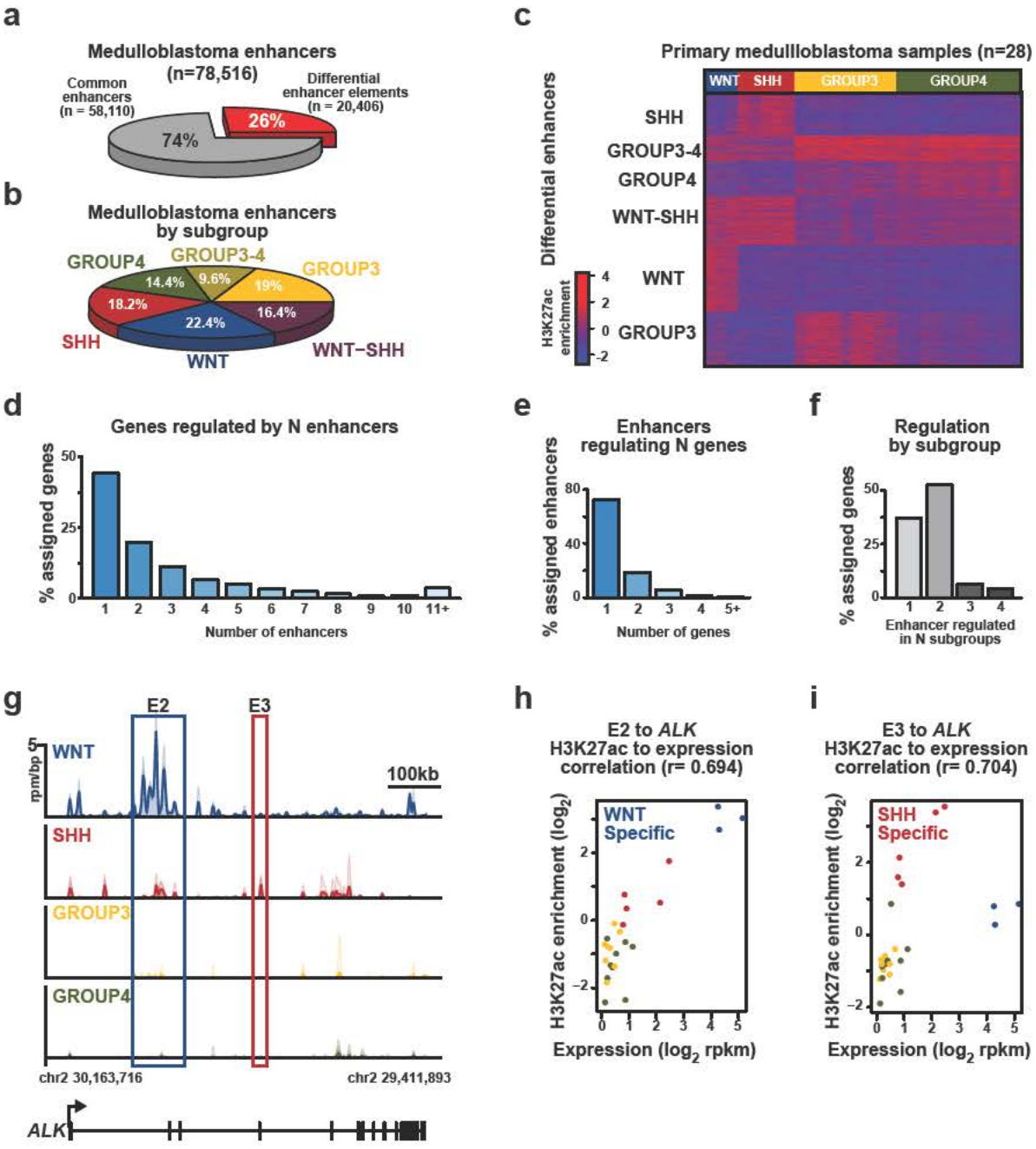

Figure 3. Functional characterization of enhancer-gene targets in medulloblastoma subgroups.

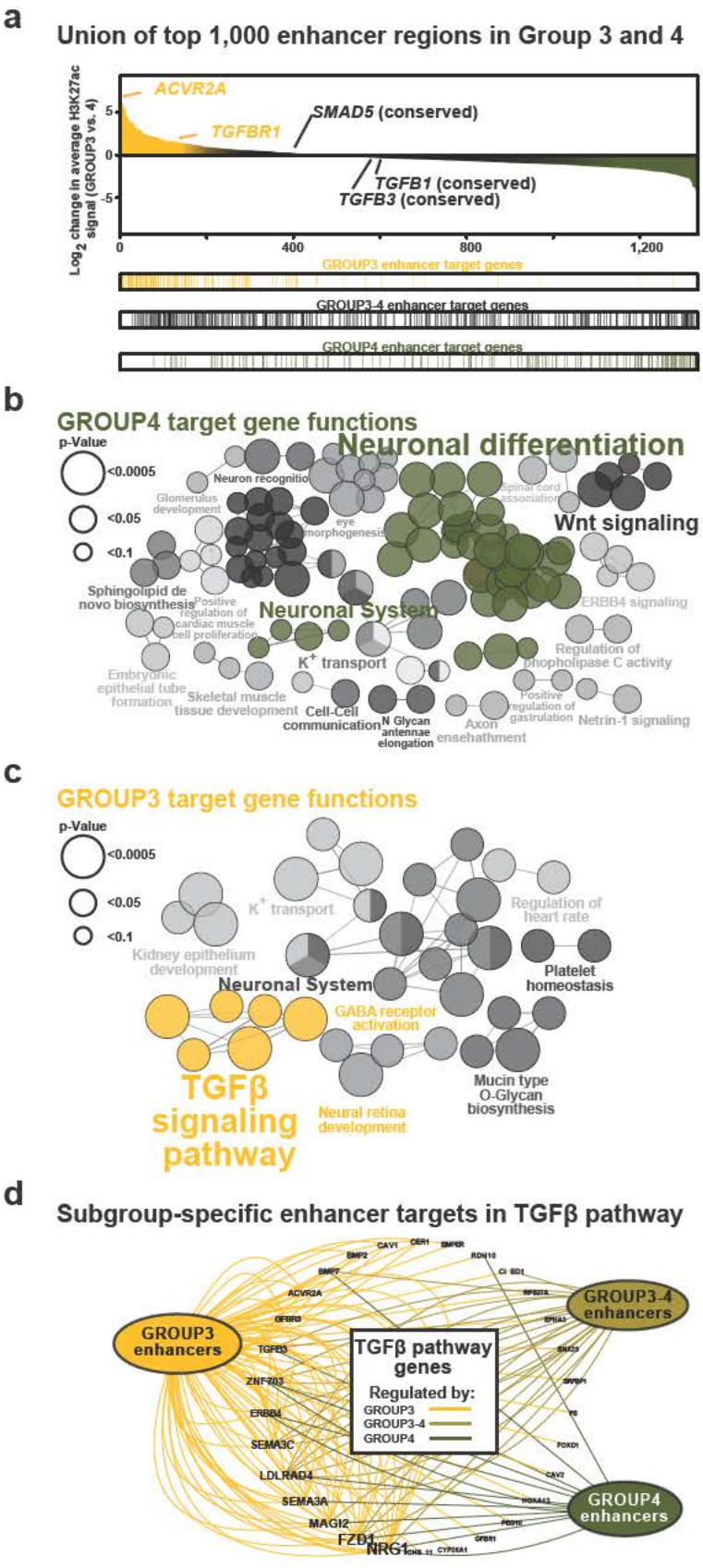

Figure 4. Medulloblastoma super-enhancers define subgroup-specific identity.

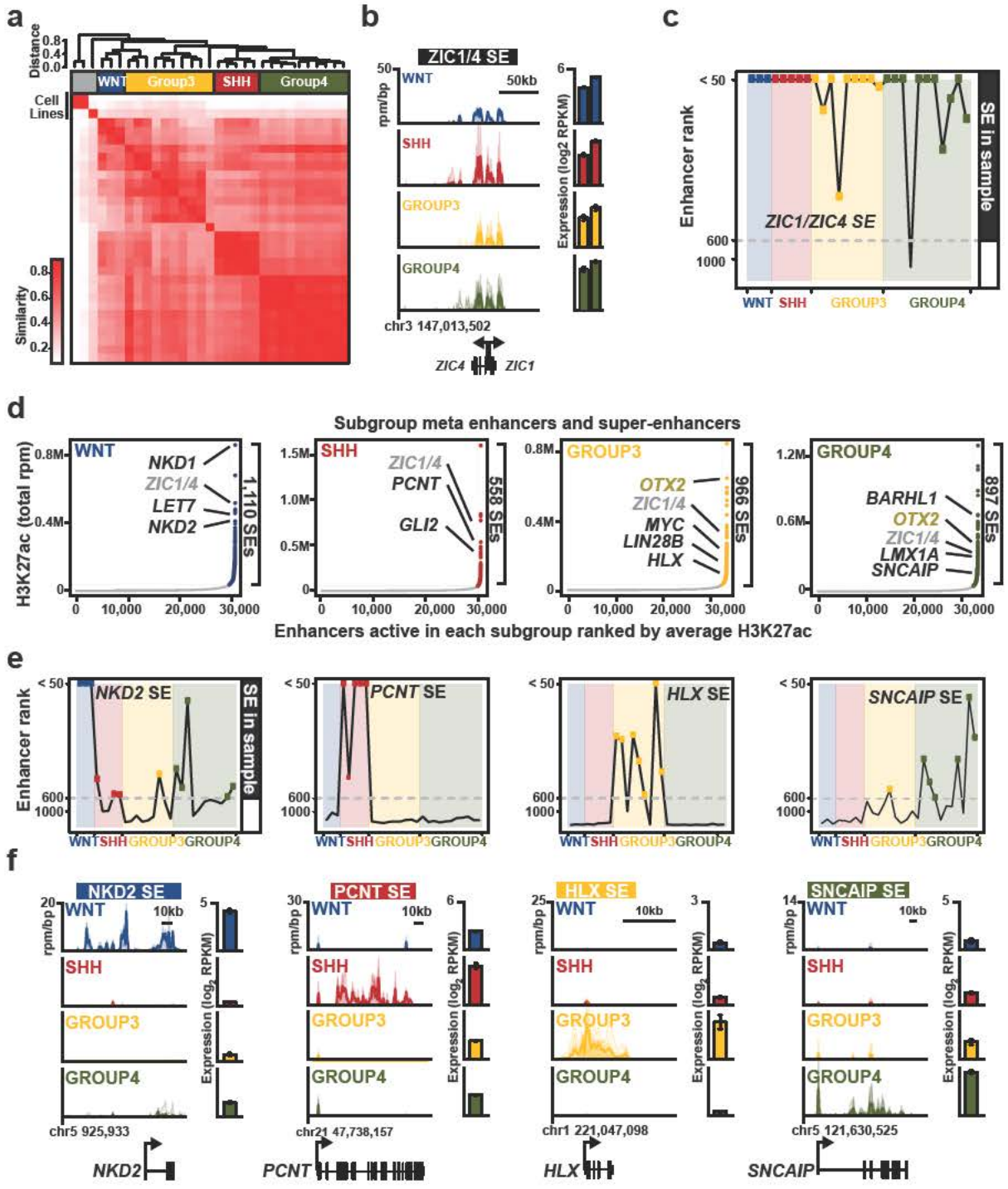

Figure 5. Super-enhancers define medulloblastoma regulatory circuitry and identify putative cellular origins.

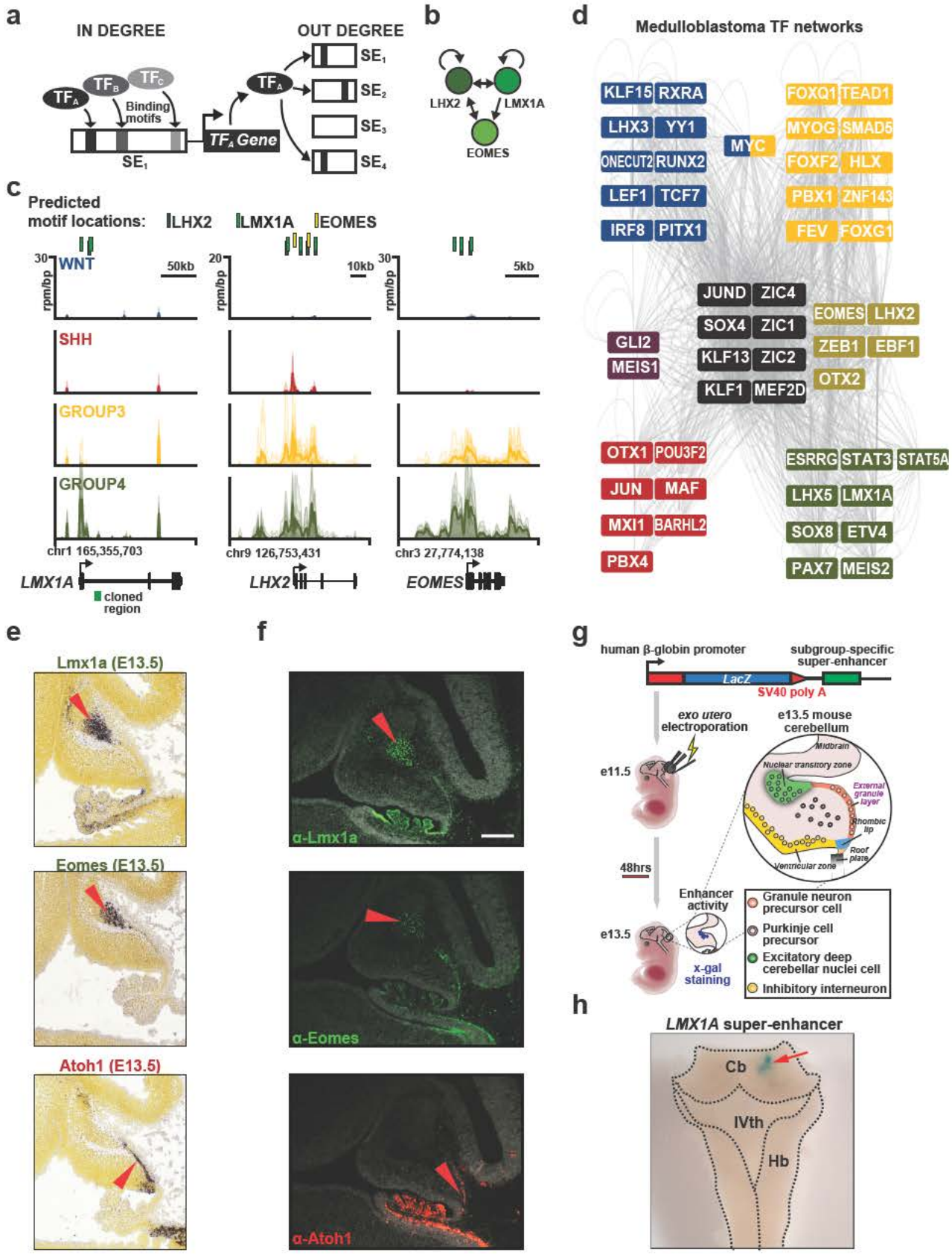

Review

CellPress

Taming of the beast: shaping Myc-dependent amplification

Elmar Wolf[1], Charles Y. Lin[2], Martin Eilers[1], and David L. Levens[3]

[1] Theodor Boveri Institute, Biocenter, and Comprehensive Cancer Center, University of Würzburg, Am Hubland, 97074 Würzburg, Germany
[2] Department of Medical Oncology, Dana Farber Cancer Institute, Harvard Medical School, Boston, MA 02115, USA
[3] Laboratory of Pathology, 10 Center Drive, Bethesda, MD 20892-1500, USA

Myc deregulation is a hallmark oncogenic event where overexpression of the transcription factor gives rise to numerous tumorigenic phenotypes. The complex consequences of Myc deregulation have prevented clear mechanistic interpretations of its function. A synthesis of recent experimental observations offers a consensus on the direct transcriptional function of Myc: when overexpressed, Myc broadly engages the established euchromatic *cis*-regulatory landscape of the cell, where the factor generally amplifies transcription. The level of Myc binding at target genes and the transcriptional output are differentially modulated by additional regulators, including Miz1. Targeting Myc oncogenic activity will require an understanding of whether amplification promotes tumorigenesis and the consequences of amplification in tumors adapted to oncogenic Myc.

Myc transcription in cancer

The intense interest in Myc proteins stems from their pervasive role in the genesis of human tumors. A large body of evidence has established that level of one out of three Myc proteins (c-Myc, N-Myc, or L-Myc) is enhanced and its expression released from its normally tight dependence on growth factors in a large fraction of all human tumors [1,2]. The three Myc genes are differentially expressed during development, but the proteins are functionally equivalent in most biological systems, allowing us to focus on c-Myc (called 'Myc' from here on) in this review [3]. Multiple experiments in transgenic models of human tumors show that this 'deregulated' expression of Myc proteins promotes tumorigenesis and that tumors generated by different oncogenes depend on elevated Myc levels [4]. Accordingly, several proof-of-principle studies suggest that targeting Myc proteins have considerable benefit for tumor therapy [5,6]. This hope awaits clinical confirmation, because therapies directed against Myc proteins have yet to enter the clinic. Myc proteins are nuclear proteins and, as such, may have several functions; however, there is consensus in the field that one major activity of Myc proteins is to regulate transcription [7]. This has stimulated a vigorous debate about why Myc-dependent transcription is so important for tumorigenesis. Here, we review the current state of this debate.

The evolution of Myc

One of the best-understood Myc transcription factor networks is that of *Drosophila*. dMyc, a basic helix-loop-helix leucine zipper protein (bHLH-Zip), binds together with a another bHLH-Zip protein, dMax, to target genes via a conserved sequence element termed an 'E-box' (CACGTG) and to activate transcription [8]. The dMyc antagonist dMnt, also pairs with dMax to repress transcription from the same DNA sequence [9]. Deletion of dMnt largely rescues the developmental defects of dMyc deletion, providing strong evidence that transcriptional activation is the critical biological function of dMyc [10]. Most target genes of dMyc and dMax encode proteins involved in RNA and protein synthesis [11]. Consistently, dMyc proteins stimulate cell growth, but not cell proliferation, and loss-of-function alleles show a 'minute' phenotype [8,12]. Transferring this model to mammalian tumorigenesis would suggest that the oncogenic activity of Myc is due to the deregulated and constitutive activation of its target genes. According to this model, sustained high levels of Myc in human tumors over-drive RNA biogenesis and protein translation, enabling growth factor-independent cell growth. Multiple observations are consistent with this model: for example, Myc-driven lymphomas, in contrast to their normal counterparts, rely on supraphysiological rates of protein translation to support growth [13].

Similar to *Drosophila* dMyc, mammalian Myc proteins, when dimerized with Max, are sequence-specific DNA-binding proteins that bind to E-boxes [7]. Unlike prokaryotic repressors that discriminate operator from nonoperator DNAs by approximately 10^{5-6}-fold, Max homodimers and, most likely, Myc/Max heterodimers have considerable affinity for variant E-boxes and even generic DNA [14]. Therefore, it is almost certain that Myc/Max heterodimers have non-negligible affinity for most promoters. Reflecting its continuum of association to targets, the intranuclear dynamics of Myc suggest engagement with intranuclear partners, indicating that Myc is globally distributed, is almost always bound directly or indirectly with chromatin, and is available to all active genes [15,16]. While broadly anticipated, there is currently only limited formal evidence that transcriptional activation is the critical oncogenic

Corresponding authors: Lin, C.Y. (Charles_lin@dfci.harvard.edu); Eilers, M. (martin.eilers@biozentrum.uni-wuerzburg.de); Levens, D.L. (levens@helix.nih.gov).
Keywords: Myc; cancer; transcription.

0962-8924/
 http://dx.doi.org/10.1016/j.tcb.2014.10.006

function of Myc. One example is the finding that inactivation of Mga, a repressive partner protein of Max, occurs commonly, but mutually exclusively with focal amplification of the Myc gene in lung cancer, suggesting that Mga inactivation is pathologically equivalent to Myc overexpression in this entity [17].

Clues to how Myc regulates gene expression are provided in the list of co-activators it recruits to induce transcription: a conserved sequence in Myc (MycBoxII) binds the adaptor protein Transformation/transcription domain-associated protein (TRRAP) via TRRAP GCN5-containing histone acetylase complexes [18,19]. Myc also recruits the p300 histone acetylase and other histone-modifying enzymes to its target sites, although the requisite interaction surfaces on Myc are less well defined [20,21]. Myc also interacts with TATA box binding protein (TBP) [22] and the chromatin regulators Tip60 [23] and switch/sucrose nonfermentable (SWI/SNF) [24], and inhibits the H3 trimethyl K4 (H3K4Me3) demethylase dKDM5/LID [25]. The ability of Myc to interact with and recruit a multitude of general chromatin regulators is consistent with its global role in regulating chromatin structure because Myc activity has been broadly linked with large nuclei/nucleoli containing high levels of euchromatic and hyperacetylated chromatin [18,26].

Myc may also interact directly with the transcription apparatus. Most notably, the extreme amino-terminus of Myc binds cyclin T1 *in vitro* [27]. Cyclin T1 is part of the positive transcription elongation factor b (P-TEFb) elongation complex, which phosphorylates the C-terminal domain of RNA polymerase at serine 2 and thereby promotes the transition from promoter binding to productive elongation. The relevance of this finding stems from observations that Myc can stimulate transcription at a step after initiation of transcription and that RNA polymerase II accumulates in the body of transcribed genes after activation of Myc [28–30]. Furthermore, ectopic expression of Myc globally enhances phosphorylation of RNA polymerase [30,31]. Together, these observations suggest that the release of RNA polymerase from a paused position is a key mechanism of transcriptional activation by Myc [30] (Figure 1). There is no doubt that other effectors of Myc remain to be defined. How Myc exploits these partners individually or in combination at any given promoter is not yet known.

The general amplifier model

The identification of Myc as a transcriptional activator raised the expectation that enumeration of the direct target genes of Myc would provide a list of critical downstream targets and biological processes that mediate the physiological and oncogenic functions of Myc. This expectation prompted a series of studies to identify the Myc-regulated genes by comparing RNA expression profiles and the genome-wide map of Myc-bound chromatin using microarray or next generation sequencing technology. Interrogation of a range of cell types surprisingly revealed mammalian Myc proteins at nearly all promoters in open chromatin [32]. This was not only true for genes transcribed by RNA polymerase II, but also for genes transcribed by RNA polymerases I and III (although rRNA promoters tend to bind less Myc compared with other promoters) [33,34]. For RNA polymerase II-transcribed genes, the presence of histone marks indicative of open chromatin, in particular H3K4Me3, highly correlated with Myc binding [35]. When overexpressed, Myc proteins also bound to many enhancers, again correlating with histone marks indicative of activity. Given that many genes encoding proteins involved in translation (e.g., ribosomal protein genes) are highly transcribed from promoters in CpG islands where E-boxes are more frequently found in an

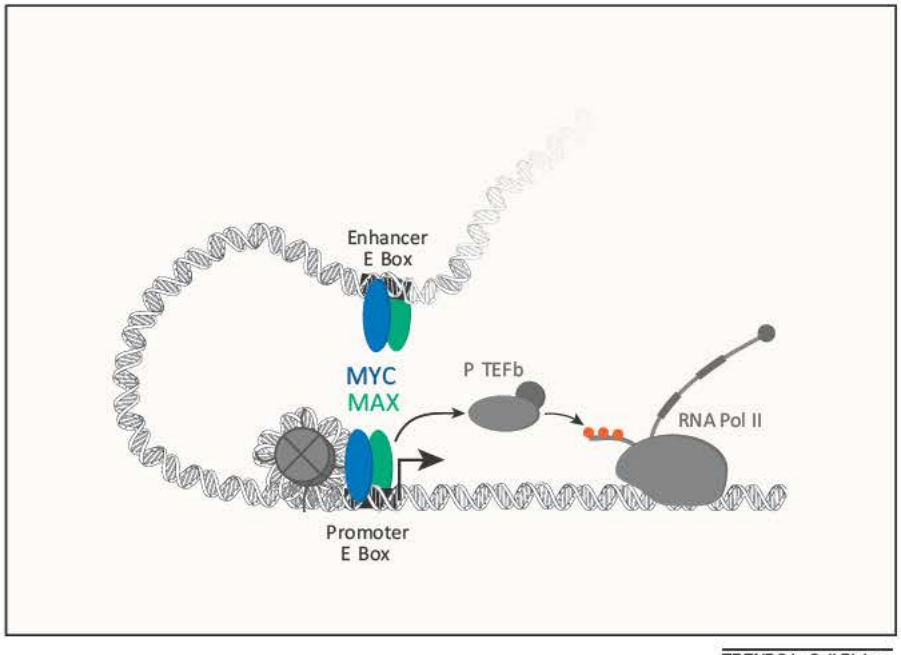

Figure 1. Schematic of transcription elongation promoting activity of MYC. MYC/MAX bind to E-box (CACGTG) sequences at enhancers and promoters and recruit the elongation factor complex positive transcription elongation factor b (P-TEFb), which promotes elongation in part by phosphorylating the C-terminal domain of RNA Polymerase II (RNA Pol II).

open chromatin conformation, these results parallel those obtained in *Drosophila*.

Collectively, these data have led to an exciting model in which Myc proteins act as general amplifiers that globally enhance transcription; the specificity and degree of amplification at individual genes is determined by the exact pattern of open promoters that pre-exists in a cell even before Myc activation [36,37]. In this model, the unique biological role of Myc stems from the ability to accelerate transcriptional activation (i.e., releasing a paused RNA polymerase from the promoter) rather than by specifying a particular program of gene expression [30]. Strong support for this model comes from the analysis of primary B cells [36]. Upon stimulation of resting B cells, Myc binds to all promoters of transcriptionally active genes in these cells and Myc binding follows the pattern of loading of RNA polymerase II that pre-exists in resting low Myc cells. In response to mitogen stimulation, there is a global increase in mRNA levels that depends on Myc, which has been confirmed by examining the mRNA levels of multiple individual genes. There are indications that the 'global amplifier' model operates not only in primary cells, but also in tumors. Comparing normal B cells with Myc-driven B cell lymphomas revealed a strong increase in total cellular mRNA content in lymphomas [38]. ChIP sequencing shows that Myc binds to 90% of all open promoters in lymphomas; an easy explanation might be that Myc broadly enhances expression of the genes to which it binds and this increases cellular mRNA content. Similarly, the comparison of human tumor cell lines with different Myc levels suggests that Myc-driven amplification accounts for differences in mRNA content between different tumor cells [37].

According to a strict amplifier model, the direct effect of Myc on promoters is always positive. The effect of Myc is not equally strong for each gene because promoters and relevant enhancers differ in their affinity for Myc: promoter binding dictates the differences in response. Moreover, the overall promoter response to Myc is not directly proportional to the amount Myc recruited there. Furthermore, at high and oncogenic levels, Myc 'invades' enhancers and promoters, enabling the pathological regulation of genes that bind little Myc at physiological levels [37–39]. Therefore, the general amplifier model can account for the observation that oncogenic levels of Myc regulate a specific set of genes in particular tumors [40]. The model can also account for apparent Myc-dependent repression. Specifically, if expression of most mRNAs is amplified and, therefore, if total mRNA content increases in a cell upon Myc stimulation, then the relative amount of mRNAs transcribed from genes that have low-affinity promoters and, thus, are poorly activated genes will decrease and, depending on the mode of normalization, these genes will appear repressed [41]. Hence, whether the general amplifier model can account for Myc-dependent repression is intimately tied to the question of whether Myc induces a general increase in cellular RNA levels and, by inference, whether cells grow as a result of Myc activation: if cells grow, seemingly repressed genes may in fact be low-affinity Myc targets that are relatively 'left behind' [41]. Myc drives both growth and proliferation of mammalian cells, unlike in *Drosophila* [42]. Given that cell proliferation and division reduce cell size, some of the apparent Myc-dependent repression may reflect the postmitotic partition of cellular contents compared with nondividing cells; therefore, a complete description of amplification will be sensitive to cell cycle parameters. Furthermore, if Myc acts at transcription, then gauging Myc action from mRNA abundance is imprecise because mRNA synthesis becomes conflated with mRNA half-lives, and cell cycle parameters. Yet, this too becomes even more complicated because the factors that regulate mRNA stability and the cell cycle may themselves be important direct or indirect Myc targets.

An important aspect of the amplifier model is the postulate that, in any given cell type, all transcription initiating genes are potential targets of Myc: individual promoters differ quantitatively in their affinity for Myc, but no sharp cut-off discriminates Myc targets from nontargets. Occupancy at each promoter changes as Myc concentrations vary and this change defines the degree of the transcriptional response. We suggest that there is a continuum of activity as Myc flickers on and off of weakly bound, weakly expressed promoters, but stays longer or more frequently at high output promoters (Figure 2). This view of Myc as a general regulator capable of interacting with all active promoters has implications for the way that ChIP sequencing data need to be interpreted, because it suggests that cut-offs that are introduced by analysis (e.g., peak-calling) programs generate artificial distinctions between target and nontarget genes.

This quantitative view also suggests that, in some experimental settings, the response of some genes to Myc plateaus as occupancy by Myc at promoters and enhancers and corresponding transcriptional output is saturated. Whereas Myc abundance is low in most, but not all primary cells (luminal cells in mammary ducts are a notable exception), recent estimates for Myc in tumor cells appear high enough to allow the saturation of some promoters [37]. A recent study provides evidence that high-affinity promoters are Myc saturated in proliferating cells and, therefore, that further increases in Myc only increase occupancy and gene expression at low-affinity promoters [39]. As a result, gene expression patterns that discriminate cells with oncogenic Myc levels from normally proliferating cells are different from the gene expression changes that occur as Myc-levels increase during the physiological transition from quiescence to proliferation.

These considerations allow the conclusion that, even within the framework of the general amplifier model, the observed effects of Myc on gene expression depend on: (i) the precise Myc levels that are being compared; (ii) whether cells grow upon Myc activation; and (iii) the precise pattern of ongoing transcription that determines which genes are accessible to Myc.

Direct and indirect transcriptional repression

In many studies, almost as many genes are downregulated by Myc as are upregulated, evoking the notion that Myc can act as a repressor [38,43]. Setting aside pseudodownregulation arising from normalization issues (above), such downregulation can stem from a direct and context-dependent repressive function of Myc that is unmasked by factors bound locally at the regulatory sequences of

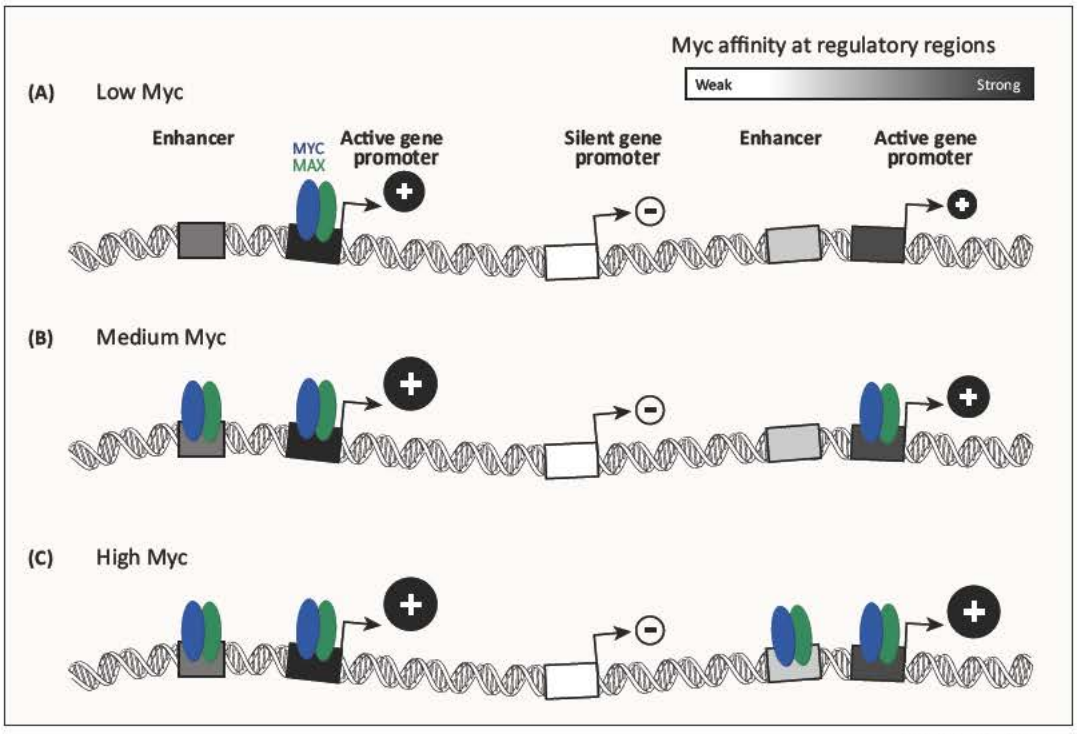

Figure 2. Schematic of MYC genomic binding at **(A)** low, **(B)** medium, and **(C)** high concentrations of the factor. *Cis*-regulatory elements (boxes) are shaded by their affinity for Myc. Myc transcriptional activity at genes is depicted as a circle sized by the impact of Myc.

particular target genes. For example, Myc blunts the induction of the cyclin-dependent kinase 4 inhibitor B (*CDKN2B*) and *CDKN1A* genes in response to transforming growth factor (TGF)-β signaling by a direct interaction with the Miz1 and Smad3 proteins at both promoters [44,45]. Alternatively, repression can be indirect; as a universal amplifier, Myc will increase the expression of repressive transcriptional and chromatin components. As repressors are upregulated, downregulation of sets of targets may ensue as the system seeks a new steady state. For example, Myc-upregulated phosphatase and tensin homolog (PTEN) inactivates Akt, which disinhibits enhancer of zeste homolog 2 (Ezh2), promoting widespread polycomb repressive complex 2 (PRC2)-mediated repression [46]. Furthermore, miRNAs, such as miR17-92 that represses SIN3 transcription regulator family member B (Sin3b), HMG-box transcription factor 1 (Hbp1), suppressor of variegation 4-20 homolog 1 (Suv420h1), and B cell translocation gene 1 (Btg1) to regulate chromatin structure as well as the apoptosis facilitator Bim [47], are repressive mediators of Myc action. Direct and indirect mechanisms may become entangled as feedforward and feedback arms of genetic circuits adjust to new conditions. In principle, the dynamics of the temporal profile of the transcriptome could help to discriminate direct from indirect regulation, because changes requiring newly synthesized protein intermediaries are expected to be delayed relative to the induction of Myc protein. However, few studies have had the temporal resolution to discriminate direct versus indirect targets. Given that they are translation independent, miRNAs and other noncoding RNAs are likely to act after only a brief delay. This rapid onset of activity is likely to hinder the discrimination of the direct and indirect effects of Myc.

Shaping transcriptional amplification

Transcriptional amplification and cell growth induced by Myc cannot continue indefinitely and unopposed. Therefore, mechanisms must exist that adjust transcriptional amplification to available metabolic resources and that provide feedback from the physiological status of a cell to Myc activity. Consequently, supraphysiological levels of Myc would be expected to elicit either compensatory measures or, if they fail, promote cell death. As Myc saturates its strongest and most highly expressed sites (these being most likely to be physiological targets), it may pathologically spill over onto other promoters and enhancers, increasing their activity and overall cellular RNA production, provided that the cell can marshal sufficient resources to augment net transcription.

There is evidence for feedback mechanisms that limit Myc-dependent transactivation operating at both physiological and supraphysiological levels. The apoptosis elicited by overexpression provides an example of an upper-bound limit for Myc levels [48]. As another example, the ribosomal protein L11, encoded by a direct target gene of Myc, inhibits Myc-dependent transactivation and expression [49,50]. Supraphysiological levels of Myc induce expression of the Arf tumor suppressor protein, which in turn interacts with Myc and inhibits Myc-dependent transactivation [51,52]. One broadly acting mechanism that limits transcriptome amplification driven by supraphysiological Myc is the recruitment of the zinc finger protein Miz1 at many promoters [53]. In primary cells, and in the

absence of high levels of Myc, Miz1 is a highly sequence-specific transcription factor that activates a relatively small number of targets that share an extended consensus sequence and that control autophagy [54]. As Myc levels rise to supraphysiological levels, Miz1 joins Myc via a protein–protein interaction at a large fraction of promoters that then decreases output [39]. Miz1 is unstable and continuously degraded by the Huwe1 ubiquitin ligase [55]; upon inhibition of Huwe1, Miz1 broadly accumulates at Myc-bound promoters, blunts activation, and enhances repression by Myc [55,56]. Interestingly, the Arf protein binds to, and inhibits, Huwe1 and promotes association of Myc with Miz1 [57,58], strongly suggesting that Arf and Miz1 are part of a common stress response to oncogenic Myc levels.

A second mechanism that is likely to limit and shape Myc amplification is competition between Myc and other bHLH-Zip dimers for binding at E-boxes and perhaps at other sites (Figure 3). Myc-Max operates against Max homodimers as well as heterodimers of Max with repressive members of the bHLH-Zip family (Mxd1-4, Mnt, etc) [9–11]. The degree to which the levels of these other complexes alter the physical distribution and activity of Myc at E-box versus non-E-box promoters remains to be rigorously evaluated. The specialized regulation of these other E-box-binding proteins (such as Mondo) have the capacity to tune the Myc response toward or away from cellular processes, such as metabolism [59] or circadian rhythms via coupling with proteins such as CLOCK [60].

Almost certainly, steady-state patterns of gene expression observed after Myc expression do not only reflect the direct action of Myc, but are also due to secondary effects of proteins or RNAs encoded by Myc target genes that feed back on gene expression [38]. In a rapidly growing cell, such as a B cell becoming activated from the naïve state, increasing synthesis of macromolecules is required to satisfy a growing demand for the transcription machinery and other components required to activate genes. Examples for such indirect effects are the induction of the Gcn5 histone acetylase that mediates a global opening of chromatin upon Myc expression and enhanced expression of phosphoribosyl-pyrophosphate synthetase 2 (PRPS2), which promotes the enhanced nucleotide biosynthesis of Myc-driven tumors [18,26,61]. At the same time, rapid growth and enhanced global transcription may induce the redeployment of limiting components of the gene expression machinery to more or less active transcription start sites. Under conditions of limiting gene expression components, increasing Myc at strongly expressed promoters might recruit transcription

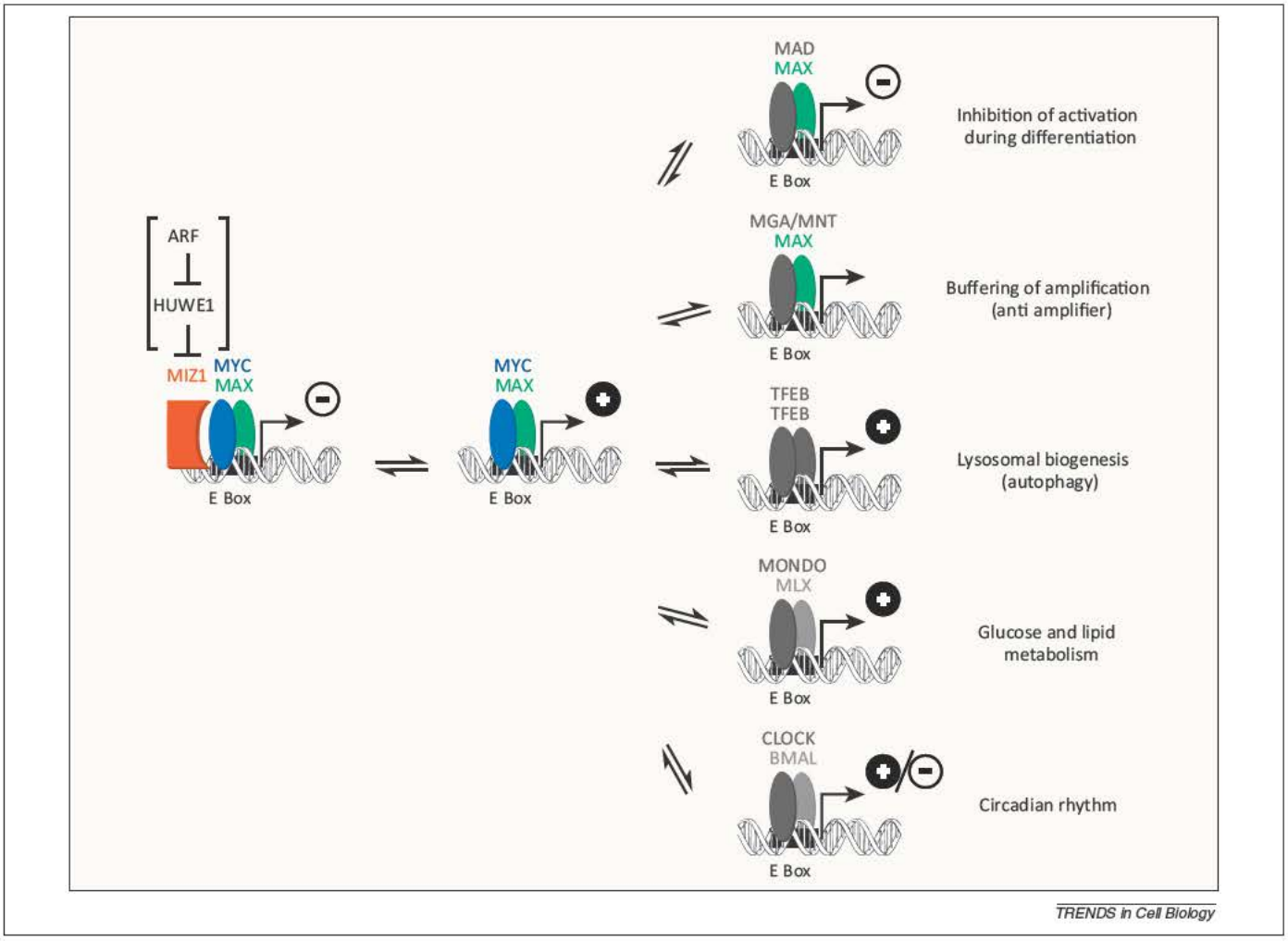

Figure 3. Schematic showing the dynamic occupancy of E-box sites by Myc and other transcriptional regulators. Multiple basic helix-loop-helix (bHLH) transcription factor pairings compete for binding at E-box sites. The net positive or negative transcriptional consequence of regulator binding at E-boxes is depicted. For definitions of abbreviations, please see the main text.

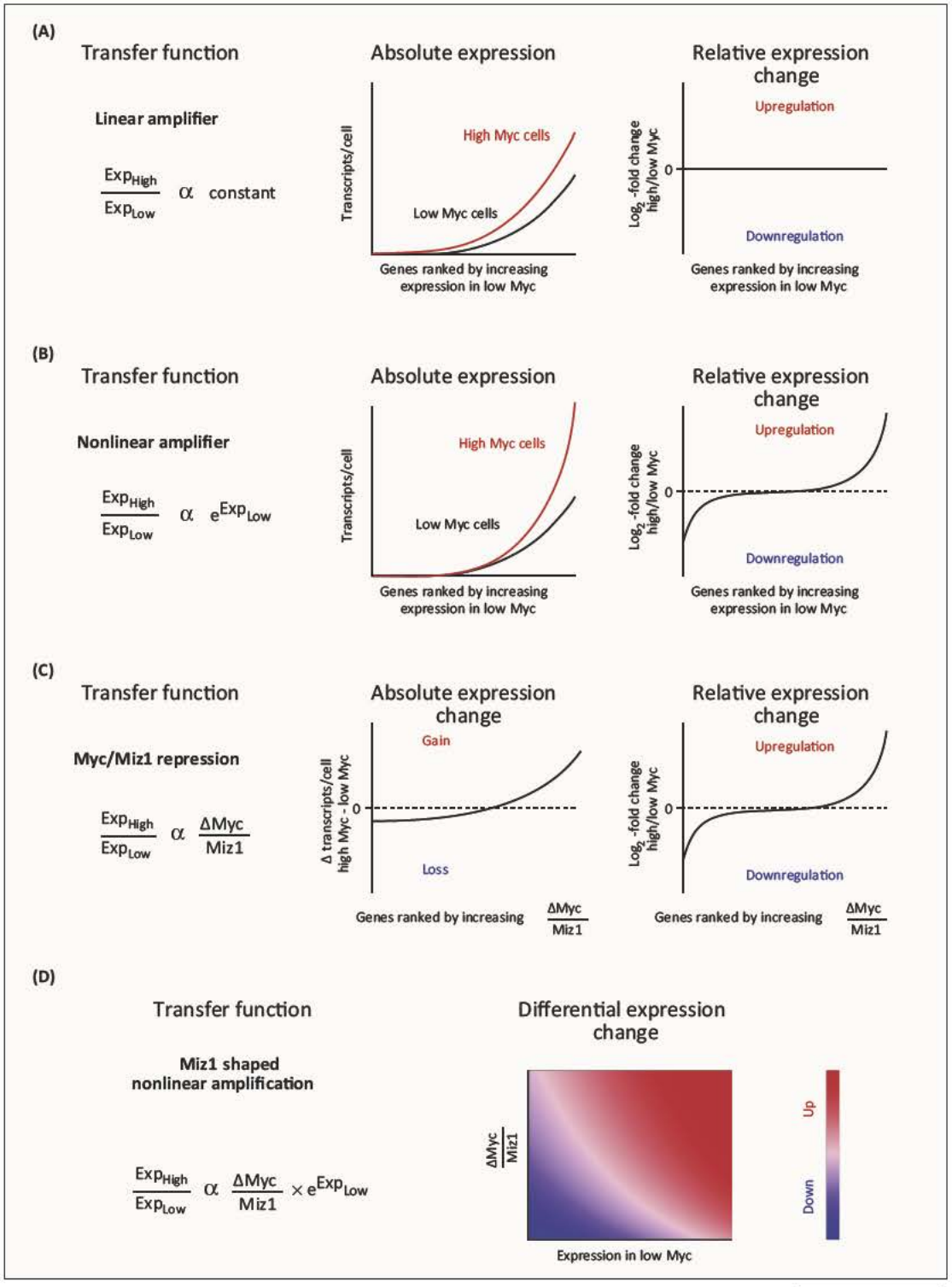

Figure 4. Schematic of Myc transfer functions. Transfer functions are shown providing the relation between expression changes at genes as a function of various parameters as measured either by absolute or relative change in expression. **(A)** A linear amplifier transfer function where the change in expression in high versus low Myc conditions is constant across all transcriptionally active genes. **(B)** A nonlinear amplifier transfer function where the change in expression in high versus low Myc conditions is proportional to the exponent of the expression in low Myc conditions. **(C)** A Myc/Miz1 repression transfer function where the change in expression is proportional to the ratio of ΔMyc binding divided by Miz1 binding. **(D)** A combined Miz1-shaped nonlinear amplifier model that combines the transfer functions in (B) and (C). A 2D heatmap is provided showing the relative change in expression as a function of both the ratio of ΔMyc binding divided by Miz1 binding (y-axis) and the initial expression in low Myc conditions (x-axis).

machinery otherwise assigned to weakly transcribed genes. Such diversion would yield the upregulation of some genes with the downregulation of others. This repression by redistribution of the transcriptional machinery has been recently observed during nuclear factor (NF)-κB activation in endothelial cells [62].

In principle, other mechanisms may act to counterbalance transcriptome amplification. For example, in yeast, rates of RNA synthesis and RNA degradation are coupled [63]. Mutations and strategies that alter the levels of one elicit compensatory changes in the other. Additional amplification counteracting pressures may arise from rate limiting levels of translation initiation in tumors. Notably, disruption of the translation initiation factor eukaryotic translation initiation factor 4 (eIF4F) is synthetic lethal in tumors with deregulated Myc, suggesting that the high levels of mRNA output need to be supported by high levels of protein expression, perhaps exposing an orthogonal vulnerability arising due to amplification [64]. For RNA levels to rise globally in response to MYC deregulation, these compensatory countermeasures may need to be defeated or overwhelmed.

Concluding remarks

Deregulated in tumors, Myc acts as a universal regulator of the pre-existing gene expression program of the cell. Whether amplification alone provides a sufficient oncogenic impulse or whether Myc-dependent repressive mechanisms are required for Myc-driven tumorigenesis warrants further investigation. Simply, as a universal regulator, mutations in other oncogenes and tumor suppressors must first specify particular genes to be turned on or off, and Myc then develops the new gene expression program. This model is also consistent with data in iPS reprogramming, where Myc overexpression increases the efficiency of an embryonic stem cell specifying Octamer 4/SRY (sex determining region Y)-box 2/Kruppel-like factor 4 (Oct4/Sox2/Klf4) transcription factors [65]. Alternatively, the pathways for growth, proliferation, apoptosis, and neoplastic metabolism do not scale linearly (i.e., increasing the components of these pathways drives them across thresholds that gate their activity as a step function). In this situation, malignant behavior would manifest as an emergent property explainable by the control theory (Box 1) and architecture of subsystems and networks whose components are upregulated by Myc.

Although predominantly an amplifier of transcription, context-specific conditions and constraints at individual genes modulate Myc transcriptional output and response. To elucidate the molecular mechanism of Myc-driven transcriptome amplification, a better description of its transfer function (the function describing how the Myc transcriptional effect depends on initial parameters at any gene; i.e., the input–output curve) will be required to account for its physiological and pathological activities. If proportional and linear, for example, all Myc targets will be upregulated equivalently, and any changes in the relative expression of particular genes would demand parallel changes in the levels of the gene-specific factors that differentially up- or downregulate these targets (Figure 4A). However, if the transfer function is nonlinear, as proposed in [66], then different zones across the expression spectrum will be disproportionately regulated. If highly expressed genes are preferentially amplified, then a Myc signature may emerge comprising genes that are highly expressed across many tissues (Figure 4B). Of course, such amplification cannot continue indefinitely and unopposed; supraphysiological levels of Myc are expected to elicit either compensatory measures or cell death (Figure 4C). Increasing amplification of all genes demands that the cell can marshal sufficient resources to augment net transcription. In the presence of limiting materials, the competition between promoters may modify the transfer function from one that supports only universal amplification to one that allows for repression at those promoters deprived of limiting factors that have been deployed to support the expression of other targets. In this scheme, repression (e.g., Miz1-dependent repression) reflects feedback control that responds to the unbalanced and excessive Myc-enforced expression of other targets (Figure 4D).

Universal activation by Myc does not preclude the functional emergence of preferred and, hence, specific targets. Moreover, the preferential up- or downregulation of specific genes that occurs as tumors achieve homeostasis in high Myc conditions may underlie the ability of Myc to act as one of the rare universal oncogenes capable of promoting tumorigenesis in a wide variety of tissues. Only when experiments challenge models that make quantitative, precise, and testable predictions will a durable consensus on the role of Myc emerge. Beyond having heuristic value as an organizing framework for diverse observations, the universal nonlinear amplifier model may yet account for quantitative differences in gene expression between cell states in health and disease.

Box 1. Control theory

Control theory is a dynamic analysis of network behavior as modeled by the effect of inputs and their consequent feedback on system output. In engineering, this can describe how different components affect the output of a system. For instance, a compressor either boosts or dampens signal depending on initial input signal. A reverb module would apply a delay to an input signal before entering it back into the system, creating a recursive feedback loop. An amplifier increases signal by an amount relative to the initial input signal. In each of these examples, the transformations are surmised through the transfer function: a mathematical representation of the relation between input and output. Thus, a control theory analysis of Myc examines the consequence of adding Myc to the transcriptional system. The Myc transfer function describes the transcriptional output of Myc activity as a function of the initial transcription parameters.

References

1 Dang, C.V. (2012) MYC on the path to cancer. *Cell* 149, 22 35
2 Meyer, N. and Penn, L.Z. (2008) Reflecting on 25 years with MYC. *Nat. Rev. Cancer* 8, 976 990
3 Kc, W. *et al.* (2014) L-Myc expression by dendritic cells is required for optimal T-cell priming. *Nature* 507, 243 247
4 Gabay, M. *et al.* (2014) MYC activation is a hallmark of cancer initiation and maintenance. *Cold Spring Harb. Perspect. Med.* 4, a014241
5 Soucek, L. *et al.* (2008) Modelling Myc inhibition as a cancer therapy. *Nature* 455, 679 683
6 Soucek, L. *et al.* (2013) Inhibition of Myc family proteins eradicates KRas-driven lung cancer in mice. *Genes Dev.* 27, 504 513
7 Eilers, M. and Eisenman, R.N. (2008) Myc's broad reach. *Genes Dev.* 22, 2755 2766
8 Gallant, P. *et al.* (1996) Myc and Max homologs in *Drosophila*. *Science* 274, 1523 1527

9 Loo, L.W. *et al.* (2005) The transcriptional repressor dMnt is a regulator of growth in *Drosophila melanogaster*. *Mol. Cell. Biol.* 25, 7078 7091
10 Pierce, S.B. *et al.* (2008) *Drosophila* growth and development in the absence of dMyc and dMnt. *Dev. Biol.* 315, 303 316
11 Orian, A. *et al.* (2003) Genomic binding by the Drosophila Myc, Max, Mad/Mnt transcription factor network. *Genes Dev.* 17, 1101 1114
12 Johnston, L.A. *et al.* (1999) Drosophila myc regulates cellular growth during development. *Cell* 98, 779 790
13 Barna, M. *et al.* (2008) Suppression of Myc oncogenic activity by ribosomal protein haploinsufficiency. *Nature* 456, 971 975
14 Sauve, S. *et al.* (2007) The mechanism of discrimination between cognate and non-specific DNA by dimeric b/HLH/LZ transcription factors. *J. Mol. Biol.* 365, 1163 1175
15 Rosales, T. *et al.* (2013) Partition of Myc into immobile vs. mobile complexes within nuclei. *Sci. Rep.* 3, 1953
16 Izeddin, I. *et al.* (2014) Single-molecule tracking in live cells reveals distinct target-search strategies of transcription factors in the nucleus. *Elife* Published online June 12, 2014, http://dx.doi.org/10.7554/eLife.02230
17 The Cancer Genome Atlas Research Network (2014) Comprehensive molecular profiling of lung adenocarcinoma. *Nature* 511, 543 550
18 McMahon, S.B. *et al.* (2000) The essential cofactor TRRAP recruits the histone acetyltransferase hGCN5 to c-Myc. *Mol. Cell. Biol.* 20, 556 562
19 McMahon, S.B. *et al.* (1998) The novel ATM-related protein TRRAP is an essential cofactor for the c-Myc and E2F oncoproteins. *Cell* 94, 363 374
20 Ullius, A. *et al.* (2014) The interaction of MYC with the trithorax protein ASH2L promotes gene transcription by regulating H3K27 modification. *Nucleic Acids Res.* 42, 6901 6920
21 Vervoorts, J. *et al.* (2003) Stimulation of c-MYC transcriptional activity and acetylation by recruitment of the cofactor CBP. *EMBO Rep.* 4, 484 490
22 Hateboer, G. *et al.* (1993) TATA-binding protein and the retinoblastoma gene product bind to overlapping epitopes on c-Myc and adenovirus E1A protein. *PNAS* 90, 8489 8493
23 Frank, S.R. *et al.* (2003) MYC recruits the TIP60 histone acetyltransferase complex to chromatin. *EMBO Rep.* 4, 575 580
24 Cheng, S.W. *et al.* (1999) c-MYC interacts with INI1/hSNF5 and requires the SWI/SNF complex for transactivation function. *Nat Genet.* 22, 102 105
25 Secombe, J. *et al.* (2007) The Trithorax group protein Lid is a trimethyl histone H3K4 demethylase required for dMyc-induced cell growth. *Genes Dev.* 21, 537 551
26 Knoepfler, P.S. *et al.* (2006) Myc influences global chromatin structure. *EMBO J.* 25, 2723 2734
27 Eberhardy, S.R. and Farnham, P.J. (2002) Myc recruits P-TEFb to mediate the final step in the transcriptional activation of the cad promoter. *J. Biol. Chem.* 277, 40156 40162
28 Eberhardy, S.R. and Farnham, P.J. (2001) c-Myc mediates activation of the cad promoter via a post-RNA polymerase II recruitment mechanism. *J. Biol. Chem.* 276, 48562 48571
29 Bouchard, C. *et al.* (2007) FoxO transcription factors suppress Myc-driven lymphomagenesis via direct activation of Arf. *Genes Dev.* 21, 2775 2787
30 Rahl, P.B. *et al.* (2010) c-Myc regulates transcriptional pause release. *Cell* 141, 432 445
31 Cowling, V.H. and Cole, M.D. (2007) The Myc transactivation domain promotes global phosphorylation of the RNA polymerase II carboxy-terminal domain independently of direct DNA binding. *Mol. Cell. Biol.* 27, 2059 2073
32 Chen, X. *et al.* (2008) Integration of external signaling pathways with the core transcriptional network in embryonic stem cells. *Cell* 133, 1106 1117
33 Gomez-Roman, N. *et al.* (2003) Direct activation of RNA polymerase III transcription by c-Myc. *Nature* 421, 290 294
34 Grandori, C. *et al.* (2005) c-Myc binds to human ribosomal DNA and stimulates transcription of rRNA genes by RNA polymerase I. *Nat. Cell Biol.* 7, 311 318
35 Guccione, E. *et al.* (2006) Myc-binding-site recognition in the human genome is determined by chromatin context. *Nat. Cell Biol.* 8, 764 770
36 Nie, Z. *et al.* (2012) c-Myc is a universal amplifier of expressed genes in lymphocytes and embryonic stem cells. *Cell* 151, 68 79
37 Lin, C.Y. *et al.* (2012) Transcriptional amplification in tumor cells with elevated c-Myc. *Cell* 151, 56 67
38 Sabo, A. *et al.* (2014) Selective transcriptional regulation by Myc in cellular growth control and lymphomagenesis. *Nature* 511, 488 492
39 Walz, S. *et al.* (2014) Activation and repression by oncogenic Myc shape tumour-specific gene expression profiles. *Nature* 511, 483 487
40 Yustein, J.T. *et al.* (2010) Induction of ectopic Myc target gene JAG2 augments hypoxic growth and tumorigenesis in a human B-cell model. *Proc. Natl. Acad. Sci. U.S.A.* 107, 3534 3539
41 Loven, J. *et al.* (2012) Revisiting global gene expression analysis. *Cell* 151, 476 482
42 Beier, R. *et al.* (2000) Induction of cyclin E-cdk2 kinase activity, E2F-dependent transcription and cell growth by Myc are genetically separable events. *EMBO J.* 19, 5813 5823
43 van Riggelen, J. *et al.* (2010) The interaction between Myc and Miz1 is required to antagonize TGFbeta-dependent autocrine signaling during lymphoma formation and maintenance. *Genes Dev.* 24, 1281 1294
44 Seoane, J. *et al.* (2001) TGFbeta influences Myc, Miz-1 and Smad to control the CDK inhibitor p15INK4b. *Nat. Cell Biol.* 3, 400 408
45 Staller, P. *et al.* (2001) Repression of p15INK4b expression by Myc through association with Miz-1. *Nat. Cell Biol.* 3, 392 399
46 Kaur, M. and Cole, M.D. (2013) MYC acts via the PTEN tumor suppressor to elicit autoregulation and genome-wide gene repression by activation of the Ezh2 methyltransferase. *Cancer Res.* 73, 695 705
47 Li, Y. *et al.* (2014) MYC through miR-17-92 suppresses specific target genes to maintain survival, autonomous proliferation, and a neoplastic state. *Cancer Cell* 26, 262 272
48 Evan, G.I. *et al.* (1992) Induction of apoptosis in fibroblasts by c-myc protein. *Cell* 69, 119 128
49 Dai, M.S. *et al.* (2007) Inhibition of c-Myc activity by ribosomal protein L11. *EMBO J.* 26, 3332 3345
50 Challagundla, K.B. *et al.* (2011) Ribosomal protein L11 recruits miR-24/miRISC to repress c-Myc expression in response to ribosomal stress. *Mol. Cell. Biol.* 31, 4007 4021
51 Qi, Y. *et al.* (2004) p19ARF directly and differentially controls the functions of c-Myc independently of p53. *Nature* 431, 712 717
52 Zindy, F. *et al.* (1998) Myc signaling via the ARF tumor suppressor regulates p53-dependent apoptosis and immortalization. *Genes Dev.* 12, 2424 2433
53 Wiese, K.E. *et al.* (2013) The role of MIZ-1 in MYC-dependent tumorigenesis. *Cold Spring Harb. Perspect. Med.* 3, a014290
54 Wolf, E. *et al.* (2013) Miz1 is required to maintain autophagic flux. *Nat. Commun.* 4, 2535
55 Inoue, S. *et al.* (2013) Mule/Huwe1/Arf-BP1 suppresses Ras-driven tumorigenesis by preventing c-Myc/Miz1-mediated down-regulation of p21 and p15. *Genes Dev.* 27, 1101 1114
56 Peter, S. *et al.* (2014) Tumor cell-specific inhibition of MYC function using small molecule inhibitors of the HUWE1 ubiquitin ligase. *EMBO Mol. Med.* Published online September 24, 2014, http://dx.doi.org/10.15252/emmm.201403927
57 Chen, D. *et al.* (2005) ARF-BP1/Mule is a critical mediator of the ARF tumor suppressor. *Cell* 121, 1071 1083
58 Herkert, B. *et al.* (2010) The Arf tumor suppressor protein inhibits Miz1 to suppress cell adhesion and induce apoptosis. *J. Cell Biol.* 188, 905 918
59 Diolaiti, D. *et al.* (2014) Functional interactions among members of the MAX and MLX transcriptional network during oncogenesis. *Biochim. Biophys. Acta* Published online May 22, 2014, http://dx.doi.org/10.1016/j.bbagrm.2014.05.016
60 Kelleher, F.C. *et al.* (2014) Circadian molecular clocks and cancer. *Cancer Lett.* 342, 9 18
61 Cunningham, J.T. *et al.* (2014) Protein and nucleotide biosynthesis are coupled by a single rate-limiting enzyme, PRPS2, to drive cancer. *Cell* 157, 1088 1103
62 Brown, J.D. *et al.* (2014) NF kB directs dynamic super enhancer formation in inflammation and atherogenesis. *Mol. Cell* 56, 219 231
63 Sun, M. *et al.* (2013) Global analysis of eukaryotic mRNA degradation reveals Xrn1-dependent buffering of transcript levels. *Mol. Cell* 52, 52 62
64 Lin, C.J. *et al.* (2012) Targeting synthetic lethal interactions between Myc and the eIF4F complex impedes tumorigenesis. *Cell Rep.* 1, 325 333
65 Takahashi, K. and Yamanaka, S. (2006) Induction of pluripotent stem cells from mouse embryonic and adult fibroblast cultures by defined factors. *Cell* 126, 663 676
66 Levens, D. (2013) Cellular MYCro economics: balancing MYC function with MYC expression. *Cold Spring Harb. Perspect. Med.* 3, a014233